EES Solar

Accepted Manuscript

This article can be cited before page numbers have been issued, to do this please use: T. H. HOANG, M. Khorsand Riabi, M. Zendehdel, M. Abdi-Jalebi and M. N. Ghazzal, *EES Sol.*, 2026, DOI: 10.1039/D6EL00019C.

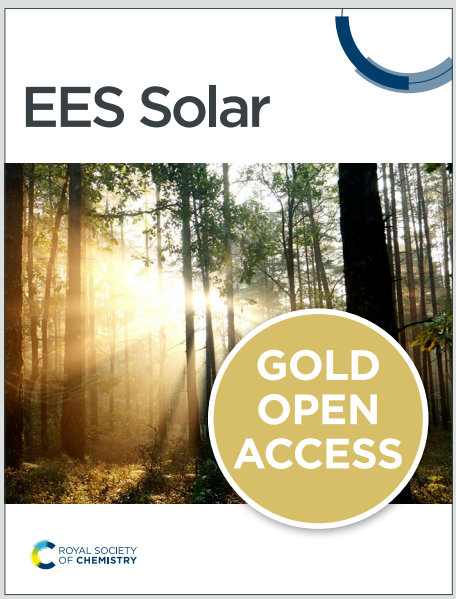

View Article Online
DOI: 10.1039/D6EL00019C

Broader Context

Metal halide perovskites have rapidly emerged as pivotal materials for solar energy conversion and a wide spectrum of optoelectronic applications due to their exceptional efficiency, low processing cost, and versatile compositional tunability. Their potential extends beyond photovoltaics to promising frontiers such as light-emitting diodes (LEDs), photodetectors, and solar-driven photocatalysis, where superior light absorption and charge transport are paramount. However, the widespread technological deployment of perovskites is critically hampered by their long-term instability under realistic operating conditions. This instability stems from a complex interplay of environmental stressors (moisture, oxygen, heat), intrinsic ion migration, and, fundamentally, defect formation. Defects act as central agents in this degradation, serving as non-radiative recombination centers that limit performance, as channels for ion migration that cause hysteresis and phase segregation, and as nucleation sites for chemical decomposition.

This review highlights defect formation as the core determinant of both efficiency losses and operational degradation in metal halide perovskites. It discusses recent, multidisciplinary strategies to mitigate these issues through advanced defect passivation. By consolidating breakthroughs across chemical doping, molecular surface engineering, and interfacial design, this work provides a comprehensive guide for enhancing material durability and electronic functionality. The insights presented are broadly relevant to the development of stable, high-performance perovskite-based technologies—not only in photovoltaics but also in LEDs, photocatalysis, and beyond—thereby accelerating progress toward sustainable and scalable energy and optoelectronic solutions.

View Article Online
DOI: 10.1039/D6EL00019C

Defect passivation of perovskites for higher efficiency and enhanced stability: applications in solar cells, photoluminescence, and photocatalysis

Thi Hieu Hoang[1], Mahdi Khorsand Riabi[2], Mahmoud Zendehdel[2,3], Mojtaba Abdi-Jalebi[4]*, Mohamed Nawfal Ghazzal[1]**.

[1] Université Paris-Saclay, CNRS UMR 8000, Institut de Chimie Physique, 91405, Orsay, France

[2] Department of Electronics Engineering, University of Rome Tor Vergata, Via del Politecnico 1, 00133 Roma, Italy.

[3] Iritaly Trading Company S.r.l., Via Volturno 58, 00185, Rome, Italy.

[4] Institute for Materials Discovery, University College London, Malet Place, WC1E 7JE, London, UK.

*Corresponding authors: mohamed-nawfal.ghazzal@universite-paris-saclay.fr ; mahmoud.zendehdel@uniroma2.it ; m.jalebi@ucl.ac.uk

Abstract: Metal halide perovskites have gained great attention for their distinctive photoelectrical properties. However, their sensitivity to some stability stressors has reduced their performance in many fields. The generation of defects has been considered a major contributor to the degradation and low performance of perovskites. Therefore, numerous passivation strategies have been proposed to mitigate the adverse effects of defects. In this review, we present various methods for passivating defects in perovskites, including polymer passivation, bulky organic cations, Lewis acid-base interactions, and metal cations. The effects of passivation on enhancing device performance and improving stability were also discussed. Finally, an outlook is presented to propose novel passivation approaches, especially in photocatalytic applications.

Keywords: Metal halide perovskites, defects, passivation, solar cells, light-emitting diodes, photocatalysis.

View Article Online
DOI: 10.1039/D6EL00019C

1. Introduction

In recent years, metal halide perovskites (MHPs), with general formula ABX_3, where A is a monovalent organic cation ($CH_3NH_3^+$, $NH_2CHNH_2^+$, etc.), or an inorganic cation (Cs^+), B is a divalent metal cation (usually Pb^{2+}), and X is a halide anion[1], have emerged as one of the most promising semiconductors with a wide range of applications. These perovskite structures have shown remarkable applications as solar cells, mainly due to their unique photoelectrical properties, such as high charge-carrier mobility, broad-spectrum light absorption, high light absorption coefficient, and high tolerance to crystal defects[2–6]. Perovskite solar cells (PSCs) have attracted significant attention from scientists for their impressive photovoltaic properties and low manufacturing costs, comparable to traditional silicon-based solar cells[7]. The power conversion efficiencies (PCE) of organic-inorganic PSCs on the lab scale had increased dramatically in just 10 years, from 3.8% in 2009[8] to 25.5% in 2020[9] and more than 26% in recent years[10–13]. Many attempts are ongoing to further enhance the PCE of perovskite solar cells and achieve a power conversion efficiency (PCE) of up to 27%[14]. Additionally, a combined analysis based on Shockley–Queisser theory and experimentally achievable photovoltaic parameters suggests that the practical efficiency potential of single-junction PSCs with a band gap of 1.5–1.6 eV could exceed 30%[15]. Achieving this goal requires significantly more effort.

The excellent performance of MHPs was also observed in light-emitting devices (LEDs), as they exhibit extremely high photoluminescence quantum yields (PLQYs) of 100%.[16] They have narrow photoluminescence (PL) peaks with a full width at half-maximum FWHM of roughly 12-40 nm, resulting in high purity of color, which is better than for conventional quantum dots (QDs) LEDs[17]. Their emission wavelengths are tunable across the entire visible and near-IR spectral regions by varying the halide composition in perovskites[18]. The first room-temperature perovskite LEDs (PeLEDs) were introduced in 2014 with the external quantum efficiencies (EQEs) of 0.76%[19]. Since then, several studies have been conducted in this field of perovskite materials, and the EQEs of PeLEDs have been boosted to an incredible 22%[20]. Moreover, the synthesis of perovskite materials is straightforward from inexpensive starting materials, potentially decreasing fabrication costs.[18] Due to the above-mentioned outstanding properties, PeLEDs have emerged as potential candidates for next-generation light-emitting devices.

View Article Online
DOI: 10.1039/D6EL00019C

In addition to remarkable applications as solar cells and light-emitting devices, MHPs have recently gained significant attention in photocatalysis, which exploits their unique photophysical properties, including a tunable bandgap, high charge-carrier mobility, and efficient electron-hole separation[2]. The potential energy gap between the valence and conduction bands of MHPs makes them well-suited to act as photocatalysts in H_2 generation and CO_2 reduction reactions[21]. Despite these excellent characteristics, industrial applications of metal halide perovskites still suffer from instability. MHPs are highly sensitive to moisture and oxygen; they exhibit poor stability under ultraviolet (UV) radiation, polar solvents (e.g., water), and thermal effects[22–25]. The degradation of conventional perovskites releases heavy metals like lead, inducing significant risks to both the environment and human health while also reducing their optical performance (Eq. 1 and 2)[26]:

$$2CsPbBr_3.H_2O + \frac{1}{2}O_2 + CO_2 \longrightarrow 2CsBr + PbCO_3 + Pb(OH)_2 + 2HBr + Br_2 \qquad (1)$$

$$Pb(OH)_2 \longrightarrow PbO + H_2O \qquad (2)$$

As a result, it is imperative to develop strategies to produce novel perovskite derivatives with superior optical performance and stability. The studies indicated that the halide composition adjustment could significantly improve the stability of perovskites. Noh et al. prepared a $CH_3NH_3Pb(I_{1-x}Br_x)_3$ perovskite by substituting I with Br.[27] Compared to the standard material $CH_3NH_3PbI_3$ ($MAPbI_3$) (x = 0), the stability of perovskite solar cells containing Br was significantly improved.[28] The mixed-halide perovskite $CsPb(Br_xCl_{1-x})$ was reported to have better stability than $CsPbBr_3$. Thus, their activity in CO_2 photoreduction was dramatically improved. The total formation rate of CO and CH_4 was approximately 4.5 times higher than that of the pristine $CsPbBr_3$. Knezevic et al. reported that adjusting the bandgap of $CsPbBr_3$ covered by a thin layer of porous TiO_2 via anion substitution at room temperature improves stability and enables reaching optimal charge-carrier separation and stabilization in aqueous media for 3 hours[29]. The encapsulation of $CsPbX_3$ into mesoporous silica films with a chiral nematic structure could enhance the perovskites' stability under ambient conditions[30]. In addition to conventional three-dimensional (3D) structures, MHPs were found to exist as two-dimensional (2D) structures. The 2D perovskites were shown to maintain unchanged optical properties in water[31]. The exposure of 2D perovskite structures to 52% of relative humidity during 46 days indicated no significant decomposition, while 3D perovskite showed new reflection peaks in X-ray diffraction (XRD) patterns, indicating the segregation of MHP and the formation of PbI_2[32]. As a result, the solar cells

View Article Online
DOI: 10.1039/D6EL00019C

fabricated from the $(PEA)_2(MA)_2[Pb_3I_{10}]$ perovskite 2D materials exhibit higher moisture resistance than devices containing 3D materials. In photocatalytic applications in water, the 2D MHPs nanosheets show greater photocatalytic activity for CO_2 reduction compared to traditional MHPs nanocrystals[31]. The PeLEDs that used quasi-2D perovskite film were also reported to show higher current efficiency and luminance than the 3D perovskite-based technology.

Nevertheless, the performance advantage of a given dimensionality is strongly dependent on the reaction environment. In non-aqueous media, 3D perovskite nanocrystals can outperform 2D nanosheets, as exemplified by CO generation rates that are 3.8 times higher for 3D nanocrystals, which also exhibit higher photoluminescence quantum efficiency (PLQE)[33]. These observations indicate that while reduced dimensionality improves stability and surface passivation in aqueous systems, it does not universally guarantee superior photocatalytic activity across all media. Elemental doping provides a powerful strategy to tune both the structural dimensionality and electronic properties of MHPs. In our work, Cu^{2+} doping preserves the three-dimensional framework of $CsPbBr_3$, whereas Bi^{3+} doping induces a transformation toward a two-dimensional structure. In toluene oxidation, an organic solvent environment, Cu-doped 3D $CsPbBr_3$ exhibits superior photocatalytic activity compared with Bi-doped 2D $CsPbBr_3$[34]. This comparison underscores a wider array of doping strategies. The introduction of extrinsic species can modify the electrical doping of the perovskite film[35]. Such changes may arise from intrinsic defect doping, extrinsic impurity incorporation, or charge transfer between the passivating species and the perovskite lattice[36]. These processes can change the concentration of free carriers and adjust the Fermi level, thereby affecting the electronic properties of the perovskite film. Additionally, changes in defect distributions may promote ionic migration pathways within the perovskite lattice, thereby further influencing local carrier density and accelerating interfacial degradation under operational conditions[37].

Encapsulating MHPs with an overlayer has been shown to be highly effective in protecting their surfaces, thereby significantly increasing their stability in air and water. Li et al. successfully increased the stability of $CH_3NH_3PbI_3$ perovskite solar cells by spin-coating the surface with butylphosphonic acid 4-ammonium chloride (4-ABPACl)[38]. Wentao group reported the successful preparation of $CsPbBr_3$ nanocrystals coated with a polymer-polyaniline (PANI), which can maintain their stability for approximately 11 days in air[39]. Metal oxides such as SiO_2 were used to

View Article Online
DOI: 10.1039/D6EL00019C

encapsulate $CsPbBr_3$ quantum dots (QDs), and it was found that the photoluminescence (PL) of $CsPbBr_3@SiO_2$ powders remained almost unchanged after 40 days of storage under ambient conditions, and their PL intensity was maintained at 80% after continuously illuminated by a UV lamp for 108 hours[40]. Our group showed that encapsulating $CsPbBr_3$ with a TiO_2 overlayer enhances the stability of H_2 generation in aqueous solutions[29].

The stability affecting MHPs also stems from defects. Defects in semiconductor crystals are either interruptions to the perfect crystal lattice or the presence of foreign atoms (impurities) in the lattice, and they can have cascading effects on device performance, as shown in **Figure 1**.[41,42] Defects are usually categorized into three types which are (1) intrinsic point defects, such as atomic vacancies (missing atoms), interstitials (extra atoms), impurity (foreign atoms) and anti-site substitutions (wrong lattice sites) (**Figure 1a**)[42]; (2) two-dimensional defects, for example, dislocation and grain boundaries (GBs) (**Figure 1b**) and (3) three-dimensional defects like precipitates and metal clusters (**Figure 1c**).[41,43] The concentration of point defects in perovskites is usually higher than that of other types, since their formation energy is much higher[44]. From point defects to three-dimensional defects, these imperfections influence key material parameters, including trap states, carrier recombination, and surface activity[45–49]. These changes directly affect device performance, including optoelectronic efficiency, photocatalytic activity, and overall stability.

The defects mainly arise from the rapid crystallization and growth processes of the perovskite films, since these steps are very difficult to control fully[7]. For example, grain boundaries form during the crystallization process when multiple crystallites grow but do not perfectly align. Other possible causes of perovskites' defects could be (i) non-stoichiometry ratio of the starting materials (e.g., lead, halide, organic cations); (ii) environmental factors (e.g., air, moisture, light); (iii) processing conditions (e.g., solvent systems, synthesis methods, temperature).[50] For instance, the diffusion of Ag^+ or Au^+ from the electrode into perovskite layers in solar cells can introduce impurity defects, or the reduction of Pb^{2+} to Pb^0 during the synthesis process is associated with a precipitation defect.

View Article Online
DOI: 10.1039/D6EL00019C

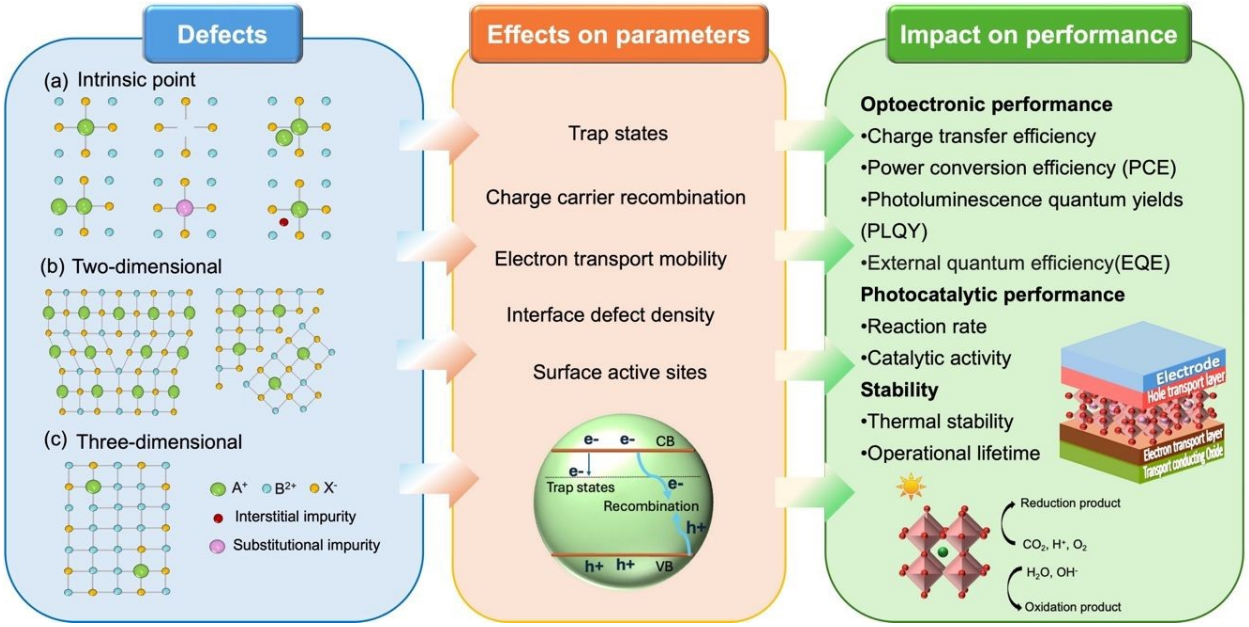

Figure 1. Left: Different forms of defects: (a) intrinsic point defects, (b) two-dimensional defects, and (c) three-dimensional defects, and the influence of the defect on device parameters and performance; Middle: The effects of defects on different parameters of materials; Right: The impacts of defects on the device's performance.

Defects play an essential role in controlling the optoelectrical and structural properties of perovskite materials. Therefore, they drastically influence the optical performance of MHPs. Defects can provide several benefits, such as active photocatalysis sites and holes for charge transportation. On the other hand, defects can be detrimental because they introduce trap states in the band gap, which may act as centers for nonradiative recombination, reducing the photoluminescent performance and stability of perovskites.[51] As a result, eliminating the negative impacts caused by defects will be a key step to further enhance the stability and the overall performance of perovskites. The preparation of single-crystalline perovskite materials can be a solution for defect problems since single-crystalline perovskites are free of grain boundaries and have a low density of defects compared to polycrystalline[43]. However, it is challenging to synthesize single-crystal perovskite materials with suitable device-scale thickness. Therefore, defect passivation is expected to be the most efficient method for mitigating the negative effects of defects in perovskites.

View Article Online
DOI: 10.1039/D6EL00019C

In this review, we will summarize different strategies for defect passivation in metal halide perovskites, including passivation by organic ions, Lewis acid-base, and metal ions. The mechanism for passivating the negatively and positively charged defects will be shown. Their effect on increasing the stability of perovskite materials will also be discussed, focusing on improving their optical performance and applications in solar cells, light-emitting diodes, and photocatalysis.

2. Defect passivation by organic molecules

In the process of advanced perovskite materials, a range of organic additives has been used to improve film morphology, interfacial properties, and long-term device stability. These additives operate through different mechanisms and therefore need to be discussed according to their functional roles.

Polymeric and biopolymeric materials, such as PMMA and chitosan, are often employed as coating or encapsulation agents[52,53]. Because nanoparticles and microparticles typically possess high surface energy and are prone to forming fissured domains, polymer coatings can effectively reduce surface roughness and enhance interfacial wettability at the polymer–polymer junction between the perovskite layer and the hole transport layer (HTL)[54,55]. In addition, polymer matrices can encapsulate physically perovskite grains and grain boundaries, thereby limiting ion migration pathways and providing partial protection against environmental factors such as moisture and oxygen. These effects improve device performance and operational stability.

In contrast, organic ammonium salts or bulky organic cations interact more directly with the perovskite crystal lattice. By intercalating between the inorganic octahedral layers, these species can promote the formation of layered or quasi-two-dimensional (2D) perovskite structures or 2D/3D heterostructures. Such architectures enhance resistance to ion migration and environmental degradation while preserving the crystalline framework of the light-absorbing material. However, due to their relatively insulating nature, excessive incorporation may hinder charge transport and reduce device performance[56].

Another important class of additives includes small-molecule ligands, which function by passivating chemical defects. These molecules can coordinate with under-coordinated metal ions or compensate ionic defects at surfaces and grain boundaries, thereby suppressing trap states and

View Article Online
DOI: 10.1039/D6EL00019C

reducing non-radiative recombination losses[57]. Organic molecules may also introduce additional functionalities into perovskite systems; for example, additives such as ethylene glycol have been reported to induce self-healing behavior or enable property tuning in composite structures[58].

Given the diversity of molecular structures and mechanisms involved, it is useful to classify organic molecules according to their primary functional roles. structured, the following sections discuss organic additives in two main categories: (i) organic capping ligands, which mainly regulate surface chemistry and interfacial interactions, and (ii) defect passivation agents based on Lewis acid-base interactions, which aim to suppress electronic defects in perovskite films.

2.1 Organic capping ligands:

Metal halide perovskite nanocrystals can be synthesized by the hot-injection method, which involves injecting Cs-oleate into a solution containing lead salts in oleic acid (OA), oleylamine (OAm), and octadecene (ODE). These capping ligands are essential in preparing perovskites since they are responsible for colloidal stability and shape control[59]. Organic capping ligands can improve surface characteristics. It would need more research in terms of surface modification of perovskites for different applications. Meanwhile, considering the long-chain OA/OAm ligands could easily desorb from the surface of perovskites, generating several defects[2], and can further lead to halide migration and segregation, inducing the decomposition of perovskites.

These surface defects not only cause the structural integrity of perovskites but also affect their optoelectronic and catalytic performance. Particularly, OA/OAm-capped perovskites are unfavorable for CO_2 photoreduction since the long-chain capping ligands hinder the efficient charge separation on the surface of MHPs and thus decrease the photocatalytic performance.[2] Therefore, developing novel ligands capable of passivating the surface defects and improving the stability of perovskite nanocrystals (NCs) is imperative, as replacements for the traditional long-chain OA/OAm.

In 2022, Li et al. employed the reactive thionyl bromide ($SOBr_2$) to replace the original ligands (OA/OAm) and compensate for bromine vacancies on $CsPbBr_3$ nanocrystals (**Figure 2a**)[60]. This approach aimed to enhance stability while also facilitating charge transfer and separation from $CsPbBr_3$ to g-C_3N_4. As a result, $CsPbBr_3$–$SOBr_2$ NCs exhibited an elevated CO_2 photoreduction activity. The photocatalytic yield is 69 μmol g^{-1} h^{-1} in terms of electron consumption, which was

View Article Online
DOI: 10.1039/D6EL00019C

approximately six times higher than that of pristine $CsPbBr_3$. Furthermore, when combined with g-C_3N_4, the CO_2 photoreduction yield reached an even higher value of 190 μmol g^{-1} h^{-1}. The utilization of tetrafluoroborate salts (BF^{4-}) was reported as a defect treatment agent and subsequently loaded Co^{2+} as a co-catalyst (Figure 2b)[61]. The results demonstrated that $CsPbBr_3$–BF_4 exhibited high photocatalytic CO2 performance, with CO and CH_4 evolution rates of 83.8 μmol g^{-1} h^{-1}.

Because surface treatment can adjust the surface characteristics of the perovskites, a post-synthesis approach was proposed to passivate the surface defects of $CsPbBr_3$ nanocrystals by using a bidentate ligand 2,2′-iminodibenzoic acid (IDA) (Figure 2c)[62]. The IDA ligand was found to be a key compound, showing much stronger binding to the perovskite surface than the OA ligand does, which can be attributed to strong interactions between the dual carboxylic groups and undercoordinated Pb^{2+} sites. The two carboxyl groups of IDA can simultaneously coordinate to surface Pb^{2+} centers, forming a bidentate chelate at the nanocrystal surface. Compared with monodentate ligands like OA, this chelating coordination offers stronger interfacial binding, helping reduce ligand desorption or dynamic surface ligand exchange during storage. The surface trap density decreased, and additional electrons were injected into perovskite NCs. The enhanced surface coordination structure helps maintain the passivated surface state, which reduces the reformation of undercoordinated sites and defect-assisted nonradiative recombination over time. The stability of the cubic perovskite phase and electronic coupling between ligands and NCs were remarkably improved. In this work, the IDA-treated $CsPbX_3$ NCs exhibited an excellent PLQY of 95%, compared to 80% recorded for the pristine ones, as illustrated in **Figure 2c**. Consequently, the EQE of the red LED device based on IDA-treated $CsPbI_3$ NCs reached a maximum value of 5%, which was almost 2-fold higher than that of the control device. Stability tests also revealed that IDA-treated NCs showed significantly improved stability, with no phase change after 40 days. Moreover, IDA-treated NCs retained 90% of PL emission after 15 days, and the PLQY remained almost the same after washing with ethyl acetate. The persistence of surface-bound IDA species after antisolvent washing, in contrast to the pronounced ligand loss observed for OA-capped nanocrystals, was supported by Fourier-transform infrared (FTIR) and X-ray photoelectron spectroscopy (XPS) analyses.

View Article Online
DOI: 10.1039/D6EL00019C

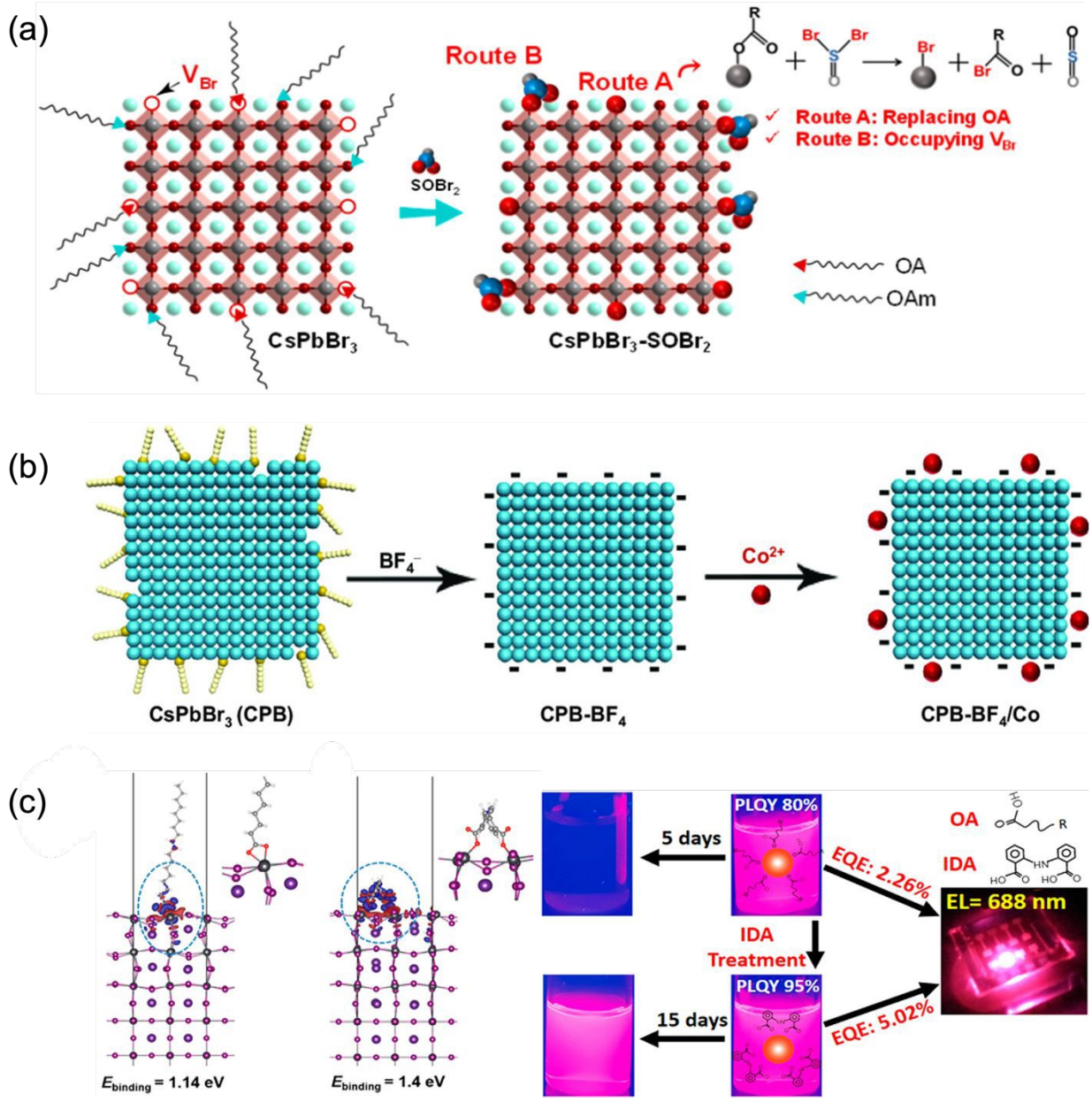

Figure 2. (a) Schematic presentation for $SOBr_2$ ligand modified-$CsPbBr_3$ NCs. Reproduced with permission.[60] Copyright 2022 American Chemical Society. (b) Schematic presentation for the treatment of $CsPbBr_3$ with BF_4^-/Co^{2+} ions. Reproduced with permission.[61] Copyright 2021 Wiley-VCH GmbH. (c) Schematic presentation for surface passivation by IDA (left); the PLQYs of OA-treated and IDA-treated $CsPbX_3$ NCs and EQE of corresponding PeLEDs devices (right). Reproduced with permission.[62] Copyright 2017 American Chemical Society.

2.1.1 Organic ammonium cations

View Article Online
DOI: 10.1039/D6EL00019C

Organic ammonium cations have been employed by many groups for perovskite defect passivation because they can readily form ionic bonds with uncoordinated ions, thereby healing defects within the perovskite crystal lattice. For instance, a straightforward method was reported to reduce the level of electronic defects at the interface between the perovskite film and the hole transport layer (HTL). To do so, the surface of perovskite was modified via the addition of organic ammonium salts, including ethylammonium iodide (EAI), imidazolium iodide (IAI), and guanidinium iodide (GuaI)[63]. Introducing salts prevented the irreversible decomposition of perovskites by fixing the A-site cation defects and enhancing the stability of the perovskite absorber. The photovoltaic devices fabricated from EAI-, IAI-, and GuaI-perovskite showed significantly improved photoconversion performance compared to the original devices, with great power conversion efficiencies up to 21.0%.

The defects' passivation by ammonium salts further increased the operational stability of perovskite solar cells, with a minor 5% efficiency loss in the best-performing devices after 550 h of exposure to maximum-power solar-intensity conditions (**Figure 3a**). The Gua cation (or GA) was employed to mitigate surface defects and enhance the stability of other types of perovskites[64]. The surface-stabilizing 1,3,5-tris(bromomethyl)-2,4,6-triethylbenzene (TBTB) was used as a healing agent for bromide vacancy (**Figure 3b**)[65]. As a result, the PLQY of passivated Perovskite increased from 79.7% for the pristine MHP to 93.3%, and the performance of green LED reached a high current efficiency of 108 cdA^{-1} and an impressive EQE of 23.4%. Liang et al. synthesized a series of phenyl and thienyl-based ammonium salts as the passivators for perovskites, including phenylmethylammonium iodide (PMAI), thienylmethylammonium iodide (TMAI), phenylformamidinium iodide (PFAI), thienylformamidinium iodide (TFAI), phenylimidazolium iodide (PImI), and thienylimidazolium iodide (TImI)[66] (**Figure 3c**). These passivators effectively passivated surface defects in as-prepared perovskite thin films, thereby enhancing optoelectronic properties and PLQY by reducing non-radiative recombination.

The introduction of the passivators also decreased the grain size and surface roughness of perovskite films. The passivated PeLEDs exhibited good color stability with no wavelength shift observed in the electroluminescent spectra under different applied bias voltages. The highest EQE of 15.6% was recorded for the $MAPbI_3$-based LEDs treated with PImI passivators, which was ten times higher than that of the pristine $MAPbI_3$ control device. Moreover, the treatment with PImI

View Article Online
DOI: 10.1039/D6EL00019C

passivators significantly improved the operational stability of the PeLEDs. The results suggested that the PImI-based device retained 50% of its initial EQE after 2 h under a constant current density of 10 mA.cm^{-2}, whereas the device treated with PMAI lasted only 6 min under the same conditions. To passivate the Br defect and increase the water resistance of the conventional perovskites, diethylenetriamine ion ($DETA^{3+}$) can be utilized in some cases.[67]

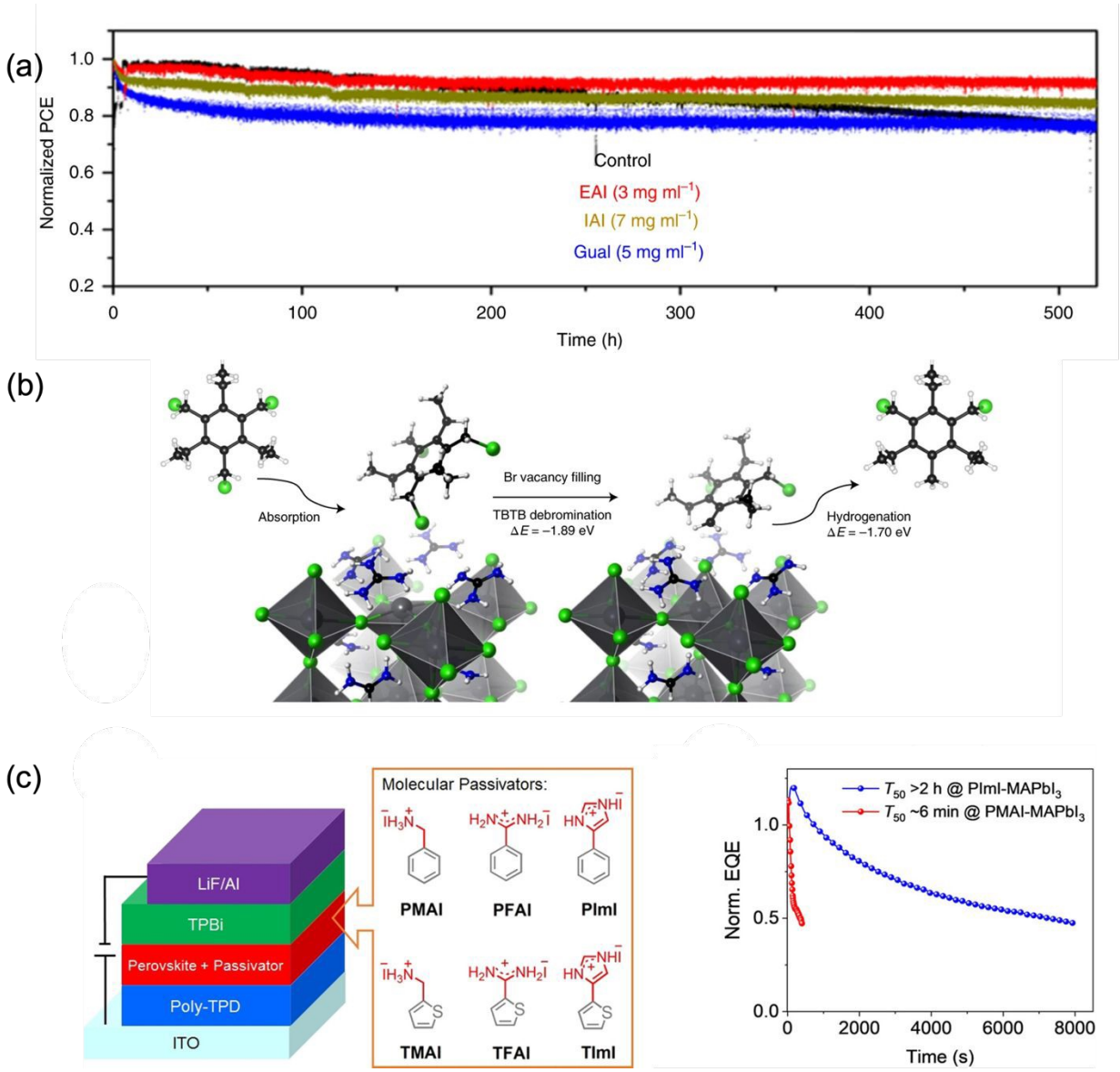

Figure 3. (a) Operational stability over time of the control and treated perovskite devices regarding power conversion efficiency. The devices were exposed to constant illumination (LED source, ~ 1 sun) at the maximum power point for 550 h. Reproduced with permission.[63] Copyright 2019 Nature Communications. (b) Schematic presentation of the DFT-proposed mechanism for bromide

View Article Online
DOI: 10.1039/D6EL00019C

vacancy passivation driven by TBTB molecules on the GA-terminated $FAPbBr_3$ surface. Reproduced with permission.[65] Copyright 2021 Nature Photonics. (c) The molecular structures of different phenyl and thienyl-based ammonium salts as the passivators for perovskites (left); Operational stabilities of the PMAI- and PImI-treated devices tested at a constant current density of 10 mA cm^{-2} (right). Reproduced with permission.[66] Copyright 2021 Wiley-VCH GmbH.

2.1.2 Dual passivation using Zwitterionic molecules

Organic cationic or anionic passivators can only act on a single defect at a time, limiting their applicability, as perovskites typically possess multiple defects. Therefore, using a zwitterionic passivator (Zw), which can heal both positive and negative defects, introduces a novel approach to enhance passivation efficiency.

A dual passivation method has been reported for perovskite defects using a bifunctional molecule, such as 4-fluorophenylmethylammonium trifluoroacetate (FPMATFA)[68]. The FPMA cations and TFA anions can form electrostatic bonds with uncoordinated lead and halide ions, respectively. Zwitterionic passivators can simultaneously passivate both lead and halide defects, as shown in **Figure 4a**. Consequently, the fabricated PeLEDs achieved an EQE of 20.9% at an excitation wavelength of 694 nm. Moreover, due to defect passivation, the FPMATFA-passivated films exhibited better thermal and optical stability than the pristine $FPMAI_{0.7}Br_{0.3}$ film. The FPMATFA device also demonstrated higher storage stability, with its EQE showing no degradation after 2 months. Similarly, 3-(decyldimethylammonio) propane-sulfonate (DPSI), a sulfonic zwitterion salt, was selected for passivating the perovskite's defects[69]. A small amount of DPSI salt (0.05wt%) was introduced into the $MAPbI_3$ precursor solution. The ammonium groups in DPSI formed ionic bonds with MA vacancies, while sulfonic groups combined with iodine vacancies to simultaneously passivate negatively and positively charged defects at the perovskite surface and grain boundaries (**Figure 4b**). The strong coordination of the S=O group in DPSI with Pb ions also passivated morphological defects during the fabrication process of the perovskite film. The stability of DPSI-treated PSC devices was then examined by exposing them under continuous AM 1.5G illumination. The DPSI devices maintain 88 % of their initial performance after 480 h, indicating their high stability under UV radiation. Moreover, the treated devices showed excellent moisture resistance, retaining 96 % of their initial performance after the 60 h test under relative humidity (RH) conditions in the range of 30-70 %. After the passivation, the pinhole as a

View Article Online
DOI: 10.1039/D6EL00019C

morphological defect formation was inhibited, thus decreasing the charge trap density and extending the electron-hole recombination lifetime. As a result, the efficiency of PSCs was boosted to an impressive value of 21.1%.

In the same context, perovskite solar cells were treated with 3-(1-pyridinio)-1-propane sulfonate zwitterion to increase their thermal stability and power conversion efficiency[70] (**Figure 4c**). The sulfonic group in the zwitterion was bonded to the SnO_2 surface to modify the SnO_2 electron transport layer (ETL), thereby increasing electron transport mobility and preventing charge recombination. The sulfonate group can strongly anchor to surface hydroxyl groups and undercoordinated metal sites on SnO_2, resulting in an interfacial coordination structure. Meanwhile, the positively charged N atoms healed Pb-I antisite defects to improve the stability of PSC devices. The zwitterionic molecular structure simultaneously interacts with both the SnO_2 ETL and the perovskite surface, thereby helping reduce interfacial ion migration, interfacial bond dissociation, and defect re-formation under thermal and humid stress. Consequently, the Zw–SnO_2-based PSCs device showed great thermal stability, maintaining 80% of its initial efficiency after 60 min under heating at 150 ^oC. Furthermore, the Zw–SnO_2-based device exhibited long-term stability, retaining 93% of its initial performance after 140 h under harsh conditions (85 °C, 85% RH). These findings indicate that zwitterion-derived interfacial passivation remains stable even under harsh aging conditions, enabling effective interfacial charge extraction and mitigating thermally induced interfacial degradation. With further optimization, the modified perovskite solar cells recorded PCE up to 21.43%. Yang et al. treated $MAPbI_3$ precursor with ammonium benzenesulfonate (ABS) to produce high-quality PSCs (**Figure 4d**). Due to the zwitterionic structure, ABS can simultaneously passivate cationic and anionic defects at grain boundaries, thus considerably reducing the trap density in perovskite. The fabricated device achieved the highest PCE of 20.62% and showed great moisture stability, with only 15% efficiency loss after storing for 1400 h under ambient conditions[71]. Other groups also employed the introduction of zwitterions onto the charge transport layer. For example, Ciro et al. utilized Rhodamine derivatives to passivate the defects on the ETL of perovskite solar cells[72] **(Figure 4e)**. The charge transport efficiency was thereby improved, and the moisture stability of MHPs was also increased since Rhodamine can act as a barrier that prevents the penetration of moisture into the perovskite layer. Therefore, an increase in PCE to 16.6% was obtained.

View Article Online
DOI: 10.1039/D6EL00019C

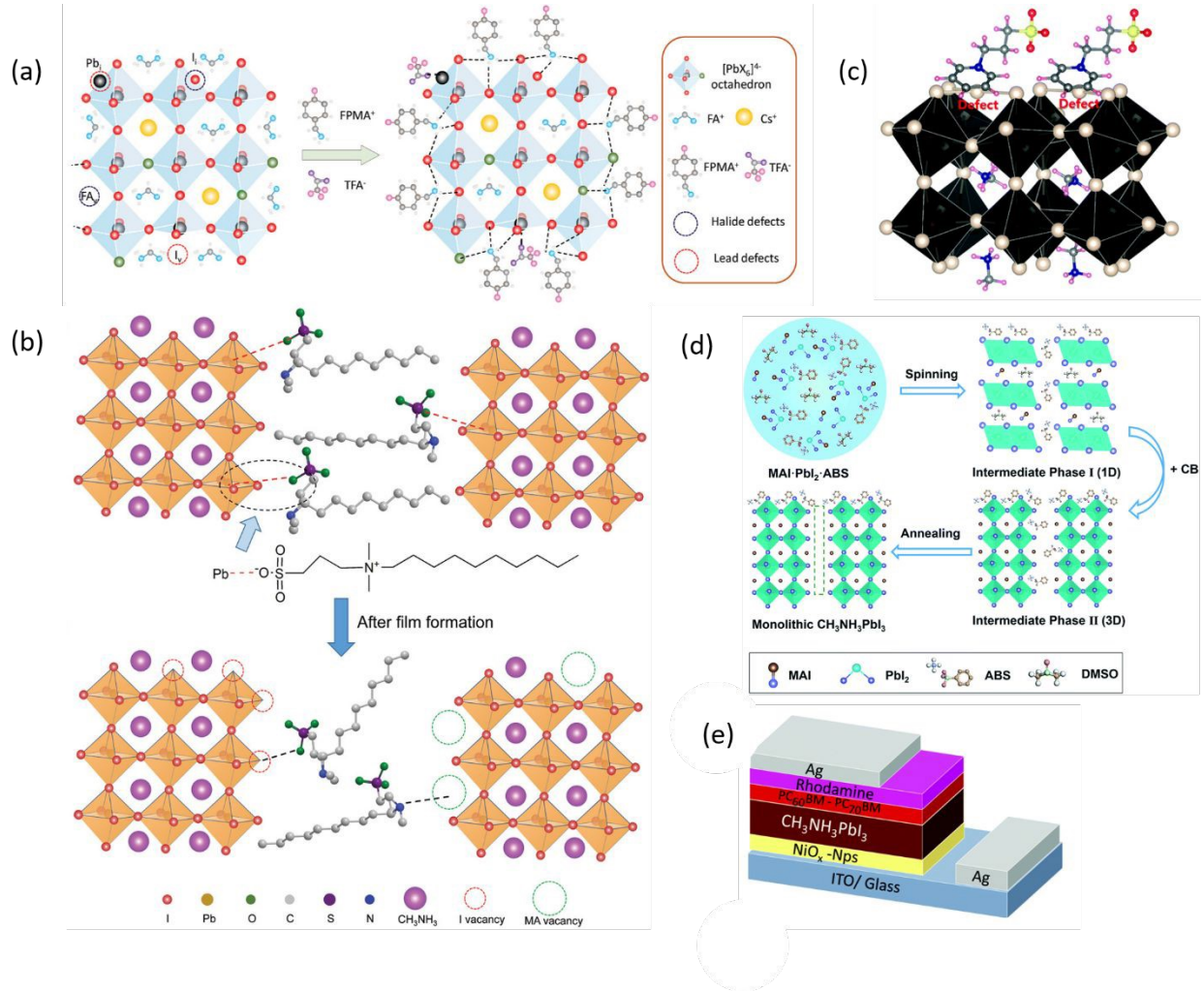

Figure 4. (a) Schematic presentation of defect passivation at perovskite grain boundaries by FPMATFA. Reproduced with permission.[68] Copyright 2020 WILEY-VCH Verlag GmbH & Co. KGaA, Weinheim. (b) Schematic presentation of DPSI mediated perovskite growth and defect passivation[69]. Copyright 2020 WILEY-VCH Verlag GmbH & Co. KGaA, Wienheim. (c) Schematic presentation for passivation of I vacancy by 3-(1-pyridinio)-1-propanesulfonate. Reproduced with permission.[70] Copyright 2018 The Royal Society of Chemistry. (d) Schematic presentation for reaction process from the precursor to monolithic perovskite grains. Reproduced with permission.[71] Copyright 2019 The Royal Society of Chemistry. (e) Device configuration for the ETL–cathode interface by employing rhodamine. Reproduced with permission.[72] Copyright 2017 The Royal Society of Chemistry.

View Article Online
DOI: 10.1039/D6EL00019C

The zwitterionic amino acid, for example, L-alanine, can be used as an additive in the perovskite precursor solution to passivate both positively and negatively charged defects[73]. Under specific pH conditions, positively charged NH^{3+} and negatively charged COO^- functional groups effectively passivated both cation and anion defects in $MAPbI_3$ PSCs (**Figure 5a**), increasing perovskite grain size and extending charge-carrier lifetime. This enhancement resulted in an improvement of PCE from 18.3% without the additive to 20.3%. Moreover, the ionic defect passivation method affected the stability of PSCs. The L-alanine-treated device retained nearly 90% of its initial PCE after 16 h of photoirradiation. In comparison, the PCE of a pure device dropped rapidly to 80% of its initial PCE after the same period (**Figure 5b**). Therefore, using the zwitterionic form of amino acids, the dual passivation method is an effective way to heal MHPs' ionic defects and fabricate highly stable PSCs. This approach was employed by many other groups with different amino acids, such as (*s*)-(-)-4-amino-2-hydroxybutyric acid molecule (AHBA)[74], which can efficiently passivate the traps/defects at grain boundaries and the surface of perovskite via the coordination with uncoordinated lead and iodide ions (**Figure 5c**). The COO^- group coordinates with undercoordinated Pb^{2+} sites, while the $–NH_3^+$ group forms hydrogen bonds with iodide ions (N–H···I). Additionally, the –OH group provides additional hydrogen bonding interactions (O–H···I). These interactions were confirmed by XPS, which showed shifts in the binding energies of Pb 4f, I 3d, N 1s, and O 1s, indicating chemical coordination between AHBA and the perovskite lattice. The multifunctional molecular structure of AHBA offers multiple interaction sites at grain boundaries and surfaces, which is expected to enhance interfacial coordination and minimize defect reactivation during long-term storage. The PCE was thus boosted from 17.96% to 20.31%, and the intrinsic stability of the devices was also improved, retaining 94% of their initial performance after 60 days of storage in the N_2 atmosphere.

View Article Online
DOI: 10.1039/D6EL00019C

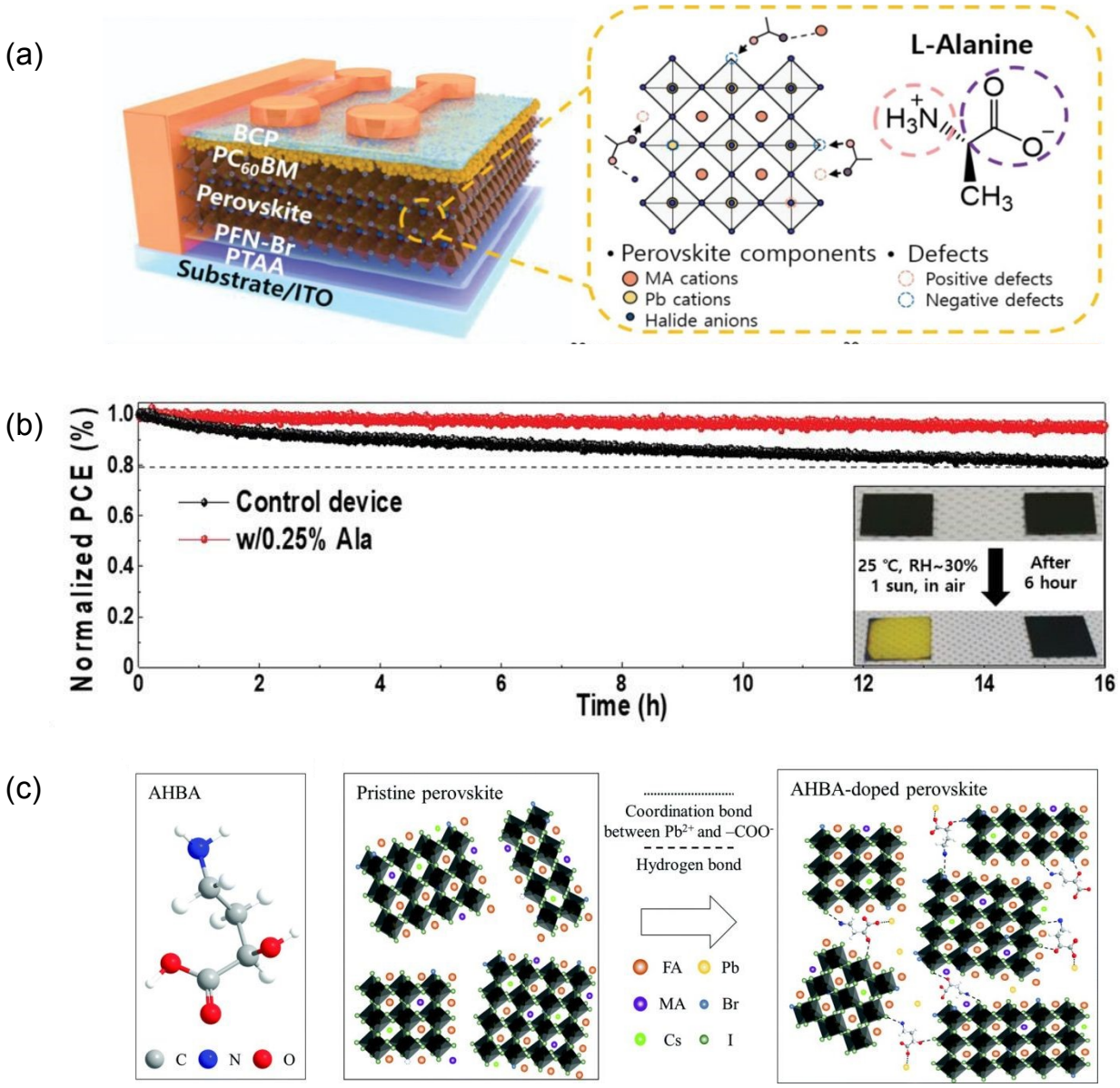

Figure 5. (a) Schematic presentations for the planar p-i-n device architecture and for the possible passivation mechanism of the L-alanine additive in the perovskite film. Reproduced with permission.[73] Copyright 2020 Wiley-VCH GmbH. (b) Normalized PCE as a function of time and photographs of the perovskite films with and without the L-alanine additive, which were exposed to 1 sun illumination in the air (inset). Reproduced with permission.[73] Copyright 2020 Wiley-VCH GmbH. (c) AHBA-passivated at perovskite surface and grain boundaries through coordination with undercoordinated Pb^{2+} and iodide-related defects. [74] Copyright 2020 Royal Society of Chemistry.

View Article Online
DOI: 10.1039/D6EL00019C

2.1.3 Organic ammonium cations as a spacer of low-dimensional perovskite overlayers

In addition to passivating defects via electrostatic interactions, organic ions, such as bulky organic ammonium cations, can form new layered perovskites, reducing recombination between light-absorbing and charge-transporting layers in PSCs. These layered perovskites have also been reported to improve MHPs' stability. For example, the incorporation of hydrophobic long-chain organic cations, such as phenylethylammonium (PEA^+), generated a 2D perovskite layer on the surface of $MAPbI_3$ (**Figure 6a**), which could act as a moisture barrier and thus increase the moisture stability of perovskites. The power conversion efficiency of PSCs was also boosted to 16.8% due to the enhanced open-circuit and fill factor[57]. A mixed passivation strategy was presented to passivate the perovskite/HTL interface using iso-butylammonium iodide (*i*BAI) and formamidinium iodide (FAI) (**Figure 6b**) to enhance both the power conversion efficiency and the stability of $(FAPbI_3)_{0.85}(MAPbBr_3)_{0.15}$ PSCs[75]. Upon optimized molar fraction of FAI and *i*BAI, the number of defects on the perovskite surface decreased, which can be attributed to the reaction between *i*BAI and excess PbI_2, forming a 2D iBA_2PbI_4 passivation layer at the perovskite/HTL interface. FAI can react with PbI_2 to passivate the FA or I vacancies. The passivation layer could inhibit ion migration and interfacial trap filling, thereby reducing hysteresis. Moreover, the formation of the iBA_2PbI_4 layer introduces a hydrophobic organic barrier that can retard the ingress of moisture into the underlying perovskite film. While hydrophobicity itself is not a defect passivation mechanism, it may enhance environmental stability by limiting water-induced degradation pathways. The stability tests of solar cell devices were carried out by storing the devices at 75% RH. After 38 days, the passivated devices exhibited moisture stability two times higher than the original ones. The PCE was thus boosted to a remarkable value of 21.7%[75]. Tavakoli et al. selected formamidinium chloride (FACl) and 1-adamantylamine hydrochloride (ADAHCl) for the mixed passivation method of the perovskite surface.[76] FACl served as a chlorine source with better solubility than other precursors such as MACl or $PbCl_2$, facilitating the efficient replacement of MA^+ ions with FA^+ ions, resulting in higher crystallinity and stability of the perovskite. Following the annealing process, Cl in FACl was released from the perovskite absorber surface via volatilization, generating surface defects (**Figure 6c**). Therefore, ADAHCl was used as an additive Cl source to passivate the perovskite surface and further improve perovskite film quality by preventing surface recombination. This passivation strategy boosted the PCE of

View Article Online
DOI: 10.1039/D6EL00019C

perovskite solar cells to achieve 21.2%. The Cl-treated PSC exhibited better stability than the reference device, as its PCE maintained 88% after 700 h under continuous illumination[76].

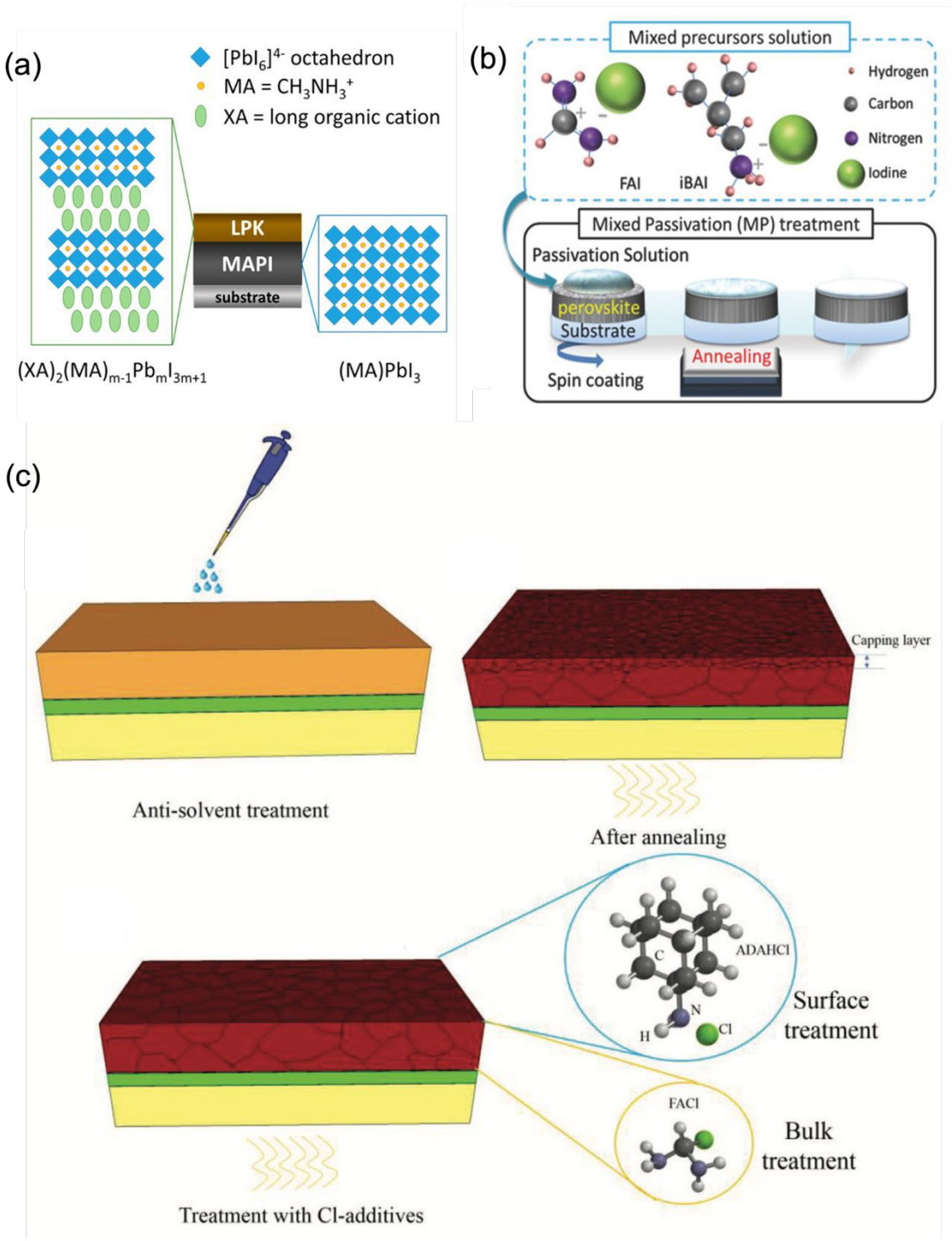

Figure 6. (a) Schematic presentation of the crystal structures of methylammonium lead iodide (MAPI) and a layered perovskite (LPK), forming the junction. Reproduced with permission.[57]

View Article Online
DOI: 10.1039/D6EL00019C

Copyright 2016 American Chemical Society. (b) Schematic presentation for the MP passivation treatment method with FAI and iBAI. Reproduced with permission.[75] Copyright 2018 WILEY-VCH Verlag GmbH & Co. KGaA, Weinheim. (c) Schematic presentation of perovskite films fabricated by the antisolvent method on SnO_2-coated FTO glass before and after treatment with ADAHCl and FACl. Reproduced with permission.[76] Copyright 2019 WILEY-VCH Verlag GmbH & Co. KGaA, Weinheim.

2.2 Defect passivation by Lewis acids and bases

Organic ions exhibited excellent defect passivation properties due to strong electrostatic interactions or ionic bonds with uncoordinated cations and anions within the perovskite crystal structure. Besides, Lewis acids and bases have also been reported to effectively passivate many defects in metal halide perovskite crystals. Lewis bases with strong electron-donating atoms, such as nitrogen and oxygen, can passivate the positively charged defects on the surfaces and grain boundaries (GBs) of perovskite layers. At the same time, Lewis acids can act as passivators of defects with lone-pair electrons, such as I^- ions and PbI_3^- antisite defects (**Figure 7**).

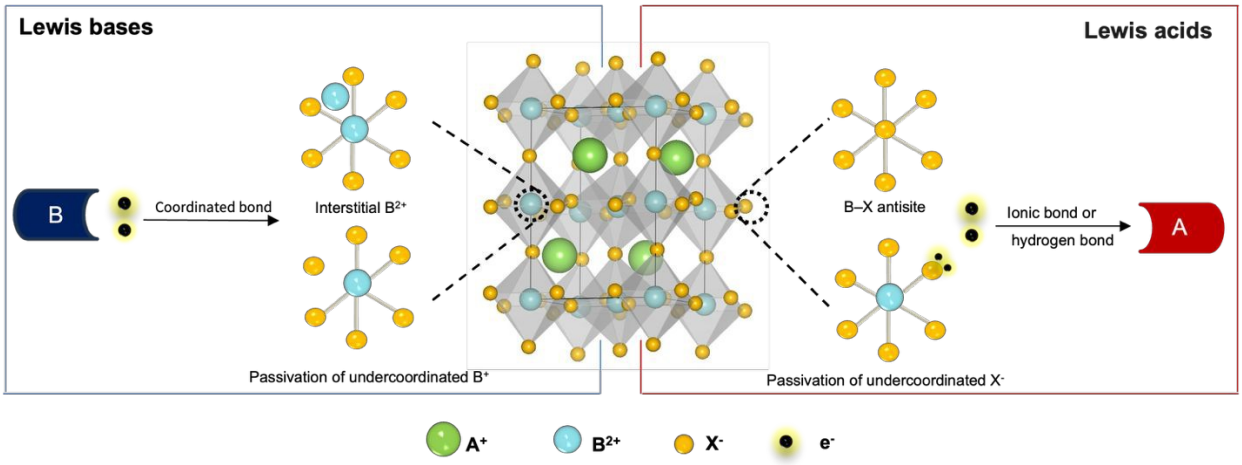

Figure 7. Schematic presentation for defect passivation by Lewis acids and bases

2.2.1 Nitrogen-based Lewis bases passivators

Amine-based passivating materials (APMs) are the most typical Lewis bases for defect healing in MHPs, mainly due to the strong coordination between nitrogen atoms and lead ions. For example, Lee et al. reported the treatment of $MAPbBr_3$ with ethylenediamine (EDA) to enhance the performance of perovskite light-emitting diodes[77]. The lone pairs of N atoms formed a strong

View Article Online
DOI: 10.1039/D6EL00019C

coordinate bonding with uncoordinated Pb atoms, thus passivating the defect sites in $MAPbBr_3$. After introducing EDA, the perovskite films exhibited enhanced PL intensities, longer PL lifetimes, and reduced PL blink, due to the inhibition of non-radiative charge-carrier recombination. Furthermore, improved surface passivation and enhanced interfacial coverage can mitigate ion accumulation at the perovskite/metal interface, thereby suppressing electrode corrosion. However, this treatment mainly improves interfacial stability rather than completely eliminating intrinsic bulk ion migration. The stability of APMs' devices was significantly improved, with almost no color change in the Ag electrode after 30 days of continuous operation (**Figure 8a**). XPS and XRD analyses further confirm that the interfacial passivation structure remains stable during long-term aging. The absence of AgBr-related signatures in the APM-treated samples after 30 days indicates that the passivated surface effectively suppresses halide migration from the perovskite layer to the metal electrode. This ongoing inhibition of ion transport suggests that the interfacial coordination environment established by the APMs is resistant to structural disruption under ambient conditions. As a result, highly efficient and stable PeLEDs were obtained, with the highest EQE of 6.2%[77]. Wang et al. selected phenylalkylamine, including aniline (A), benzylamine (BA), and phenethylamine (PA), as APMs for $FAPbI_3$ films[78]. The amino groups passivated the undercoordinated Pb site defects by coordinating with Pb ions or forming hydrogen bonds with I ions. Moreover, the benzene rings exhibited strong hydrophobicity and formed an ordered edge-on packing in benzylamine-modified $FAPbI_3$ films. Cooperative interactions between amino groups and surface ions, along with the ordered molecular packing of benzyl moieties, are expected to enhance the stability of the surface coordination structure by reducing molecular desorption, preventing surface rearrangement, and minimizing moisture-induced disruption during long-term aging. The perovskite films showed almost no degradation after more than 2900 h of air exposure under RH level of 50 ± 5 %, as presented in **Figure 8b**. BA-modified films showed significantly better moisture stability compared to PA-modified films, despite the fact that the two molecules differ by only one additional $–CH_2–$ group. This finding suggests that long-term stability is heavily influenced by the molecular configuration and structural integrity of the passivation layer rather than solely by the presence of amine functional groups. The electronic properties of MHPs were simultaneously enhanced, resulting in a significant increase in PCE to reach 19.2%[78]. Benzylamine (BA) was further employed to fabricate high thermal-photostability and photovoltaic performance PSCs[79]. After the treatment with BA

View Article Online
DOI: 10.1039/D6EL00019C

molecules, the defects on the perovskite film surface and GBs were effectively passivated, thereby inhibiting the phase transformation and perovskite decomposition. The BA-treated PSCs showed greatly enhanced thermal-photostability. The PL mapping image showed that the pristine film had already turned dark after 8 h of exposure under white LED illumination at 85 °C, whereas the BA-treated film showed only minor changes in its PL emission under the same conditions (**Figure 8c**). Owing to these advantages, the BA-treated solar cells exhibited high photovoltaic performance, with a champion efficiency of 17.1%.

Zheng et al. reported that a tertiary amine, hexamethylenetetramine ($(CH_2)_6N_4$, HMTA), had a positive effect on stabilizing perovskites[80]. HMTA can form a strong Pb–N bond, passivating grain boundary defects and preventing the formation of PbI_2 as a decomposition product. Simultaneously, HMTA treatment inhibited water adsorption at the surface and enhanced the water resistance of perovskite solar cells. The HMTA-perovskite showed a very weak PbI_2 peak in the XRD pattern after 10 days of air exposure, indicating much lower degradation (**Figure 8d**). Moreover, HMTA enhanced the binding between the perovskite layer and the ZnO ETL, thereby improving interfacial charge transport. As a result, the PCE of HMTA-treated PSCs increased significantly from 12.70% to 17.87%[80]. Kim et al. reported the introduction of melaminium iodide into a perovskite precursor solution. Besides the coordination of the $–NH_2$ group with PbI_2, the –C=N– group in the melamine ring interacted with FAI impurity via hydrogen bonding, thus healing the defects on the surface of perovskites and suppressing non-radiative recombination[81]. The photovoltaic performance of melamine-treated PSCs was significantly improved, yielding a PCE of 17.3%, compared to 15.9% for the pristine PSCs. The influence of melamine on the humidity stability of perovskite was also investigated by exposing it to 65% relative humidity (RH) in the dark. The pristine perovskite showed a significant decrease in PCE from 18% to 16.4% during a reverse scan after 96 h of testing. In contrast, the PCE of melaminium-treated perovskite experienced a much smaller loss, from 18.4% to 17.4% (**Figure 8e**). Moreover, the pristine perovskite exhibited significant surface morphological degradation after a 24 h aging test. In contrast, the melamine-modified perovskite exhibited minimal change in the morphology due to the rear-surface passivation and the low aqueous solubility of melamine (**Figure 8f-i**). A large hysteresis was observed in the pristine perovskite after 96 h, mainly due to increased trap states resulting from moisture intrusion. This issue was effectively addressed when the melaminium additive was incorporated into the perovskite surface[81].

View Article Online
DOI: 10.1039/D6EL00019C

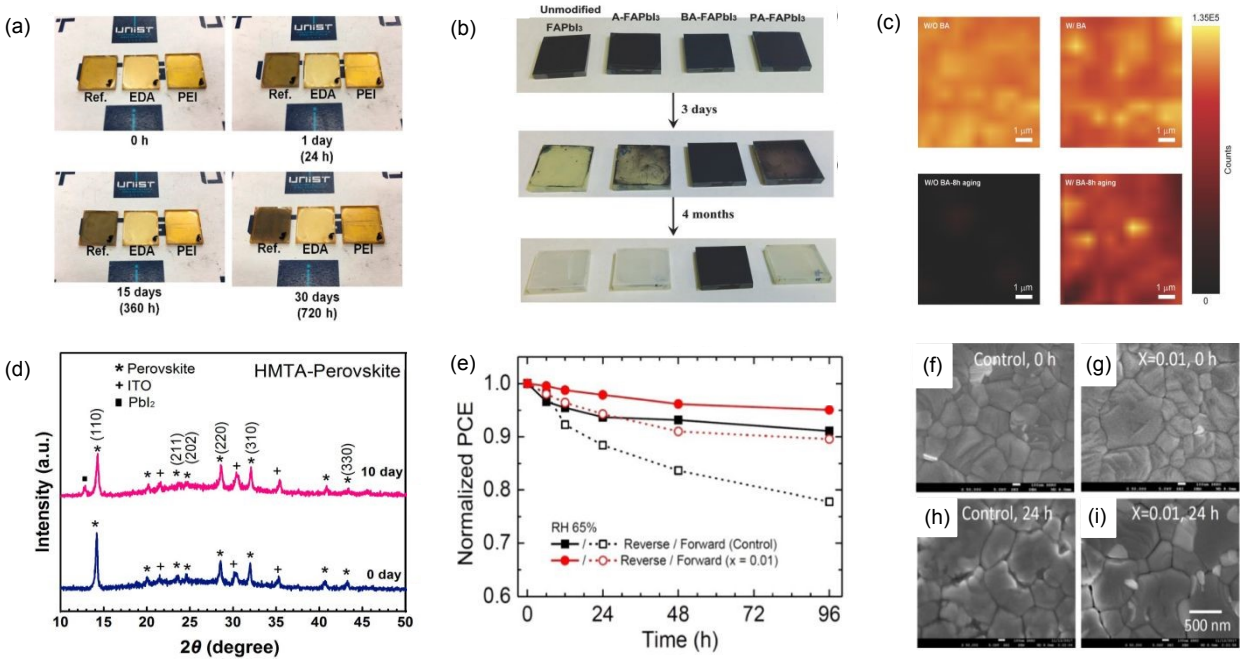

Figure 8. (a) Stability test of Ag electrode on $MAPbBr_3$ materials with and without APMs under ambient conditions over time. Reproduced with permission.[77] Copyright 2017 American Chemical Society. (b) Stability test of pristine $FAPbI_3$, A-$FAPbI_3$, BA-$FAPbI_3$, and PA-$FAPbI_3$ films under different durations (fresh, 3 days, and 4 months) of exposure under 50 ± 5 RH% air. Reproduced with permission.[78] Copyright 2016 WILEY-VCH Verlag GmbH & Co. KGaA, Weinheim. (c) PL mapping for pristine and BA-treated films aged 8 h under a white LED light source with an intensity of 200 mW cm^{-2} at 85 °C. Reproduced with permission.[79] Copyright 2017 WILEY-VCH Verlag GmbH & Co. KGaA, Weinheim. (d) XRD pattern HMTA-perovskites after exposure for 10 days under ambient air with a relative humidity of 55%. Reproduced with permission.[80] Copyright 2017 Elsevier B.V. (e) Normalized PCE of pristine and melaminium-treated perovskites over time under RH of 65% in the dark. Reproduced with permission.[81] Copyright 2018 American Chemical Society. (f-i) Scanning electron microscopy (SEM) images of the pristine perovskite (control) and melaminium-treated perovskite (x = 0.01) after 24 h under RH of 65% in the dark. Reproduced with permission.[81] Copyright 2018 American Chemical Society

2.2.2 Oxygen-based Lewis bases passivators

Oxygen-containing Lewis bases have been proven to exhibit passivation ability like nitrogen-containing Lewis bases. For instance, a bilateral interfacial passivation strategy by using

View Article Online
DOI: 10.1039/D6EL00019C

diphenylphosphine oxide-4-(triphenylsilyl)phenyl (TSPO1) as the passivator was proposed.[82] The TSPO1 molecules passivated both the top and bottom of the perovskite emitting layer via the interaction between uncoordinated Pb and the P=O functional group (**Figure 9a**). By doing so, interfacial nonradiative recombination was significantly suppressed, leading to enhanced PLQY. Consequently, the passivated PeLEDs reached a maximum EQE of 18.7% and the current efficiency of 75 cd A^{-1}. Moreover, the addition of TSPO1 also significantly improved the stability of PeLEDs. The PL emission intensity of bilateral-passivated perovskite films remained above 85% of the initial value after 10 h of continuous irradiation in ambient air with 40% RH. In contrast, pristine films lost 60% of the original efficiency after the same period. As a result, the operational lifetime of passivated PeLEDs was dramatically increased, which was 20 times longer than the control device, reaching 15.8 h.[82] The carbonyl group C=O has demonstrated great coordination with lead ions, prompting several studies on its utilization as a perovskite passivator. Wang et al. incorporated theophylline, caffeine, and theobromine into perovskite films and investigated their impact on defect passivation[83]. The results indicated that the –C=O group in the xanthine core of the theophylline molecule strongly interacted with the Pb antisite, while the neighboring N–H on the imidazole ring coordinated to PbI_6^- via a hydrogen bond, thus passivating the surface defects (**Figure 9b**). The PCE of theophylline-treated device was boosted to reach 23.48%. For caffeine, the hydrogen bond between the xanthine core and PbI_6^- was eliminated since a methyl group was linked to N on the imidazole ring. A weak interaction between caffeine and Pb_I defect was obtained, resulting in a decrease in PCE of the caffeine-treated device to 22.32%. When the N–H and C=O groups were located next to each other on the same six-membered ring to form theobromine, the interaction between N–H and I was disabled, leading to an even weaker interaction. The theobromine-treated device exhibited a significant decrease in PCE to 20.24%. The passivated devices also showed long-term stability, with their PCE remaining more than 90% of the initial value after storage at 40% RH for 500 h.[83] An organic dye (AQ310) was employed to passivate trap states at the surfaces and GBs of hybrid perovskite solar cells[84]. The passivation mechanism is due to the coordination of the –COOH group in AQ310 with uncoordinated Pb ions (**Figure 9c**). The trap states were thereby reduced, leading to higher stability. Eventually, the PSC with AQ310 passivator recorded the best power conversion efficiency of 19.43%, 1.5% higher than the original PSC.

View Article Online
DOI: 10.1039/D6EL00019C

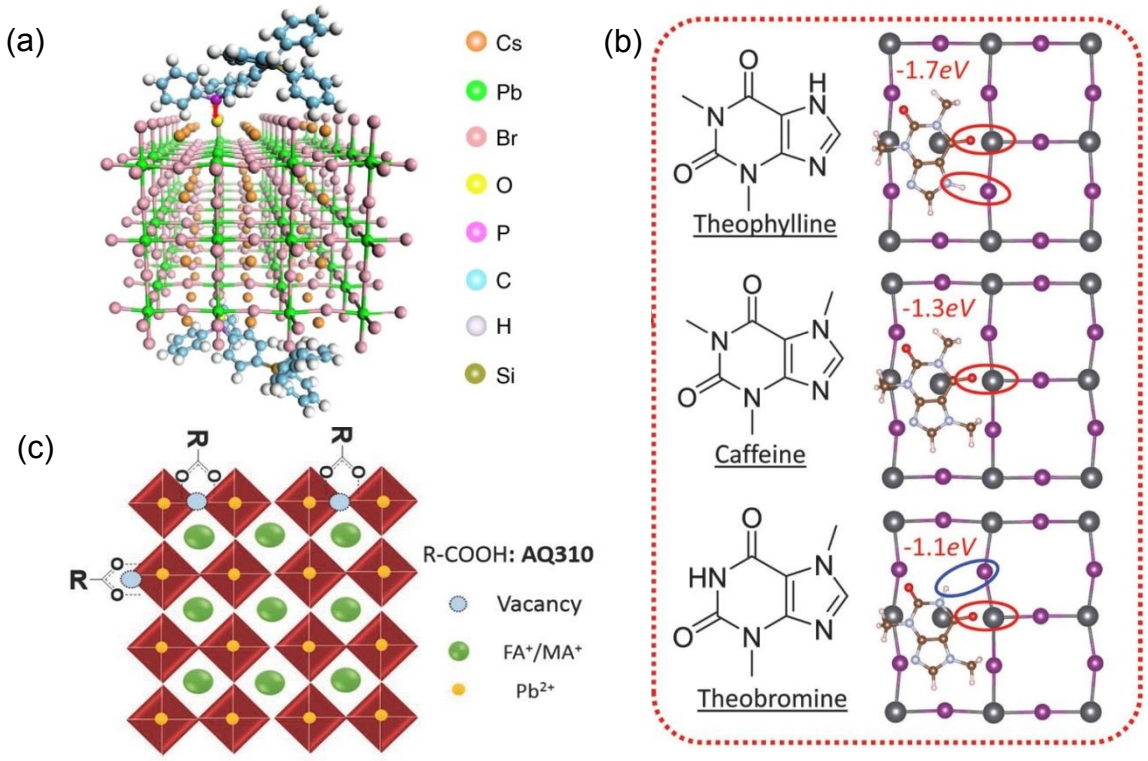

Figure 9. (a) Schematic presentation for defect passivation by TSPO1. Reproduced with permission.[82] Copyright The Author(s) 2020. (b) Schematic presentation for surface passivation by theophylline, caffeine, and theobromine. Reproduced with permission.[83] Copyright Science 2019. (c) Schematic presentation for passivation mechanism of AQ310. Reproduced with permission.[84] Copyright 2018 WILEY-VCH Verlag GmbH & Co. KGaA, Weinheim.

2.2.3 Sulphur-based Lewis bases passivators

Besides N-containing and O-containing Lewis bases, many S-containing bases were also investigated to have good passivation effects on perovskites[85]. For example, two thiophene isomers (named S2 and S3) were used to passivate the defects in PSCs through the strong interaction of S atoms with uncoordinated Pb^{2+} sites[86]. The coordination between the lone pair of S atoms and the Pb ion slowed down the crystallization process and prevented the migration of ions. The non-radiative recombination and trap density were significantly reduced, while the charge extraction ability improved. The thiophene-functionalized perovskites further showed excellent thermal stability with minimal decomposition observed at 289 °C. Moreover, the introduction of two

View Article Online
DOI: 10.1039/D6EL00019C

thiophene isomers improved perovskite's moisture stability, as much lower PbI_2 diffraction intensities were observed in XRD patterns after 14 days at 65 ± 0% RH. Consequently, the highest PCE of 18% was achieved for the S3-passivated device, which was 6.69 % higher than that of the reference device (**Figure 10a**).[86] The thiophene-based interlayers, including 3-phenolic acid (TA 1), thiophene-3-acetic acid (TA 2), and 3-thiophene propanoic acid (TA 3), were reported to increase the conductivity and decrease the work function of SnO_2 ETLs in perovskite solar cells[85]. The sulfur atoms in the thiophene ring can coordinate with the uncoordinated Pb^{2+} ion in $MAPbI_3$, thereby passivating ionic defects, reducing trap states, and reducing charge-carrier recombination at SnO_2/$MAPbI_3$ interfaces (**Figure 10b**). Meanwhile, the –COOH groups of the thiophene-based interlayers chemically anchor to the SnO_2 surface and passivate surface –OH dangling bonds, improving the electrical properties of the electron transport layer. In addition, treatment with thiophene-based interlayers improves perovskite crystallinity, resulting in larger grain size and lower defect density. The TA interlayer-modified PSCs also showed better thermal stability, retaining roughly 80% of the initial PCE after 130 h of thermal annealing at 85 °C. As a result, the TA 1, TA 2, and TA 3 interlayer-modified $MAPbI_3$ achieved PCE of 19.59%, 18.67%, and 20.61%, respectively, compared to 17.54% of the original one.[85] Apart from thiophene and its derivatives, another example of an S-containing passivator was p-mercaptobenzoic acid (HOOC-Ph-SH), which was introduced into the TiO_2/$MAPbI_3$ interface.[87] The carboxylic group of the passivator was coordinated with TiO_2, while the –SH group was combined with Pb on the perovskite absorber, facilitating the electron transfer from perovskite to TiO_2 and increasing the photovoltaic performance of PSCs (**Figure 10c**). Moreover, the perovskite surface was modified with the highly hydrophobic pentafluorobenzenethiol (HS-PhF_5). HS-PhF_5 covered the perovskite surface via the coordination of Pb-S, inhibiting the escape of MA ion and the penetration of water into the perovskite absorber (**Figure 10c**). The HS-PhF_5 modified device thereby showed enhanced water resistance, with no significant color change after 8 days and remaining at almost 80% of its initial performance after 10 days of storage in ambient conditions with a relative humidity of 45%. Finally, the highest PCE of 14.1% was achieved for the modified PSCs[87].

Recently, Xu et al. introduced a very interesting strategy to improve photocatalytic hydrogen evolution using metal halide perovskites. In particular, MHPs were bi-functionalized with PbS and amorphous molybdenum sulfide (MoS_x) as co-catalysts.[88] The uncoordinated Pb^{2+} defects on the surface of MHPs were effectively passivated by PbS, thanks to the strong chemical interaction

View Article Online
DOI: 10.1039/D6EL00019C

between Pb^{2+} and S^{2-} and thus increased charge transfer efficiency. Meanwhile, MoS_x can significantly promote the hydrogen evolution yield due to its high catalytic activity (**Figure 10d**). Consequently, a maximum solar-to-chemical conversion efficiency of *ca.* 4.63% was achieved on the bi-functionalized $FAPbBr_{3-x}I_x$. Taking advantage of a strong Pb–S bond, Meng et al. demonstrated a passivation method by growing $CsPbBr_3$ quantum dots into a thiol-functionalized covalent-organic framework (COF-SH)[89]. The strong interaction between the Pb atom in the perovskites and the S atom in COF-SH significantly reduced crystal defects and also prevented ion migration. Therefore, the $CsPbBr_3$@COF-SH composite showed much better thermal and air stability, as well as higher PLQY compared to those of pristine $CsPbBr_3$. Moreover, $CsPbBr_3$@COF-SH was further used in photocatalytic systems with eosin Y (EY) and rose bengal (RB). The results indicate that ESY-$CsPbBr_3$@COF-SH and RB-$CsPbBr_2I$@COF-SH systems showed better performances in photocatalytic C–H selection and cross-coupling/annulation reactions, respectively, compared to ESY or RB alone.

View Article Online
DOI: 10.1039/D6EL00019C

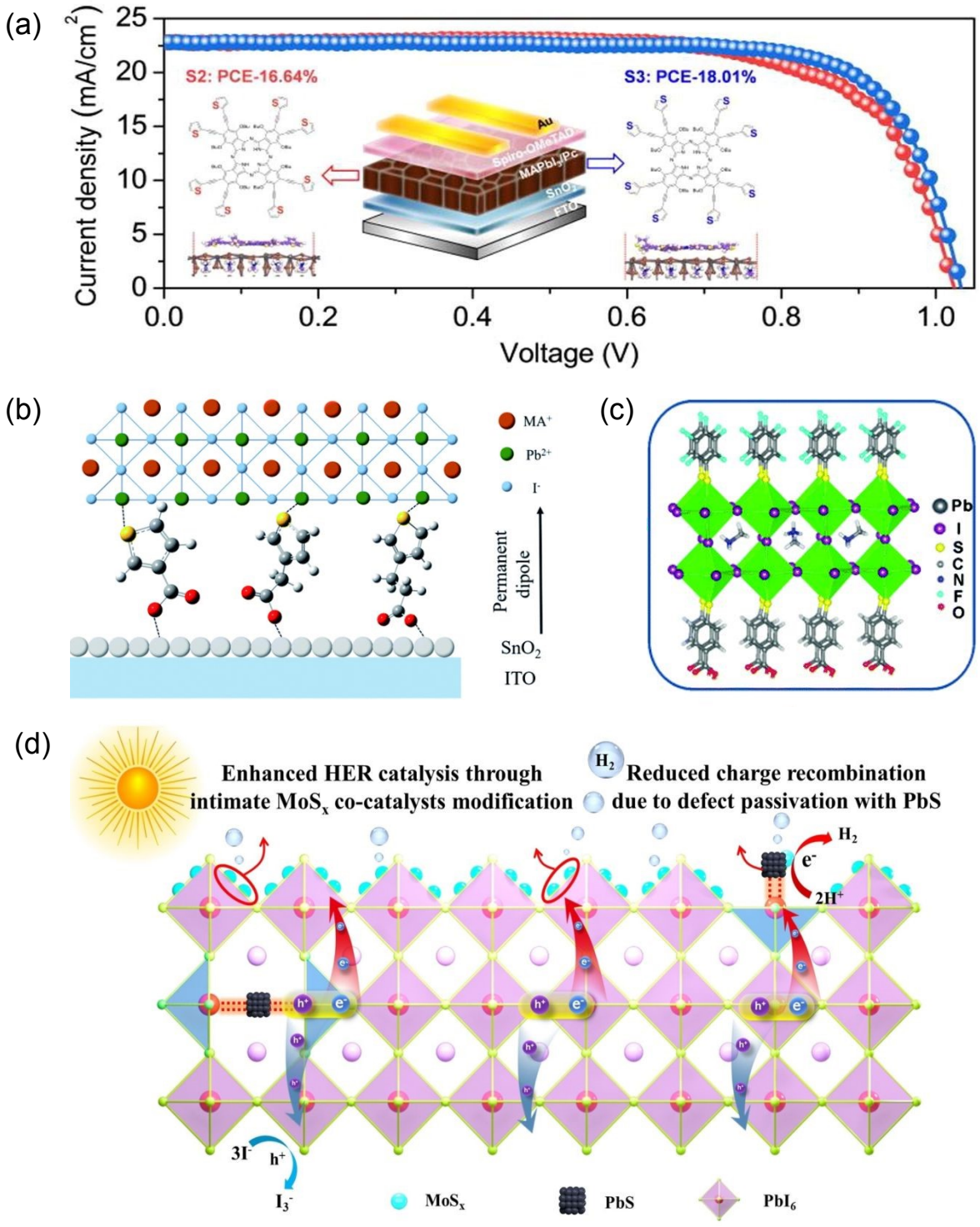

Figure 10. (a) Molecular structure of two isomers used for passivation for perovskite solar cells and their maximum power conversion efficiency. Reproduced with permission.[86] Copyright 2021 Science Press and Dalian Institute of Chemical Physics, Chinese Academy of Sciences. (b) Schematic presentation for defect passivation by 3-thenoic acid (TA 1), thiophene-3-acetic acid

View Article Online
DOI: 10.1039/D6EL00019C

(TA 2), and 3-thiophenepropanoic acid (TA 3). Reproduced with permission.[85] Copyright 2021 The Royal Society of Chemistry. (c) Schematic presentation for defect passivation by p-mercaptobenzoic acid and pentafluorobenzenethiol. Reproduced with permission.[87] Copyright 2015 The Royal Society of Chemistry. (d) Schematic presentation for photocatalytic hydrogen evolution on bi-functionalized MHPs. Reproduced with permission.[88] Copyright 2024 Wiley-VCH GmbH.

2.2.4 Polymer passivators

Polymer is another typical example of an effective passivator for MHPs' defects. Additionally, due to their long alkyl chains, the polymer passivators exhibit strong hydrophobicity and thus enhance the water resistance of perovskites. For example, Li et al. reported the introduction of an interfacial polystyrene (PS) layer between the perovskite film and spiro-OMeTAD layer[90]. The presence of the PS layer passivated the interface traps and defects. As a result, the PL intensity and carrier lifetime were significantly increased due to suppressed nonradiative recombination. In addition to defect passivation, the hydrophobic polymer chains form a protective interfacial barrier that limits moisture penetration and helps preserve the interfacial passivation structure during environmental exposure. The efficiency of PSCs incorporated polystyrene reached 20.46%. The passivated device retained almost 85% of its initial PCE after 60 days of storage under open-air conditions, which is 20% higher than the control device[90] (**Figure 11a**). Contact angle measurements indicated that PS-modified perovskite films had higher water contact angles (approximately 92.5°) compared to pristine films (around 75.1°). Additionally, the PS-modified films exhibited a smaller reduction in contact angle over time, suggesting that the hydrophobic interfacial layer remained effective despite environmental exposure. Furthermore, after 2 months of storage, the PS-modified devices retained their black, opaque appearance, whereas the pristine devices showed significant signs of decomposition.

Similar to polystyrene, polyethylene oxide (PEO) can be inserted into the perovskite absorption layer and the charge extraction layer to passivate anion vacancies via the coordination of the C–O group with Pb ions[91] (**Figure 11b**). In addition, PEO can absorb water molecules, thereby hindering water penetration into the perovskite layer and significantly improving the moisture stability of PSCs (Figure 11b). The PEO-treated device thereby retained 80% of its initial performance after 120 h of exposure to 88% humidity, while the untreated device showed

View Article Online
DOI: 10.1039/D6EL00019C

continuous degradation of PCE from 15% to 1%. For the application of efficient perovskite LEDs, Feng et al. demonstrated an infiltrative treatment method for perovskites using poly(vinylidene fluoride) (PVDF), in which the polymer chains were added into the perovskite films before crystallization[92] (**Figure 11c**). The Fluorine atoms in PVDF can interact with MA^+/FA^+ and Pb^{2+} ions via hydrogen and ionic bonds, passivating defects on the surfaces and along GBs of perovskites. As a result, high-quality perovskite films were obtained, and the corresponding PeLEDs achieved an EQE of 22.29%, nearly 7.5% higher than that of the control device. The operating stability of PeLED devices was then measured, and the half-times of polymer-treated devices were nearly 7 times higher than those of the control device, indicating that PVDF significantly improved the stability of perovskite LEDs[92]. Therefore, it can be inferred that the polymer-assisted passivation method was efficient for increasing the efficiency and stability of PeLEDs, and various polymer passivators were employed for this strategy, such as poly(methyl methacrylate) (PMMA)[93], poly(vinylpyrrolidone) (PVP)[94], and polyethylene glycol (PEG)[95].

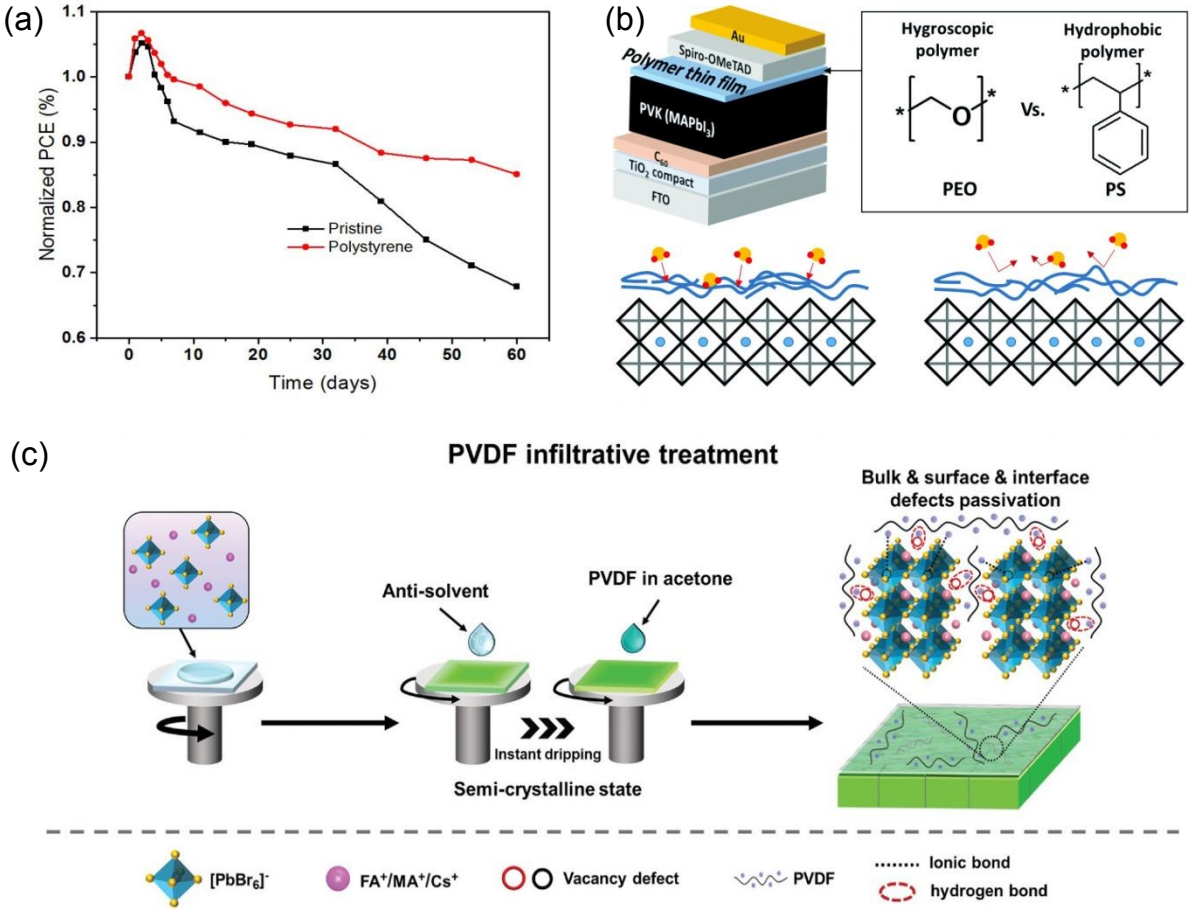

View Article Online
DOI: 10.1039/D6EL00019C

Figure 11. (a) Normalized PCE of pristine and polystyrene-treated device after stability test in ambient air. Reproduced with permission.[90] Copyright 2018 American Chemical Society. (b) Schematic presentation for the perovskite solar cell devices with PEO and PS as the interfacial layers. Reproduced with permission.[91] Copyright 2018 The Royal Society of Chemistry. (c) Infiltrative treatment process of perovskites with poly(vinylidene fluoride) (PVDF). Reproduced with permission.[92] Copyright 2022 Wiley-VCH GmbH.

2.2.5 π-conjugated bases passivators

π-conjugated molecules are a class of molecules characterized by variable carbon hybridization, enabling the unrestricted movement of π-electrons within the system.[96] This feature enhanced the stability and electrical conductivity of π-conjugated molecules and their adducts[96]. Moreover, π-conjugated molecules can coordinate with lead atoms in perovskite via electron donors. Therefore, some π-conjugated materials can act as Lewis base passivators for perovskite, for example, indacenodithiophene end-capped with 1,1-dicyanomethylene-3-indanone (IDIC)[97], and with 4-bromo-7-dicyanovinyl-2,1,3-benzothiadiazole (SM2)[98]. IDIC was introduced as an interlayer between the perovskite and the cathode. **Figure 12a** showed that the O atom in the carbonyl group, the N atom in the cyano group, and the S atom in the thiophene group of IDIC could effectively passivate the Lewis acid traps (e.g., uncoordinated Pb^{2+} and Pb clusters) on the surface and at GBs of $MAPbI_3$ via formation of Lewis adducts. IDIC can promote electron extraction and transport from the perovskite layer due to its n-type semiconducting property. As a result, the $MAPbI_3$/IDIC-based solar cells achieved a high PCE of 19.5%, whereas the control device without IDIC achieved only 13.5%. Moreover, the introduction of IDIC enhanced the stability of PSCs when stored under a dry inert atmosphere, maintaining almost 90% of the initial PCE, which is better than the nearly 80% observed for devices without an IDIC layer[97]. On the other hand, SM2 molecules can be added to the perovskite precursor (**Figure 12b**) and then passivate surface and GB defects via strong coordination of two cyano groups to uncoordinated Pb^{2+}. It could also increase the charge separation and transport at the perovskite interface due to an appropriate alignment in the energy of its LUMO with the conduction band minimum (CBM) of perovskite[98]. Thanks to these benefits, the PSCs treated with SM2 molecules achieved a high PCE of 21.2%.

Moreover, the hydrophobic nature of SM2 can retard the penetration of water molecules into the perovskite layer. Combined with defect passivation via Lewis acid-base interactions, this

View Article Online
DOI: 10.1039/D6EL00019C

contributes to improved moisture stability of the perovskite solar cells. The SM2-treated device retained almost 80% of its initial PCE after 2000 h of storage at 25% RH, whereas the control device showed a significant loss, dropping to 61%.[98] The defect passivation at GBs by SM2 can also enhance the thermal stability of perovskite since the grain boundaries can serve as channels for the rapid diffusion of atoms and ions, and they are vulnerable to thermal stress. While the control device degraded to 52% of its initial PCE after heating for 60 h at 80 °C, the one treated with SM2 remained at 71% of the original PCE[98].

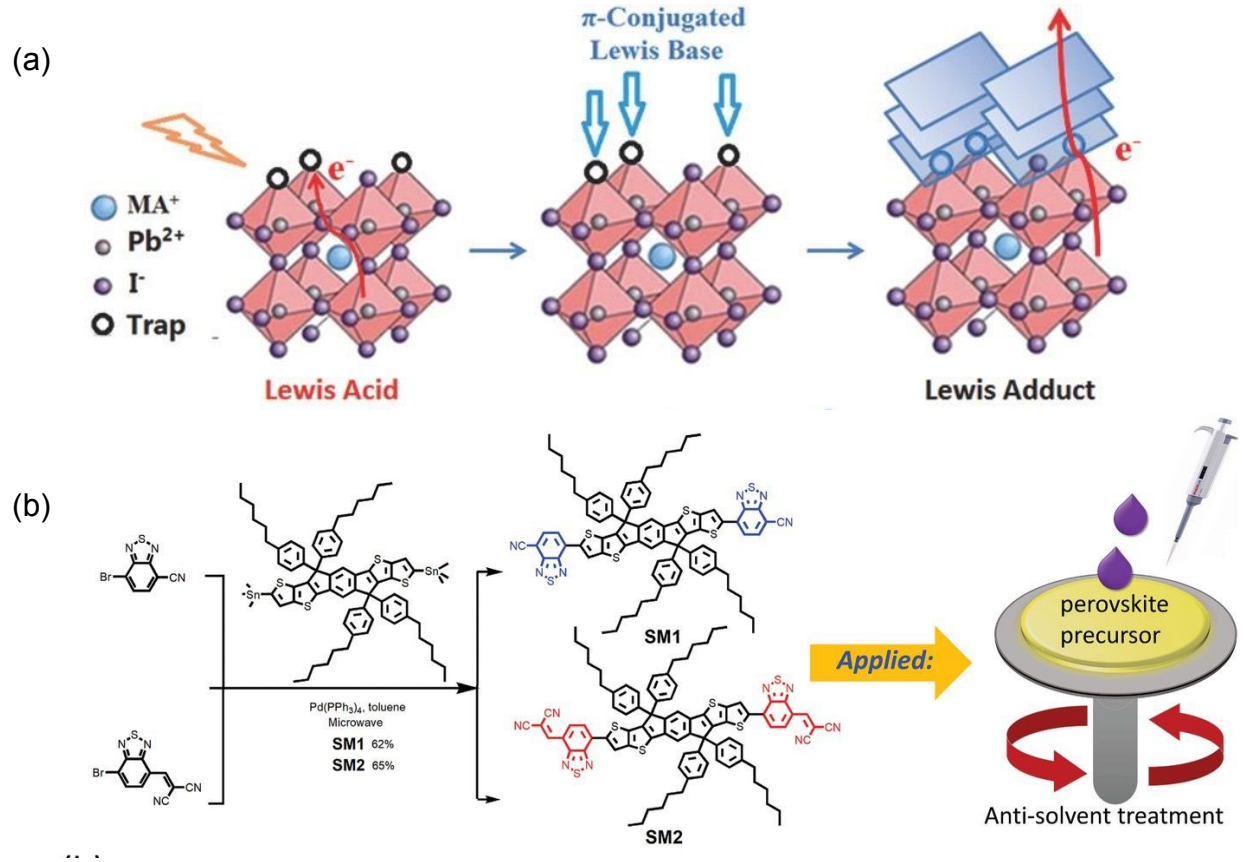

Figure 12. (a) Schematic presentation for defect passivation in perovskites by forming Lewis adducts with IDIC. Reproduced with permission.[97] Copyright 2016 WILEY-VCH Verlag GmbH & Co. KGaA, Weinheim. (b) Synthesis of SM2 and treatment of perovskite with SM2 to passivate defects. Reproduced with permission.[98] Copyright 2020 WILEY-VCH Verlag GmbH & Co. KGaA, Weinheim.

View Article Online
DOI: 10.1039/D6EL00019C

2.2.6 Other Lewis bases passivators

Beyond conventional Lewis bases passivators, graphene oxide (GO), oligomeric silica (OS), and graphitic carbon nitride (gC_3N_4) have also been identified as promising Lewis-base passivators for improving the structural and optical stability of metal halide perovskites.

The encapsulation of graphene oxide can not only mitigate surface defects but also improve the stability of MHPs by forming a protective shell, thereby enhancing their optical performance.[99] For example, the treatment of $CsPbBr_3$ with GO slightly increased the photocatalytic activity of MHPs in CO_2 reduction, with the CO and CH_4 generation yield of 58.8 and 29.6 μmol g^{-1}, respectively, while the amounts of CO and CH_4 for reaction using pristine $CsPbBr_3$ were 49.5 and 22.9 μmol g^{-1}, respectively (**Figure 13a**).[100]

Bai et al. demonstrated a facile strategy to wrap perovskite grains with an oligomeric silica (OS) matrix, forming a core-shell structure[101]. The $-OCH_2CH_3$ group in the OS layer can simultaneously passivate the defects at the surface and GBs of perovskites via a coordination bond of an oxygen atom with an uncoordinated Pb^{2+} ion (**Figure 13b**). As a result, the trap density was significantly reduced, and the charge-carrier recombination lifetime was prolonged, thereby enhancing the PCE of $MAPbI_3$ PCs to 21.1%. Furthermore, the OS shell could serve as a physical barrier to prevent the penetration of external moisture and atmospheric gases. It might also inhibit internal ion migration and decomposition by blocking degradation pathways from internal and external sources in perovskite films. As a result, the moisture and operational stabilities of corresponding PSCs were dramatically improved. There was no impurity peak observed in the XRD pattern of $MAPbI_3$@OS film after 60 days of exposure to the air, while the pattern of the pristine $MAPbI_3$ film showed the impurity peak for PbI_2 after exposure to air for 10 days. Moreover, the performance of the $MAPbI_3$ film drops rapidly due to degradation, whereas the MAPbI3@OS film maintained almost 90% of its initial PCE after 1200h.

View Article Online
DOI: 10.1039/D6EL00019C

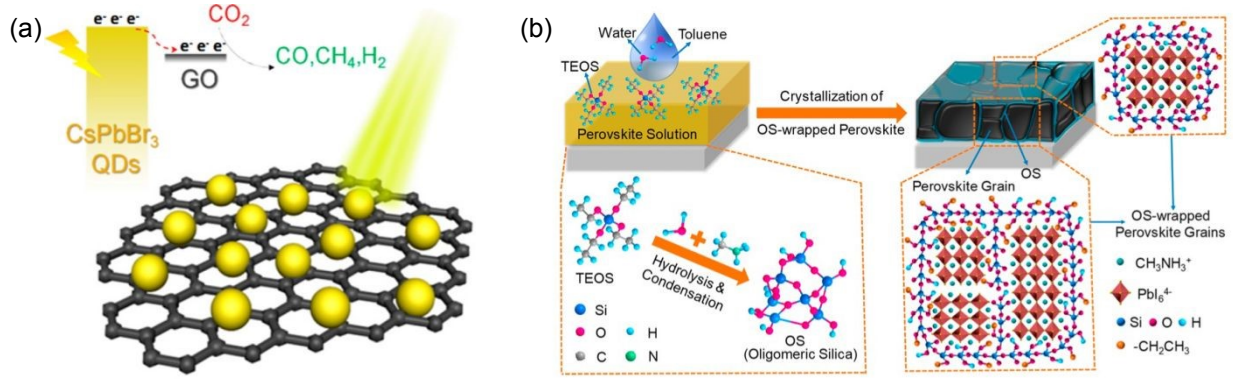

Figure 13. (a) Schematic for photocatalytic CO_2 reduction by $CsPbBr_3$/GO quantum dots. Reproduced with permission.[100] Copyright 2017 American Chemical Society. (b) Schematic presentation for forming an OS-wrapped perovskite thin film and the hypothesized perovskite-OS nanostructures. Reproduced with permission.[101] Copyright 2019 American Chemical Society.

Graphitic carbon nitride (gC_3N_4, GCN), which shares structural similarities with graphene, can also be used to passivate intrinsic defects and grain boundaries in perovskites. The $Cs_2AgBiBr_6$-GCN composites showed a reduced trap density due to defect passivation by GCN, resulting in a better photocurrent response compared to that of pristine $Cs_2AgBiBr_6$[102]. In addition, GCN can serve as a supporting matrix and reduce the hydrophilicity of $Cs_2AgBiBr_6$, thereby increasing the moisture stability of the perovskites. In terms of photocatalysis, GCN already displayed high photoactivity[102], $Cs_2AgBiBr_6$-GCN composites exhibited 3 times and nearly 10 times higher in CO and CH_4 production, respectively, compared to pure $Cs_2AgBiBr_6$ in photocatalytic CO_2 reduction.

2.2.7 Fullerenes-based Lewis acid passivators

Fullerenes (C_{60}) and their derivatives are renowned for their high electron affinity and transport capability, which come from their distinctive spherical shape. They have been widely used as electron-transport layers and trap passivators in the design of perovskite solar cells.[103] Phenyl-C61-butyric acid methyl ester (PCBM) is the most representative fullerene derivative as a Lewis acid passivator. Huang et al. discovered that the deposition of PCBM onto the $MAPbI_3$ layer leads to a significant reduction in perovskite film trap-states by two orders of magnitude, accompanied by the suppression of photocurrent hysteresis (**Figure 14a**). [104] The PCE of the PSC device with

View Article Online
DOI: 10.1039/D6EL00019C

PCBM layer increased by more than 200% to reach 14.9%. They also found that the high trap concentration can be attributed to the low thermal stability of perovskite materials, which decompose at the surface, and that eliminating photocurrent hysteresis can increase the stability of these devices. Niu et al. employed PCBM to passivate Pb-I antisite defects via the formation of a PCBM-halide radical.[105] The device with a $MAPbI_3$ film passivated with PCBM showed a maximum PCE of 18.41%, compared to 17.34% for the original device. The long-term stability of this perovskite film was also examined by exposure to ambient conditions (RH 50%) for 60 days without encapsulation. The perovskite film treated with PCBM remained unchanged, while the control film faded from black to yellow. Moreover, the PCBM passivated device retained 76% of its initial PCE after 40 days in the dark room, whereas the control device's PCE dropped to 64%. The passivated device also showed significant enhancement in thermal stability, with PCE remaining at almost 85% of the original value after heating at 80 oC for 24 h, compared to 55% for the control. This improvement in stability can be attributed to the combined effects of defect passivation at grain boundaries, strong molecular interactions with MAPbI3, and the enhanced hydrophobicity of the passivated film (**Figure 14b**).[105] In 2017, Zhang and co-workers prepared the α-bis-PCBM-containing perovskite film, which exhibited a higher crystal quality and lower defect concentration.[106] The α-bis-PCBM network could passivate voids or pinholes that may form in the bulk active layer, thereby increasing the electron extraction efficiency of PSCs. The stability tests also showed that the α-bis-PCBM-containing perovskite-based device exhibited significant stability improvements, retaining 90.1% of its original PCE after 44 days under ambient conditions at 40% RH. On the other hand, under the same conditions, the PCE of the pristine control device and the PCBM-containing perovskite-based device decreased to 45.4% and 72.6% of their original values, respectively (**Figure 14c**). The enhanced stability was further confirmed under additional stress conditions. The device showed minimal degradation of less than 10% after 44 days at 65 °C. Additionally, there was only a 4% drop in efficiency after 600 hours of continuous full-sun illumination with maximum power point tracking. This suggests that the passivation network derived from α-bis-PCBM remains stable even under prolonged environmental and operational stresses. By maintaining a compact microstructure with fewer pinholes and less prominent grain boundaries, the α-bis-PCBM network effectively provides interfacial protection. Moreover, the α-bis-PCBM-containing perovskite-based device showed higher thermal resistance at 85 °C than the other two corresponding devices. As a result, an excellent PCE of 20.8% for the α-bis-PCBM-

View Article Online
DOI: 10.1039/D6EL00019C

containing device was obtained, compared to 19.9% for PCBM and 18.8% for the control device (**Figure 14d**). Following that, in 2018, bis-PCBM mixed isomers, acting as Lewis acids, were added to the antisolvent, and N-(4-bromophenyl)thiourea (BrPh-ThR), acting as a Lewis base, was added to the perovskite precursor solution (**Figure 14e**). Bis-PCBM can passivate the negatively charged defects by accepting an electron from PbI_3^- or uncoordinated halide ions, while BrPh-ThR can simultaneously passivate positively charged defects by binding with uncoordinated Pb^{2+} ions[107]. The synergistic effect of a Lewis base and a Lewis acid not only passivated the defects but also improved the perovskite grain size and increased charge-carrier separation and transport. As a result, the PCE of the corresponding perovskite solar cell device was improved to achieve 21.7%. Moreover, introducing this Lewis acid and base increased the hydrophobicity of the perovskite film and improved its structural and interfacial properties, thereby enhancing moisture stability. After 30 days of exposure to an ambient environment of 45% relative humidity, the color of the perovskite film incorporated with bis-PCBM and BrPh-ThR remained persistent, whereas the control perovskite film almost faded to yellow. Cheng et al. employed the same strategy to simultaneously passivate positive and negative defects at the surface through the self-assembly of 4,4′-bipyridine (4,4′-BiPy) and 2,2′-bipyridine (2,2′-BiPy) as Lewis bases from PCBM (a Lewis acid) onto the perovskite layer[108]. By using 4,4′-BiPy, the trap density was reduced after the passivation, and the electron transport ability was also enhanced (**Figure 14f**). Therefore, the $CsPbI_2Br$-based devices treated with PCBM:4,4′-BiPy showed greatly enhanced performance, increasing PCE from 10.74% to 12.09%. Compared to 4,4′-BiPy, the ligand 2,2′-BiPy can also passivate trap states, but it may cause phase transformation in perovskites; the PCE of devices treated with PCBM:2,2′-BiPy was lower.[108] Furthermore, the introduction of 4,4′-BiPy can improve the thermal stability of PSCs, showing that the all-inorganic PSCs device containing 4,4′-BiPy retained 76% of its initial PCE after being heated for 52 h in air. In contrast, the all-inorganic PSC reference device retained only 51% of its original PCE after 41 h of heating.[108] Another derivative of fullerene, Lewis-acid-featured fullerene skeleton after iodide ionization (PCBB-3N-3I, the structure was shown in **Figure 14g**, was reported to effectively passivate the positively charged surface defects of perovskites via the electrostatic interaction with iodide ions, resulting in an enhancement in PCE from 17.7% to 21.1%[109]. Furthermore, the reduction in surface defects also improved the ambient stability of the device treated with PCBB-3N-3I, which remained at 87% of its initial PCE after 150 h stored under ambient conditions with RH of 40-50%. On the

View Article Online
DOI: 10.1039/D6EL00019C

other hand, the device treated with PCBB-3N (the fullerene before iodide ionization, the structure was shown in **Figure 14g** displayed lower stability and smaller PCE value because PCBB-3N exhibited less efficient defect passivation than PCBB-3N-3I[109].

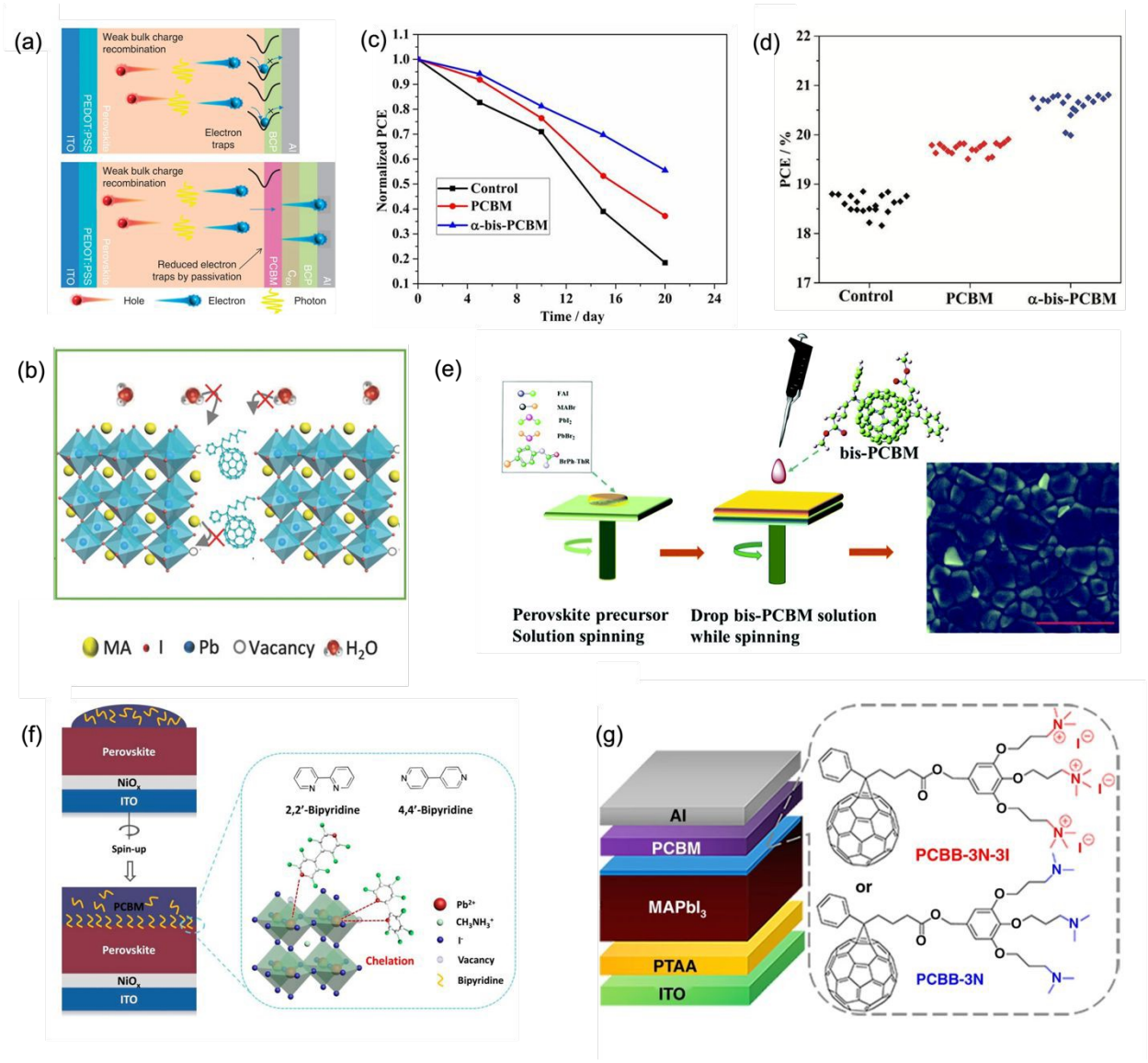

Figure 14. (a) Schematic presentation for electron trap passivation by PCBM. Reproduced with permission.[104] Copyright 2014 Nature. (b) The prevention of MA loss and moisture attacks induced by PCBM. Reproduced with permission.[105] Copyright 2018 WILEY-VCH Verlag GmbH & Co. KGaA, Weinheim. (c) The PCE stability of the pristine, PCBM- and α-bis-PCBM perovskite solar cells in an ambient environment with 40% relative humidity. Reproduced with permission.[106] Copyright 2017 WILEY-VCH Verlag GmbH & Co. KGaA, Weinheim. (d) Maximum power

View Article Online
DOI: 10.1039/D6EL00019C

conversion efficiency of the pristine, PCBM- and α-bis-PCBM perovskite solar cells devices. Reproduced with permission.[106] Copyright 2017 WILEY-VCH Verlag GmbH & Co. KGaA, Weinheim. (e) Schematic presentation of the antisolvent process to incorporate bis-PCBM to perovskites. Reproduced with permission.[107] Copyright 2018 The Royal Society of Chemistry. (f) Schematic presentation for defect passivation by 4,4′-BiPy and 2,2′-BiPy. Reproduced with permission.[108] Copyright 2019 International Solar Energy Society. (g) Structure of PCBB-3N and PCBB-3N-3I. Reproduced with permission.[109] Copyright 2019 The Author(s).

2.2.8 Fluorine-containing Lewis acid passivators

Due to their unique passivation mechanisms, many aromatic compounds containing fluorine atoms have gained considerable interest as Lewis acid passivators for perovskites. The strongly electronegative F-atoms can inductively withdraw electrons, making another atom in the molecule partially positively charged. This partially positively charged atom can passivate uncoordinated halogen ions and PbI_3^- antisite defects by accepting an electron from them. For example, Yang et al. designed a tris(pentafluorophenyl) phosphine (TPFP) agent as a surface passivator for perovskite solar cells[110]. Due to the strong electron-withdrawing effect of 15 electronegative F atoms, the central phosphorus atom was positively charged, which can be used to heal halide defects at the surface (**Figure 15a**). The positively charged phosphorus center can interact strongly with surface sites that lack halides, while the fluorinated aromatic groups create a highly hydrophobic interfacial environment. As a result, the recombination rate and phase segregation were reduced, leading to a significant enhancement in PCE to 22%. Moreover, the TPFP-treated perovskite solar cell device showed greater moisture resistance, retaining 63% of its initial PCE after 336 h at 75% RH, compared to just 21% for the control device. The slower optical and electrical degradation observed in the TPFP-treated films indicates that the passivation layer is sufficient to effectively suppress the formation of ion-migration pathways assisted by halide vacancies, even under humid conditions. This structural stability of the passivated surface is crucial, as moisture-induced degradation in mixed-halide perovskites is closely linked to the migration of halide and Cs ions, which can lead to irreversible phase segregation. Stronger hydrophobicity and defect passivation effect are responsible for the slower degradation rate of the TPFP-treated device. Abate et al. prepared a Lewis passivator, iodopentafluorobenzene (IPFB), to encapsulate the perovskite crystal (**Figure 15b**)[111]. In this molecule, F atoms with strong

View Article Online
DOI: 10.1039/D6EL00019C

electronegativity can withdraw the electron from the aromatic ring due to inductive effects, leading to a decrease in the electron density of the iodine atom bonded to the ring. The iodine atom carries a partial positive charge, enabling it to engage in halogen bonding with electron-rich species such as halide anions (X^-), forming a directional –C–I···X^- interaction. As a result, the uncoordinated halogen ions and Pb-X antisite defects were passivated, leading to slower recombination. Consequently, the IPFB-treated solar cells showed an increase in power conversion efficiency from 13% to more than 15.7%, and the efficiency stabilized at over 15% under a fixed 0.81 V forward bias. Another Lewis acid, 2,3,5,6-tetrafluoro-7,7,8,8-tetracyanoquinodimethane (F4TCNQ), exhibits the same passivation mechanism as IPFB molecules, in which the passivation group carries a partial positive charge due to the inductive electron-withdrawing effect of the F atoms. F4TCNQ was introduced as a dual-function interfacial layer that passivated the surface defects and was doped in the perovskite (**Figure 15c**). As a result, the F4TCNQ-modified PSCs exhibited an excellent efficiency of 18.1% and improved long-term stability without encapsulation, retaining 60% of their initial PCE after 1000 h of storage in ambient atmosphere.[112]

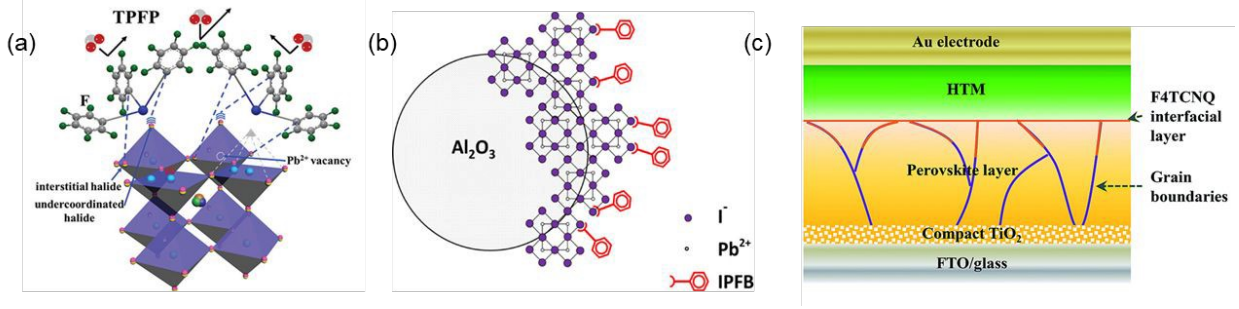

Figure 15. (a) Schematic presentation of TPFP-induced passivation and prevention of water contact. Reproduced with permission.[110] Copyright 2020 WILEY-VCH Verlag GmbH & Co. KGaA, Weinheim. (b) Schematic presentation for the binding of IPFB to supramolecular perovskites. Reproduced with permission.[111] Copyright 2014 American Chemical Society. (c) Schematic presentation of a perovskite solar cell with F4TCNQ as an interfacial layer. Reproduced with permission.[112] Copyright 2016 The Royal Society of Chemistry.

3. Passivation of metal halide perovskite using metal cations

Metal cations with different valence states (monovalent, divalent, and trivalent) have been incorporated into perovskite systems to modulate defect chemistry and electronic properties. Depending on their oxidation state, ionic radius, and chemical environment, these cations may

View Article Online
DOI: 10.1039/D6EL00019C

induce defect passivation, substitutional doping, alloying, or secondary-phase formation[113–116]. In the following sections, we discuss their roles according to valence classification.

3.1. Passivation by monovalent cations:

Many alkali metal ions have been studied for passivating the defects in perovskites. For instance, Na-passivated $CsPbBr_3$ nanocrystals can be synthesized by the ligand-assisted reprecipitation (LARP) method, in which NaBr and a precursor perovskite solution were mixed[117]. Bromide anions can passivate the vacancies in perovskites, while Na^+ cations prevent the immigration of bromide ions from the surface of NCs by binding with them. As a result, the non-radiative recombination pathways were eliminated, and the passivated $CsPbBr_3$ NCs exhibited enhanced optical performance, achieving a PLQY of 66%. Furthermore, introducing Na^+ improved the thermal and water stability of perovskite NCs. The PL intensity of passivated NCs retained 80% of the initial value after storing in water for 11 h, while the pristine NCs maintained only 20% of the original intensity (**Figure 16a**). Na^+ ions were reported to have a similar size to the MA^+ organic cation in perovskite structures[118]. Therefore, Na^+ can be easily introduced into the A-site vacancy of perovskite via doping to passivate the negatively charged defects, such as uncoordinated halogen ions. Zhang et al. successfully prepared perovskite solar cell devices with significant improvements in both efficiency and stability via surface modification with sodium p-toluenesulfonate (STS)[119]. The Na^+ cation and sulfonate anion of STS can passivate the surface of perovskite by interacting with uncoordinated Pb^{2+} and I^-/Br^- ions, respectively. Consequently, the PCE of the STS-treated device increased to 20.05% compared to 18.7% of the non-passivated device (**Figure 16b**). Moreover, the impact of STS passivation on the stability of the PSC device was investigated. The results revealed that the STS-treated device showed greater stability, with only 21% degradation in PCE after 950 h of exposure to an RH of 40-70%, compared to nearly 53% for the control device under the same conditions. This enhanced stability can be attributed to the hydrophobicity of the toluene group, which prevented the attacks of water and oxygen gas on the surface of perovskites.

The same surface passivation strategy was employed in another report, in which sodium dodecyl sulfate (SDS) was used to replace the traditional OA ligand[120]. SDS passivation significantly reduced trap density, thereby boosting the PLQY of SDS-$CsPbI_3$ NCs to nearly 100%. In addition, the incorporation of SDS significantly increased the stability of $CsPbBr_3$ NCs. The results showed

View Article Online
DOI: 10.1039/D6EL00019C

that the red emission from pristine $CsPbI_3$ NCs disappeared after 20 min of water treatment. In comparison, the SDS-$CsPbI_3$ NCs retained over 70% of their original performance after 40 min under the same conditions. The SDS-$CsPbI_3$ NCs retained 40% of their initial PL intensity at high temperatures and showed no phase transformation under ambient conditions. On the other hand, the pristine $CsPbI_3$ NCs experienced a rapid reduction in PL intensity to zero at the same temperature. They transformed into the δ phase after exposure to ambient air for 5 days. DFT calculations revealed that improvements in both stability and photoluminescence can be attributed to the strong binding affinity of the SDS ligand, which preserves the perovskite surface. Consequently, the red PeLEDs fabricated from SDS-$CsPbI_3$ NCs showed superior color purity and performance, achieving a maximum EQE of 8.4%, compared to 2.1% of those using pristine $CsPbI_3$ NCs (**Figure 16c**).

Son et al. reported a strong relationship between hysteresis and trap states generated by defects. As trap density decreased, hysteresis decreased gradually. Therefore, they proposed a strategy to synthesize hysteresis-free perovskite solar cells through defect passivation using alkali metal salts (LiI, NaI, KI, RbI, and CsI)[121]. The results showed that KI had the greatest effect on eliminating the hysteresis phenomenon. This can be attributed to the well-suited placement of K^+ ions within the O_h interstitial site, preventing the migration of I ions. Consequently, the formation of iodide Frenkel defects, the primary contributors to hysteresis, was minimized. Removing hysteresis can improve the stability and optical performance of PCSs. As a result, an average PCE of 17.55% was obtained for KI-doped perovskite solar cells, compared with 17.14 % for the pristine one. Adbi-Jalebi et al. employed a K^+ passivator to prepare perovskite films with superior photoluminescence quantum efficiency (PLQE) and high photostability[122]. With an appropriate amount of K+ doping, the PLQE reached 66%, corresponding to an internal yield of more than 95% (**Figure 16d**). After passivation, the perovskite films showed very high photostability at the optimal bandgap under irradiation, while the pristine sample exhibited significant redshifts and changes in bandgap over time. Ion migration was also prevented, eliminating hysteresis. As a result, the PCE of the device based on passivated perovskites increased remarkably from 17.3% to 21.5%. In another study, it was demonstrated that a quadruple-cation perovskite $K_xCs_{0.05}(FA_{0.85}MA_{0.15})_{0.95}Pb(I_{0.85}Br_{0.15})_3$ in which K^+ ion showed self-passivation properties[123]. The passivation induced an improvement in the crystallinity and an increase in the grain size of the perovskite films. The trap states at GBs and interfaces were thus reduced, resulting in a slower

View Article Online
DOI: 10.1039/D6EL00019C

recombination rate and longer carrier lifetime. Moreover, introducing the K+ cation significantly improved the long-term stability of the corresponding device, with no degradation in PCE after 1000 h under ambient conditions with RH of about 10 ± 5 % (**Figure 16e**). Consequently, a hysteresis-free, stable, and highly efficient PSC with a PCE of 20.56% was obtained. In the field of photocatalysis, the doping of K^+ cation into $MAPbBr_3$ to form K-$MAPbBr_3$ was revealed to efficiently prevent the formation of Pb^0 and Br^0 defects, and thus boosted the photostability of the perovskite in H_2 generation reaction[124]. After depositing the K-$MAPbBr_3$ with $Mo_3S_{13}^{2-}$ nanoclusters, the amount of H_2 generated by K-$MAPbBr_3$/ $Mo_3S_{13}^{2-}$ significantly increased to nearly 80 μmol g^{-1}, which is 7.4 times higher than that of $MAPbBr_3$/ $Mo_3S_{13}^{2-}$ (**Figure 16f**).

Compared with K^+, the Rb^+ ion shows a lower passivation capability. K^+ and Rb^+ were doped into triple cation perovskite $(Cs_{0.06}MA_{0.15}FA_{0.79})Pb(I_{0.85}Br_{0.15})_3$ to passivate the negatively charged defects, then the optical performance and chemical stability of passivated perovskite films were examined[125]. The K-passivated films showed a significant increase in PLQE from 18% to 41%, while no change in PLQE was observed for the Rb-passivated ones. After exposure to RH level of 50% for 24 h, the PLQE of K-passivated films increased to 49.2%, while the PLQE of Rb-passivated films dropped to 12.9% (**Figure 16g**). These results suggested that potassium has a greater tolerance than rubidium. This is because, under high relative humidity conditions, both K- and Rb-passivated films degraded into non-perovskite phases. However, the Rb-rich phase had lower solubility and a negative effect on the film's photoluminescence, resulting in lower PLQE for Rb-passivated films. Nevertheless, Rb^+ ions still have a specific passivation impact on perovskites. In particular, the Rb-doped $CsPbI_2Br$ film had less recombination and lower defect density than the pristine one, which induced an increase in the PCE of the corresponding PSCs device to reach a maximum value of 12%[126] (**Figure 16h**). The air stability of PSCs based on Rb-doped $CsPbI_2Br$ film was also enhanced, in which more than 90% of the initial PCE was maintained after exposure to 20% humidity for 94 h. Meanwhile, the PCE of the device based on pristine $CsPbI_2Br$ dropped to only 0.14% under the same conditions.[126] By adding an appropriate amount of RbI into perovskite precursor solution, Rb-introduced $(FAPbI_3)_{0.85}(MAPbBr_3)_{0.15}$ perovskites with enhanced performance were fabricated[127]. In this case, Rb^+ was reported to occupy the A-site and passivate the iodine vacancies in both grain interiors and grain boundaries. The electronic passivation effect of Rb resulted in significantly improved intrinsic photostability for the 5% Rb-introduced perovskites, exhibiting three times higher photoluminescence intensity

View Article Online
DOI: 10.1039/D6EL00019C

(**Figure 16i**) and a longer carrier lifetime compared to those of pristine perovskites. Furthermore, introducing Rb into perovskite materials can lead to the formation of Rb-containing secondary phases (e.g., $RbPbI_3$) at the surface, which modify interfacial energetics, as Rb was not incorporated into the main perovskite lattice[128].

Cesium ion has been widely used as a suitable cation to occupy the A-site in the perovskite structure. Inorganic cesium salts can be incorporated with perovskites to serve as surface passivators. Ling et al. reported that the post-treatment of $CsPbI_3$ quantum dots (QDs) with various inorganic cesium salts, including cesium acetate (CsAc), cesium iodide (CsI), cesium carbonate (Cs_2CO_3), cesium nitrate ($CsNO_3$) can passivate the vacancies at the perovskite surface and prolong the carrier lifetime[129] (**Figure 17a**). As a result, the maximum PCE of 14.10%, 13.14%, 13.74%, and 13.67% were obtained for CsAc-, Cs_2CO_3-, CsI-, and $CsNO_3$-treated $CsPbI_3$ QD solar cells, respectively, surpassing the control device which showed a PCE of 12.59%.

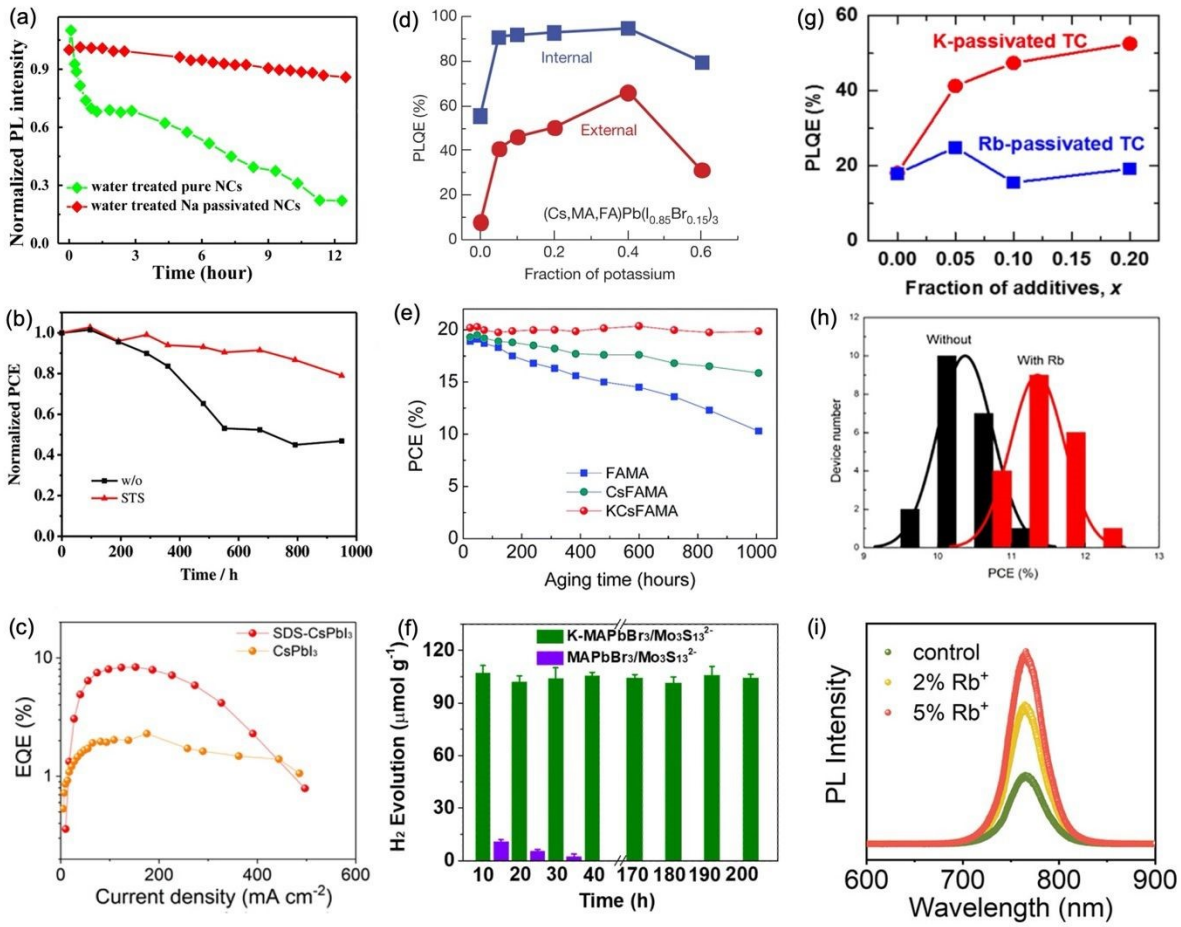

View Article Online
DOI: 10.1039/D6EL00019C

Figure 16. (a) Normalized PL intensity of pristine and Na-passivated CsPbBr3 NCs in deionized water. Reproduced with permission.[117] Copyright 2021 Elsevier B.V. (b) Normalized PCE of PSC devices with and without STS modification stored in ambient condition without encapsulation (temperature: 25 ºC, relative humidity: 40–70%). Reproduced with permission.[119] Copyright 2020 WILEY-VCH Verlag GmbH & Co. KGaA, Weinheim. (c) EQEs of PeLEDs fabricated from SDS-$CsPbI_3$ NCs and pure $CsPbBr_3$ NCs. Reproduced with permission.[120] Copyright 2021 American Chemical Society. (d) PLQE of perovskite thin films passivated with different fractions of potassium *x*. Reproduced with permission.[122] Copyright 2018 Macmillan Publishers Limited, part of Springer Nature. (e) Long-term stability of passivated and non-passivated perovskite devices after more than 1000 hours under an average humidity of $10 \pm 5\%$. Reproduced with permission.[123] Copyright 2017 The Royal Society of Chemistry. (f) H_2 evolution in experiments using K-$MAPbBr_3/Mo_3S_{13}^{2-}$ and $MAPbBr_3/Mo_3S_{13}^{2-}$ as photocatalysts. Reproduced with permission.[124] Copyright 2020 The Authors. EcoMat is published by John Wiley & Sons Australia, Ltd on behalf of The Hong Kong Polytechnic University. (g) PLQE of K- and Rb-passivated perovskite films with different fractions of additives. Reproduced with permission.[125] Copyright 2018 American Chemical Society. (h) The PCE of devices with and without Rb^+ doping. Reproduced with permission.[126] Copyright 2019 WILEY-VCH Verlag GmbH & Co. KGaA, Weinheim. (i) PL intensity of undoped- and Rb-doped perovskites. Reproduced with permission.[127] Copyright 2022 WILEY-VCH Verlag GmbH & Co. KGaA, Weinheim.

Moreover, CsAc treatment could improve the stability of $CsPbI_3$ crystals. This effect should be attributed to cooperative ionic interactions in CsAc, where Ac^- coordinates with undercoordinated Pb^{2+} defects, while Cs^+ contributes to lattice stabilization, thereby protecting the surface of perovskite QDs from moisture attack. The device based on CsAc-treated $CsPbI_3$ QDs retained 70% of its original PCE after storage for 54 h under a relative humidity of 40%, while the PCE of the control device dropped to 52% of its initial PCE under the same conditions[129]. Yuan et al. pointed out that incorporating CsAc into $FA_{0.85}MA_{0.15}PbI_3$ film reduced the defect density and improved the stability of perovskites due to the strong interaction of Ac^- with Pb^{2+} ions. The CsAc-treated PSCs exhibited an increase in maximum PCE from 19.47% to 21.95% and maintained 97% of their initial PCE after exposure for 55 days without encapsulation in air[130] (**Figure 17c**). The passivation with CsBr positively impacted the performance and stability of $CsPbI_2Br$ PSCs, where Br^- compensates halide vacancies, and Cs^+ helps stabilize the perovskite lattice, resulting in an

View Article Online
DOI: 10.1039/D6EL00019C

increased PCE from 11.8 % to 16.3 %. Additionally, the PCE of CsBr-passivated $CsPbI_2Br$ PSCs only decreased to 86% of the initial value after storage for 1368 h in N_2. In contrast, the device without CsBr passivation retained only 57% of the initial PCE after 384 h under the same conditions[131] (**Figure 17b**). Guo et al. proposed a surface passivation strategy using cesium oleate (Cs-oleate), in which oleate anions coordinate with Pb^{2+} surface defects while Cs^+ assists in structural stabilization. The device fabricated from Cs-oleate-treated perovskite films slightly improved maximum PCE from 18.01% to 18.31%. Moreover, it maintained 88% of the initial efficiency after 720 h stored at room temperature under RH of 69%, without the use of any encapsulation[132]. Besides alkali metal ions, monovalent metal cations such as Ag^+ and Cu^+ can be doped into perovskite lattice since they have similar ionic radii as Pb^{2+} ion[133], leading to significant modification of the electronic structure. The Ag doped- $CsPbI_3$ films showed enhanced stability against moisture and light irradiation, in which their PLQY retained 80% of the initial value after 48 h under ambient conditions. The LED device fabricated from Ag doped-passivated $CsPbI_3$ films showed stronger PL intensity and a higher EQE of 11.2%, compared with 7.3% of the non-passivated device[134] (**Figure 17e**). Abdi-Jalebi et al. reported that the PLQE of Cu-doped $CH_3NH_3PbI_3$ films reached 12%, and the PCE of Cu-doped perovskite solar cells achieved a best value of 19.2%[133] (**Figure 17f**). In addition, it should be noted that using an excess amount of Ag^+ and Cu^+ doping can result in a negative effect on the performance of perovskites; thus, in many cases, only low concentrations of Ag- and Cu-salts could be used[133,135].

View Article Online
DOI: 10.1039/D6EL00019C

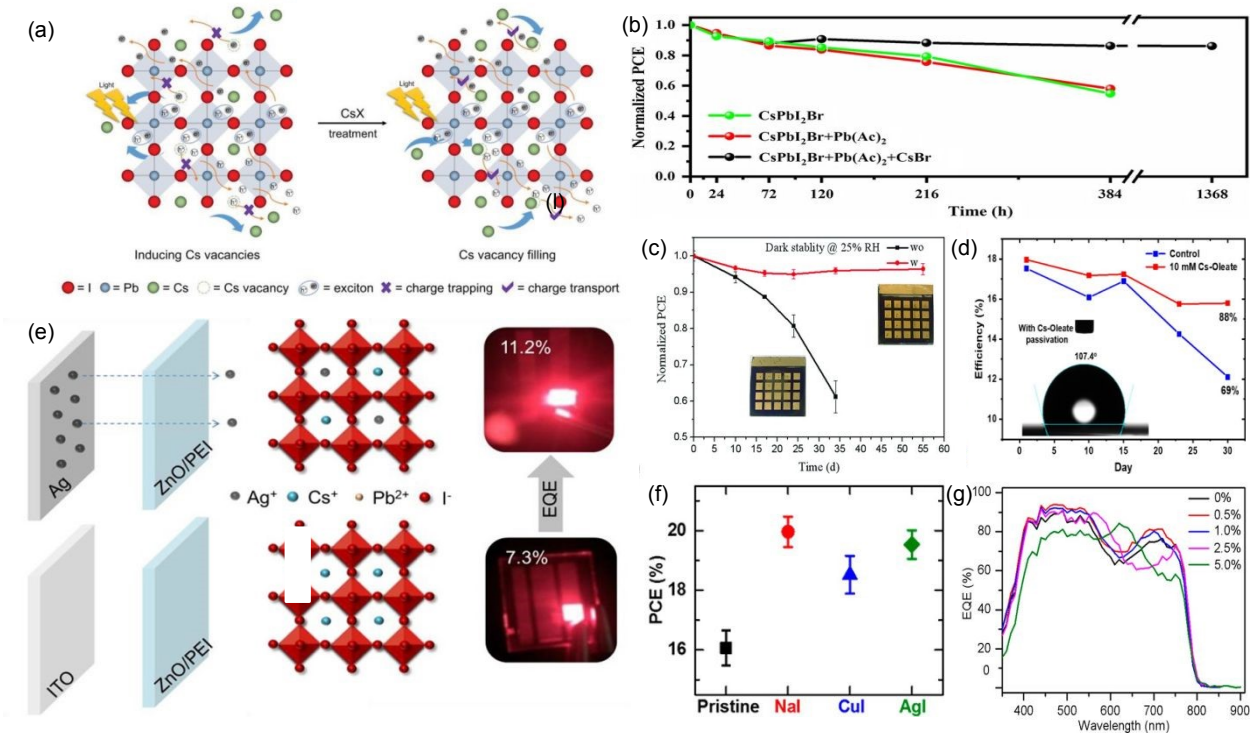

Figure 17. (a) Schematic presentation for the CsX post-treatment process to passivate the Cs vacancy. Reproduced with permission.[129] Copyright 2019 WILEY-VCH Verlag GmbH & Co. KGaA, Weinheim. (b) Long-term stability of $CsPbI_2Br$ PSCs with and without CsBr treatment. All the devices were stored in N_2, while PCE was measured under ambient conditions. Reproduced with permission.[131] Copyright 2019 WILEY-VCH Verlag GmbH & Co. KGaA, Weinheim. (c) The stability of the pristine and CsAc-treated PSCs in the dark under ambient conditions. Reproduced with permission.[130] Copyright 2019 WILEY-VCH Verlag GmbH & Co. KGaA, Weinheim. (d) Stability of the pristine and Cs-oleate PSCs devices at room temperature under RH of 69%, without encapsulation. Reproduced with permission.[132] Copyright 2019 American Chemical Society. (e) There is an increase in the EQE of PeLEDs after Ag^+ passivation. Reproduced with permission.[134] Copyright 2018 American Chemical Society. (f) The PCE of the PSCs device was treated with NaI, CuI, and AgI. Reproduced with permission.[133] Copyright 2018 American Chemical Society. (g) The EQE of PeLED devices with different Ag^+ doping concentrations. Reproduced with permission.[135] Copyright 2017 American Chemical Society.

View Article Online
DOI: 10.1039/D6EL00019C

3.2 Divalent metal cations

Divalent metal cations are typically doped into the perovskite lattice to replace the position of Pb^{2+} in the B-site. Many transition metals (e.g., Ni^{2+}, Cu^{2+}, Mn^{2+}, Cd^{2+}, and Zn^{2+}) and alkaline earth metals (e.g., Mg^{2+}, Ca^{2+}, Sr^{2+}) can be incorporated to effectively passivate negatively charged defects. For example, incorporating Ni^{2+} can reduce the trap density in $MAPbI_3$ perovskite. This is because Ni^{2+} passivated PbI_3^- antisite defects and restrained the formation of Pb^0 via interactions with uncoordinated halogen ions and halide-rich antisites[136] (**Figure 18a**). The PSCs fabricated from 3% Ni^{2+}-added $MAPbI_3$ films showed a significant increase in PCE, rising from 17.25% to 20.61%. The stability test also revealed that Ni^{2+} positively improved the air stability of PSCs device. The strong interaction of Ni^{2+} with I^- and MA^+ not only affected the ordered arrangement of MA cations but also enhanced the crystallinity of perovskite, consequently enhancing stability. Mn^{2+}-doped perovskite NCs show a characteristic yellow-orange emission but have a very low PLQY due to a nonradiative recombination process at defect states. Co-doping with Mn^{2+} and Cu^{2+} can effectively passivate these trap states. Therefore, the Cu^{2+}-Mn^{2+}-codoped $CsPbCl_3$ NCs showed significantly enhanced photoluminescence performance to reach a best PLQY of 80% (**Figure 18b**), compared to only 11% for that of Mn^{2+}-doped NCs[137]. Moreover, Cu^{2+} exhibits better thermal stability, potentially improving the stability of perovskite NCs. Cd^{2+} is reported in many publications as an efficient ionic dopant for defect passivation in perovskites. Zhao et al. presented an interfacial passivation method for synthesizing high-efficiency, stable PSCs by incorporating CdS into perovskite layers. Cd^{2+} cations can passivate iodide vacancy defects by forming a strong Cd-I bond. At the same time, S^{2-} anions simultaneously fill the iodide vacancy, reducing the trap density in perovskites and improving charge transport ability. As a result, the PSCs device based on CdS-treated perovskites achieved an excellent PCE of 21.62%, compared to the 19.97% PCE of the control device. Additionally, the long-term stability of the device was improved after the introduction of CdS, with CdS-modified PSCs retaining 87.5% of the initial efficiency after storage in N_2 for 410 h. In comparison, the control device dropped by 30% of its initial PCE under the same conditions[138] (**Figure 18c**). The surface passivation with CdI_2 can yield perovskite solar cells with even higher efficiency and stability.

Wu et al. reported that CdI_2-treated PSCs exhibited a PCE of 21.9% with improved operational stability, maintaining 92% of the initial efficiency after 1000 h under continuous irradiation at 1

View Article Online
DOI: 10.1039/D6EL00019C

sun intensity[139] (**Figure 18d**). By monitoring the content of the CdI_2 additive, Ji et al. obtained a champion PSCs device with a very high PCE of 21.95% at 0.5% Cd^{2+}-doped amount. Moreover, this device showed good long-term stability in which its PCE degraded only 12% after exposure for 42 days in ambient air with a RH of 50%). On the other hand, the PCE of the control device experienced about 17% loss under the same conditions[140]. The efficiency of Cd^{2+}-incorporated perovskite solar cells can be further boosted to achieve 22.75% by additional interfacial passivation by KCl[140] (**Figure 18e**). Zn^{2+} has been found to aggregate at grain boundaries when a high concentration of ZnI_2 was added to perovskite precursor[141]. This aggregation of Zn^{2+} can heal the defect at GBs, leading to a reduction in non-radiative recombination. Furthermore, the formation of the non-perovskite phase and PbI_2 precipitate were minimized after introducing the Zn ion. As a result, the device based on Zn^{2+}-doped PSCs showed an improved overall performance and higher stability, resulting in an increased power conversion efficiency from 18.4% (for the control device) to 20.7%, with only a 5% loss of the initial PCE after continuous illumination for 300 h[141] (**Figure 18f**). Another halide salt of zinc, $ZnBr_2$, was used to passivate the surface defects of $CsPbBr_3$, as it allowed Br^- to fill the vacancy on the surface[142]. Moreover, Zn^{2+} ion was revealed to act as catalytic sites for CO_2 reduction. As a result, the $ZnBr_2$-$CsPbBr_3$ showed approximately three times higher CO formation yield than that of pure $CsPbBr_3$ in photocatalytic CO_2 reduction. Chen et al. employed a hot-injection method to synthesize Mg^{2+}-treated $CsPbI_3$ NCs. They discovered that Mg^{2+} ions were not incorporated to replace Pb^{2+} but mainly dispersed on the surface of perovskite NCs and then passivating the defects in this region. The non-radiative recombination pathways were thereby reduced, increasing the PLQY of as-prepared Mg-$CsPbI_3$ NCs from 77% to 95%[143]. Following surface passivation with Mg^{2+}, the optical and structural stability of perovskite NCs were improved. As shown in **Figure 18i**, the Mg-$CsPbI_3$ NCs maintained over 80% of their initial PLQY after storage in air for 80 days and showed no obvious color change or phase transformation after 9 days. The improved stability can primarily be attributed to Mg^{2+}-derived surface species on nanocrystals. These species effectively passivate surface defects and partially isolate the nanocrystals from their external environment. The fact that the cubic phase remains evident in the XRD results even after 9 days suggests that the surface passivation structure stays sufficiently stable during aging. This stability helps prevent surface reconstruction and moisture-induced phase transitions. Consequently, a high-efficiency, stable red LED device based on Mg-$CsPbI_3$ NCs was successfully fabricated, demonstrating an external

View Article Online
DOI: 10.1039/D6EL00019C

quantum efficiency of 8.4%, four times that of the pristine $CsPbI_3$ LED. Ca^{2+} doping has been reported as a powerful method to boost the optical performance and stability of perovskite films. Ca^{2+}-doped $CsPbI_3$ NCs showed a maximum PLQY of 93%, 4% higher than the undoped ones. Moreover, Ca^{2+}-doped $CsPbI_3$ NCs can retain up to 83% of their initial PL intensity after storage for 147 days under 20 ± 5°C and 40-50% of RH (**Figure 18g**). The improved long-term stability is linked to the preservation of the nanocrystal surface and crystal structure upon Ca^{2+} incorporation. In contrast to pristine $CsPbI_3$ NCs, which became nonuniform, aggregated, and lost their cubic shape during storage, the Ca^{2+} -doped nanocrystals maintained a uniform cubic form and exhibited stable red emission. In solid films, Ca^{2+} -doped $CsPbI_3$ retained the cubic α-phase after 58 days in ambient conditions, while the undoped films gradually transitioned to the orthorhombic δ -phase. These findings indicate that Ca^{2+} incorporation stabilizes the local lattice environment and reduces structural changes induced by ion migration, thereby preserving the passivated structure under prolonged ambient and thermal stress. As a result, the red LED fabricated from Ca^{2+}-doped $CsPbI_3$ NCs demonstrated a nearly three-fold increase in maximum EQE to achieve 7.8%[144] (**Figure 18h**). These improvements were primarily attributed to the beneficial impact of Ca^{2+} doping, which led to a reduction in defect density and a lower hole injection barrier in perovskite films. The incorporation of Ca^{2+} can yield perovskite NCs with high efficiency and unique violet emission (**Figure 18j**). However, the stability of Ca^{2+}-doped NCs was not discussed in this case[145]. The ionic radius of Sr^{2+} (1.18 Å) is almost the same as that of Pb^{2+} (1.19 Å). Therefore, Sr^{2+} is very suitable for doping into perovskite to replace Pb^{2+}. Many publications on employing Sr^{2+} doping to synthesize perovskite films with high PLQY and improved stability have been reported[120]. The red PeLEDs based on $CsPbI_3$:1.8% Sr^{2+} showed high stability under ambient conditions and demonstrated a maximum EQE of 17.1%, a world record at the time. On the other hand, Ba^{2+} has a much larger ionic radius (1.35 Å) than Pb^{2+} ions[145]. Therefore, the introduction of Ba^{2+} to replace Pb^{2+} can generate more defects in the perovskite lattice. Consequently, Ba^{2+}-doped perovskite NCs showed extremely poor PLQY when compared to other alkaline earth metals-doped NCs[145].

View Article Online
DOI: 10.1039/D6EL00019C

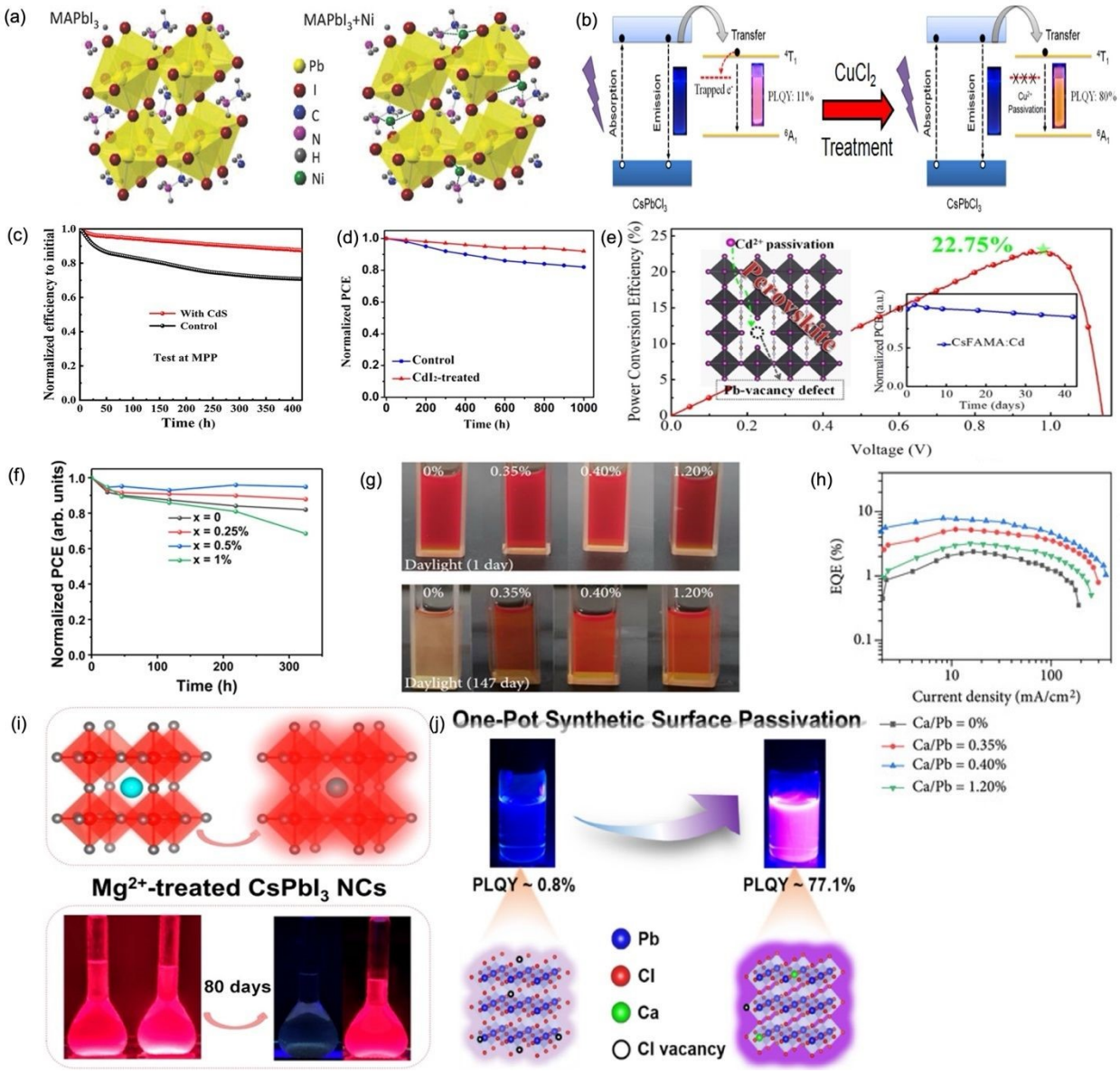

Figure 18. (a) Schematic for defect passivation in $MAPbI_3$ by Ni^{2+} ions[136]. Copyright 2018 WILEY-VCH Verlag GmbH & Co. KGaA, Weinheim. (b) The PLQY of Mn^{2+}-doped $CsPbI_3$ NCs before and after treatment with $CuCl_2$. Reproduced with permission.[137] Copyright 2021 American Chemical Society. (c) Stability of the control and CdS-treated devices in N_2 air. Reproduced with permission.[138] Copyright 2021 American Chemical Society. (d) Stability of the control and CdI_2-treated PSCs under continuous 1 sun illumination with encapsulation. Reproduced with permission.[139] Copyright 2022 American Chemical Society. (e) Schematic presentation for defect passivation in perovskites by Cd^{2+} and the PCE after further treatment with KCl. Reproduced with permission.[140] Copyright 2021 American Chemical Society. (f) The photostability of

View Article Online
DOI: 10.1039/D6EL00019C

unencapsulated devices with different content of Zn under extended light illumination at 100 mW/cm^2 in a N_2 glovebox. Reproduced with permission.[141] Copyright 2020 AIP. (g) Stability of the Ca^{2+}-doped $CsPbI_3$ NCs solutions under daylight before and after 147-day storage (from left to right: Ca/Pb = 0%, 0.35%, 0.40%, 1.20%). Reproduced with permission.[144] Copyright 2021 Wei Shen et al. Exclusive Licensee Science and Technology Review Publishing House. (h) The EQEs of PeLEDs at different Ca/Pb ratios. Reproduced with permission.[144] Copyright 2021 Wei Shen et al. Exclusive Licensee Science and Technology Review Publishing House. (i) The stability of the pristine and Mg^{2+}-treated $CsPbI_3$ NCs in solution after 80 days. Reproduced with permission.[143] Copyright 2021 American Chemical Society. (j)The PLQY and violet emission of Ca^{2+}-doped perovskite solution. Reproduced with permission.[145] Copyright 2019 American Chemical Society.

3.3 Trivalent metal ions

Despite the mismatch in oxidation states with Pb^{2+}, some trivalent metal ions still have the potential to be doped into perovskite lattice, such as group III metals (Al^{3+}, In^{3+})[149,150], group V metals (Bi^{3+}, Sb^{3+})[151,152], and lanthanide metals (Sm^{3+}, Yb^{3+})[153,154].

Al-Br and Pb-Br bonds have shown similar dissociation energy, thereby Al^{3+} can be easily incorporated into perovskite lattice[155]. In 2016, Wang et al. reported that Al^{3+} doping can reduce the electronic defect density and thereby improve the PLQE of perovskite films from 15% to 35% (**Figure 19a**). The PSCs based on Al^{3+}-doped films achieved a maximum PCE of 19.1% and a stabilized power output of 18.2%[156]. Subsequently, Yang et al. proposed a strategy using aluminum(III) acetylacetonate ($Al(acac)_3$) for doping Al^{3+} into $CsPbBr_3$ QDs[149]. The incorporation of Al^{3+} facilitated the Cl^- anion-exchange process to afford a stable mixed Br/Cl perovskite QDs with deep-blue emission[149]. The results showed that Al^{3+} doping significantly reduced defects in the as-prepared $CsPb(Br/Cl)_3$:Al QDs, leading to an increased radiative recombination ratio and an extended average lifetime. In addition, the Al-doped QDs exhibited remarkable moisture stability, with negligible phase degradation and spectral shifts after storage in water for 240 h. Consequently, a deep-blue LED was fabricated from $CsPb(Br/Cl)_3$:Al QDs**, demonstrat**ing good spectral stability and a maximum EQE of 1.38%, exceeding that of an LED device based on pristine perovskite QDs (**Figure 19b**). Recently, indium has been widely used to synthesize lead-free perovskite mainly due to its non-toxic nature[157,158]. Therefore, In^{3+} is a potential candidate for replacing Pb^{2+} in perovskite lattice. By controlling the dopant concentration, Zhu et al. successfully

View Article Online
DOI: 10.1039/D6EL00019C

prepared an In-doped perovskite sample with enhanced crystallinity and less boundary defects at 4% $InBr_3$ additive[150]. The PSCs based on $CsPbI_{2.5}Br_{0.5}$-4%-$InBr_3$ films exhibited a remarkably enhanced PCE of 12.05%, compared to a PCE of 7.5% of those based on undoped films. Furthermore, the $CsPbI_{2.5}Br_{0.5}$-4%-$InBr_3$-based PSCs displayed superior thermal resistance, in which their PCE maintained 80% of the initial value after being heated for more than 1600 h at 100 ^oC (**Figure 19c**). On the other hand, the PSCs based on pristine $CsPbI_{2.5}Br_{0.5}$ only retained 50% of the initial PCE after 800 h under the same temperature[150]. Zhou et al. obtained high-efficiency and stable indium-doped perovskite quantum dots (PeQDs) at 10% In^{3+} dopant[158] using the same concentration-controlled strategy. The 10% In^{3+}-doped $CsPbBr_xI_{3-x}$ PeQDs displayed an impressive near-unity PLQY of 99.8% and extremely high stability. These PeQDs retained over 70% of their initial PLQY after storage in n-hexane for more than six months under ambient conditions, with no considerable change in red emission color. These improvements in photoluminescence and stability can mainly be attributed to the effective passivation of surface vacancy defects induced by In^{3+} doping. Benefiting from these enhancements, the pure red PeLED based on 10% In^{3+}-doped $CsPbBr_xI_{3-x}$ PeQDs displayed an increased maximum EQE (11.2%) and higher stability than that of the pristine PeLED[159].

Bi^{3+} doping has attracted significant interest among trivalent metal cations because of its similar electron configuration to that of Pb^{2+} ions ($6s^26p^0$)[160]. Incorporating Bi^{3+} can afford perovskite materials with a narrow bandgap and near-infrared (NIR) luminescence.[161,162] However, Bi^{3+} doping was also reported to increase the structural defects in perovskites[163]. Therefore, Bi^{3+} ion might not be used as a perovskite passivator. Similarly, introducing Sb^{3+} might induce some defects (e.g., Pb vacancies), thus reducing the electron mobility in perovskite materials.[164] Incorporating lanthanide ions into the perovskite lattice can provide many benefits in photoluminescent performance and improve the stability of materials. For example, a 3% Sm^{3+}-doped $CsPbBr_3$-based PSCs device can retain more than 90% of the initial PCE after 60 days under 80 ^oC and 0% humidity, while the PCE of undoped PSCs dropped to 80% of the initial value under the same conditions.[153] Yb^{3+}-doped $CsPbCl_3$ NCs exhibited NIR emission with outstanding PLQY of approximately 200% due to the quantum cutting phenomenon[154]. However, a limited number of publications have considered the passivation effects of lanthanide ions on lead halide perovskites. Wang et al. demonstrated that the Eu^{3+} doping can simultaneously eliminate the Pb^0 and I^0 defects in the perovskite lattice. This occurred because Eu^{3+} initially oxidized Pb^0,

View Article Online
DOI: 10.1039/D6EL00019C

generating Eu^{2+}, which then reduced I^0. After passivation, the Eu^{3+}-doped device displayed an increase in maximum PCE to 21.52% (Figure 19e) and long-term stability[165] (**Figure 19f**).

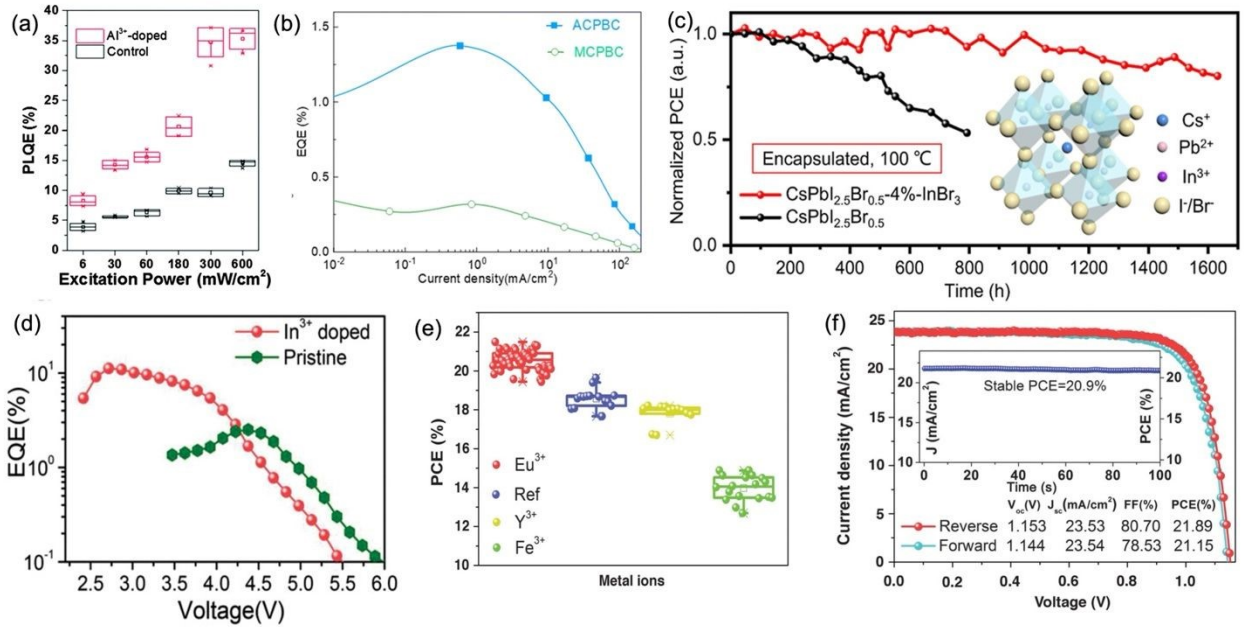

Figure 19. (a) The PLQEs of the control and Al^{3+}-doped perovskite films as the function of excitation power. Reproduced with permission.[156] Copyright 2016 The Royal Society of Chemistry. (b) The EQE of $CsPb(Br/Cl)_3$:Al QDs (ACPBC) and $CsPb(Br/Cl)_3$ QDs (MCPBC) as the function of current density. Reproduced with permission.[149] Copyright 2023 The Royal Society of Chemistry. (c) Thermal stability of the pristine and $InBr_3$-treated PSCs under heating at 100 °C. Reproduced with permission.[150] Copyright 2023 American Chemical Society. (d) EQEs of the pristine and In^{3+}-doped PeLEDs. Reproduced with permission.[159] Copyright 2021 Wiley-VCH GmbH. (e) PCE of Eu^{3+}-doped PSCs. Reproduced with permission.[165] Copyright 2019 Science. (f) Stability of Eu^{3+}-doped PSCs. Reproduced with permission.[165] Copyright 2019 Science.

4. Conclusion and outlook

In conclusion, organic ions, organic Lewis acids and bases, and metal cations have all demonstrated the ability to passivate various defect types in metal halide perovskites. Various organic ions can heal the negatively charged defects by forming ionic bonds. While Lewis bases can passivate positively charged defects at perovskite surfaces and GBs by electron donation, Lewis acids can accept electrons to passivate negatively charged defects, such as uncoordinated halogen and Pb-X antisite defects. In addition, metal cations with different covalent bonds can be

View Article Online
DOI: 10.1039/D6EL00019C

doped into the perovskite lattice, thereby passivating surface or grain-boundary defects. The positive influence of defect passivation is evident in the enhanced performance and stability of perovskite-based devices. Consequently, the passivated perovskite solar cells and perovskite light-emitting diodes exhibit significantly improved power conversion efficiency and external quantum efficiency, respectively, along with enhanced thermal and moisture stability.

However, there are few reports on boosting the photocatalytic activity of metal halide perovskites through defect passivation (summarized in **Table 1**). The key points for a semiconductor to become a good photocatalyst are strong absorption of visible light, efficient charge generation and transfer, abundant active sites and large surface areas, and high thermal and optical stability[166]. Defects in the semiconductor can affect all these features, offering both advantages and disadvantages. Therefore, further experimental and theoretical studies are needed to develop novel passivation strategies to improve the photocatalytic performance of perovskite catalysts.

In this context, distinguishing between intrinsic and extrinsic degradation mechanisms is crucial for developing effective stabilization strategies. Intrinsic instability originates from material-inherent processes such as ion migration, phase segregation, and defect evolution, whereas extrinsic instability is driven by environmental stressors including moisture, oxygen, and thermal stress. Future passivation approaches should be tailored to address both classes of degradation. While extrinsic pathways are often mitigated through encapsulation or surface protection, intrinsic degradation requires targeted passivation of defects and interfaces. In this context, multi-functional passivators that combine defect binding with environmental barrier properties represent a promising route to simultaneously suppress multiple degradation pathways and enhance long-term stability.

Defect passivation can tune the bandgap to match the energy requirements for specific photocatalytic reactions, such as CO_2 reduction. Morphology modification, which specifically alters the perovskite phase beyond the conventional cubic phase, can be a viable and promising approach, since it can provide more active sites for the catalysis. The 2D/3D mixed perovskites have been widely reported to enhance the performance of perovskite LEDs[167], so the preparation of 2D/3D perovskite materials can become another effective passivation method. In these systems, the 2D layer can act as a protective barrier that passivates surface defects and inhibits ion migration, while the 3D layer with a higher surface area is responsible for catalysis. Replacing the

View Article Online
DOI: 10.1039/D6EL00019C

Pb^{2+} ion in traditional halide perovskites with other metal ions, such as Sn^{2+} or In^{2+}, might prevent defect formation during synthesis and reduce the environmental toxicity of Pb. Defect passivation with a co-catalyst can significantly increase the catalytic activity of the materials by leveraging the synergy between the perovskite and the co-catalyst. Interfacial passivation would be essential at the perovskite/co-catalyst interfaces, particularly with optimal charge-transport layers, where significant non-radiative recombination and instability can occur. While conventional approaches often focus on single interfaces, emerging strategies such as graded passivation, bilayer architectures, and deliberate interface engineering aim to simultaneously suppress interfacial defects and enhance charge extraction. These approaches are expected to play a central role in reducing interfacial losses while improving both device efficiency and long-term stability. Moreover, this approach offers the opportunity to make perovskites active in new catalytic reactions beyond CO_2 reduction and H_2 generation.

In addition, operational stability under realistic conditions must be established. Stability should be assessed under practical operating conditions, including continuous illumination, electrical bias, elevated temperature, and humidity, to accurately evaluate passivation strategies. The adoption of standardized testing protocols that combine multiple stress factors would enable more meaningful comparison of passivation efficacy across studies and accelerate the translation of laboratory advances into reliable devices. For instance, Advanced in-situ and operando characterization techniques, such as photoluminescence, X-ray diffraction, and transmission electron microscopy, are crucial for tracking defect evolution and interfacial changes under operating conditions. These approaches can provide direct insight into dynamic passivation mechanisms that are inaccessible to ex-situ measurements. In parallel, DFT calculations and machine learning approaches offer powerful tools to predict effective passivators and unravel structure–property relationships at the atomic scale, enabling more rational and accelerated passivation design.

Table 1. Summary of the performance of passivated perovskites in photocatalysis

Photocatalyst	Defect's type	Passivator	Catalyzed reaction	Performance	Year	Ref
$CsPbBr_3$-$SOBr_2$	Surface defect	$SOBr_2$	CO_2 reduction	Total CO and CH_4 production rates: 190 μmol g^{-1} h^{-1}	2022	[60]
$CsPbBr_3$-$SOBr_2$/g-C_3N_4	Surface defect	$SOBr_2$	CO_2 reduction	CO_2 photoreduction yield of 190 μmol g^{-1} h^{-1}	2022	[60]
$CsPbBr_3$-BF_4/Co^{2+}	Surface defect	BF^{4-}	CO_2 reduction	Total CO and CH_4 evolution rates of 83.8 μmol g^{-1} h^{-1}	2021	[58]
MoS_x/S-$FAPbBr_{3-x}I_x$	Uncoordinated Pb^{2+}	S^{2-}	H_2 generation	Solar-to-chemical (STC) conversion efficiency of ca. 4.63 %	2024	[88]
K-$MAPbBr_3$/$Mo_3S_{13}^{2-}$	Pb^0 and Br^0 defects	K^+	H_2 generation	H_2 generation yield of 80 μmol g^{-1}, which is 7.4 times higher than that of $MAPbBr_3$/$Mo_3S_{13}^{2-}$	2020	[124]
$ZnBr_2$-$CsPbBr_3$	Br vacancy	Br^-	CO_2 reduction	The yield is three times higher than that of pristine $CsPbBr_3$	2024	[142]
ESY-$CsPbBr_3$@COF-SH	Surface defects	COF-SH	C–H selenation	Yield up to 99.3%	2021	[89]
(DETA)$BiBr_6$/$Cs_2AgBiBr_6$	Br defect	DETA	Toluene oxidation	Up to 100%	2023	[67]
RB-$CsPbBr_2I$@COF-SH	Surface defects	COF-SH	Cross-coupling/annulation	Yield up to 95.5%	2021	[89]
$Cs_2AgBiBr_6$-GCN	Intrinsic defect and grain boundaries	GCN	CO_2 reduction	12.14 μmol g^{-1} h^{-1} of CO and 8.85 μmol g^{-1} h^{-1} of CH_4 generation.	2023	[102]

View Article Online
DOI: 10.1039/D6EL00019C

Acknowledgements

T. H. Hoang acknowledges her PhD funding from the France Exellence program. The authors gratefully acknowledge funding from the European Union's Horizon Europe research and innovation program for the SUNPEROM project (Grant Agreement No. 101223212). M. N. GHAZZAL acknowledges funding from the M-ERA.NET joint Call 2023 for the project with Reference Number: project11468. M. Abdi-Jalebi acknowledges University College London's Research, Innovation and Global Engagement, UCL – Korea University Strategic Partner Fund, for their financial support.

5. References

(1) Fu, Y.; Zhu, H.; Chen, J.; Hautzinger, M. P.; Zhu, X.-Y.; Jin, S. Metal Halide Perovskite Nanostructures for Optoelectronic Applications and the Study of Physical Properties. *Nat. Rev. Mater.* **2019**, *4* (3), 169–188. https://doi.org/10.1038/s41578-019-0080-9.

(2) Knezevic, M.; Hoang, T.-H.; Rashid, N.; Abdi-Jalebi, M.; Colbeau-Justin, C.; Ghazzal, M. N. Recent Development in Metal Halide Perovskites Synthesis to Improve Their Charge-Carrier Mobility and Photocatalytic Efficiency. *Sci. China Mater.* **2023**, *66* (7), 2545–2572. https://doi.org/10.1007/s40843-023-2469-4.

(3) Miyazawa, Y.; Ikegami, M.; Chen, H.-W.; Ohshima, T.; Imaizumi, M.; Hirose, K.; Miyasaka, T. Tolerance of Perovskite Solar Cell to High-Energy Particle Irradiations in Space Environment. *iScience* **2018**, *2*, 148–155. https://doi.org/10.1016/j.isci.2018.03.020.

(4) Ramasamy, P.; Lim, D.-H.; Kim, B.; Lee, S.-H.; Lee, M.-S.; Lee, J.-S. All-Inorganic Cesium Lead Halide Perovskite Nanocrystals for Photodetector Applications. *Chem. Commun.* **2016**, *52* (10), 2067–2070. https://doi.org/10.1039/C5CC08643D.

(5) Shamsi, J.; Urban, A. S.; Imran, M.; De Trizio, L.; Manna, L. Metal Halide Perovskite Nanocrystals: Synthesis, Post-Synthesis Modifications, and Their Optical Properties. *Chem. Rev.* **2019**, *119* (5), 3296–3348. https://doi.org/10.1021/acs.chemrev.8b00644.

(6) Cao, M.; Damji, Y.; Zhang, C.; Wu, L.; Zhong, Q.; Li, P.; Yang, D.; Xu, Y.; Zhang, Q. Low-Dimensional-Networked Cesium Lead Halide Perovskites: Properties, Fabrication, and Applications. *Small Methods* **2020**, *4* (12), 2000303. https://doi.org/10.1002/smtd.202000303.

(7) Lei, Y.; Xu, Y.; Wang, M.; Zhu, G.; Jin, Z. Origin, Influence, and Countermeasures of Defects in Perovskite Solar Cells. *Small* **2021**, *17* (26), 2005495. https://doi.org/10.1002/smll.202005495.

(8) Kojima, A.; Teshima, K.; Shirai, Y.; Miyasaka, T. Organometal Halide Perovskites as Visible-Light Sensitizers for Photovoltaic Cells. *J. Am. Chem. Soc.* **2009**, *131* (17), 6050–6051. https://doi.org/10.1021/ja809598r.

(9) Yoo, J. J.; Seo, G.; Chua, M. R.; Park, T. G.; Lu, Y.; Rotermund, F.; Kim, Y.-K.; Moon, C. S.; Jeon, N. J.; Correa-Baena, J.-P.; Bulović, V.; Shin, S. S.; Bawendi, M. G.; Seo, J. Efficient

View Article Online
DOI: 10.1039/D6EL00019C

Perovskite Solar Cells via Improved Carrier Management. *Nature* **2021**, *590* (7847), 587–593. https://doi.org/10.1038/s41586-021-03285-w.

(10) Tao, M.; Wang, Y.; Zhang, K.; Song, Z.; Lan, Y.; Guo, H.; Guo, L.; Zhang, X.; Wei, J.; Cao, D.; Song, Y. Molecule-Triggered Strain Regulation and Interfacial Passivation for Efficient Inverted Perovskite Solar Cells. *Joule* **2024**, *8* (11), 3142–3152. https://doi.org/10.1016/j.joule.2024.08.003.

(11) Su, Z.; Cui, M.; Dong, B.; Zhang, Y.; Ran, Y.; Qi, G.; Yang, Y.; Edvinsson, T.; Hagfeldt, A.; Jiang, L.; Fan, Q.; Ma, W.; Liu, Y. Stereo-Hindrance Induced Conformal Self-Assembled Monolayer for High Efficiency Inverted Perovskite Solar Cells. *Small* **2024**, *20* (52), 2407387. https://doi.org/10.1002/smll.202407387.

(12) Yang, Y.; Chen, H.; Liu, C.; Xu, J.; Huang, C.; Malliakas, C. D.; Wan, H.; Bati, A. S. R.; Wang, Z.; Reynolds, R. P.; Gilley, I. W.; Kitade, S.; Wiggins, T. E.; Zeiske, S.; Suragtkhuu, S.; Batmunkh, M.; Chen, L. X.; Chen, B.; Kanatzidis, M. G.; Sargent, E. H. Amidination of Ligands for Chemical and Field-Effect Passivation Stabilizes Perovskite Solar Cells. *Science* **2024**, *386* (6724), 898–902. https://doi.org/10.1126/science.adr2091.

(13) Li, Y.; Xie, Z.; Duan, Y.; Li, Y.; Sun, Y.; Su, C.; Li, H.; Sun, R.; Cheng, M.; Wang, H.; Xu, D.; Zhang, K.; Wang, Y.; Lei, H.; Peng, Q.; Guo, K.; Liu, S.; Liu, Z. Successive Reactions of Trimethylgermanium Chloride to Achieve > 26% Efficiency MA-Free Perovskite Solar Cell With 3000-Hour Unattenuated Operation. *Adv. Mater.* **2025**, *37* (7), 2414354. https://doi.org/10.1002/adma.202414354.

(14) Kazmerski, L. Best Research Cell Efficiencies Chart. *Natl. Renew. Energy Lab. NREL* **2012**.

(15) Ma, C.; Park, N.-G. A Realistic Methodology for 30% Efficient Perovskite Solar Cells. *Chem* **2020**, *6* (6), 1254–1264. https://doi.org/10.1016/j.chempr.2020.04.013.

(16) Milstein, T. J.; Kroupa, D. M.; Gamelin, D. R. Picosecond Quantum Cutting Generates Photoluminescence Quantum Yields Over 100% in Ytterbium-Doped CsPbCl3 Nanocrystals. *Nano Lett.* **2018**, *18* (6), 3792–3799. https://doi.org/10.1021/acs.nanolett.8b01066.

(17) Lu, M.; Zhang, Y.; Wang, S.; Guo, J.; Yu, W. W.; Rogach, A. L. Metal Halide Perovskite Light-Emitting Devices: Promising Technology for Next-Generation Displays. *Adv. Funct. Mater.* **2019**, *29* (30), 1902008. https://doi.org/10.1002/adfm.201902008.

(18) Liu, X.-K.; Xu, W.; Bai, S.; Jin, Y.; Wang, J.; Friend, R. H.; Gao, F. Metal Halide Perovskites for Light-Emitting Diodes. *Nat. Mater.* **2021**, *20* (1), 10–21. https://doi.org/10.1038/s41563-020-0784-7.

(19) Tan, Z.-K.; Moghaddam, R. S.; Lai, M. L.; Docampo, P.; Higler, R.; Deschler, F.; Price, M.; Sadhanala, A.; Pazos, L. M.; Credgington, D.; Hanusch, F.; Bein, T.; Snaith, H. J.; Friend, R. H. Bright Light-Emitting Diodes Based on Organometal Halide Perovskite. *Nat. Nanotechnol.* **2014**, *9* (9), 687–692. https://doi.org/10.1038/nnano.2014.149.

View Article Online
DOI: 10.1039/D6EL00019C

(20) Chu, Z.; Ye, Q.; Zhao, Y.; Ma, F.; Yin, Z.; Zhang, X.; You, J. Perovskite Light-Emitting Diodes with External Quantum Efficiency Exceeding 22% via Small-Molecule Passivation. *Adv. Mater.* **2021**, *33* (18), 2007169. https://doi.org/10.1002/adma.202007169.

(21) Wang, Z.; Hong Mak, C.; Feng, J.; Shen, H.-H.; Han, B.; Permatasari Santoso, S.; Yuan, M.; Li, F.-F.; Song, H.; Lee, D.-J.; Carlos Colmenares, J.; Hsu, H.-Y. Nanoscale Halide Perovskites for Photocatalytic CO 2 Reduction: Product Selectivity, Strategies Implemented, and Charge-Carrier Separation. *J. Mater. Chem. A* **2024**, *12* (32), 20542–20577. https://doi.org/10.1039/D4TA02446J.

(22) Sun, J.; Yang, J.; Lee, J. I.; Cho, J. H.; Kang, M. S. Lead-Free Perovskite Nanocrystals for Light-Emitting Devices. *J. Phys. Chem. Lett.* **2018**, *9* (7), 1573–1583. https://doi.org/10.1021/acs.jpclett.8b00301.

(23) Luo, J.; Hu, M.; Niu, G.; Tang, J. Lead-Free Halide Perovskites and Perovskite Variants as Phosphors toward Light-Emitting Applications. *ACS Appl. Mater. Interfaces* **2019**, *11* (35), 31575–31584. https://doi.org/10.1021/acsami.9b08407.

(24) Lei, L.-Z.; Shi, Z.-F.; Li, Y.; Ma, Z.-Z.; Zhang, F.; Xu, T.-T.; Tian, Y.-T.; Wu, D.; Li, X.-J.; Du, G.-T. High-Efficiency and Air-Stable Photodetectors Based on Lead-Free Double Perovskite Cs2AgBiBr6 Thin Films. *J. Mater. Chem. C* **2018**, *6* (30), 7982–7988. https://doi.org/10.1039/C8TC02305K.

(25) Creutz, S. E.; Crites, E. N.; De Siena, M. C.; Gamelin, D. R. Colloidal Nanocrystals of Lead-Free Double-Perovskite (Elpasolite) Semiconductors: Synthesis and Anion Exchange To Access New Materials. *Nano Lett.* **2018**, *18* (2), 1118–1123. https://doi.org/10.1021/acs.nanolett.7b04659.

(26) Li, J.; Wang, L.; Yuan, X.; Bo, B.; Li, H.; Zhao, J.; Gao, X. Ultraviolet Light Induced Degradation of Luminescence in CsPbBr3 Perovskite Nanocrystals. *Mater. Res. Bull.* **2018**, *102*, 86–91. https://doi.org/10.1016/j.materresbull.2018.02.021.

(27) Guo, S.-H.; Zhou, J.; Zhao, X.; Sun, C.-Y.; You, S.-Q.; Wang, X.-L.; Su, Z.-M. Enhanced CO2 Photoreduction via Tuning Halides in Perovskites. *J. Catal.* **2019**, *369*, 201–208. https://doi.org/10.1016/j.jcat.2018.11.004.

(28) Noh, J. H.; Im, S. H.; Heo, J. H.; Mandal, T. N.; Seok, S. I. Chemical Management for Colorful, Efficient, and Stable Inorganic–Organic Hybrid Nanostructured Solar Cells. *Nano Lett.* **2013**, *13* (4), 1764–1769. https://doi.org/10.1021/nl400349b.

(29) Knezevic, M.; Quach, V.-D.; Lampre, I.; Erard, M.; Pernot, P.; Berardan, D.; Colbeau-Justin, C.; Ghazzal, M. N. Adjusting the Band Gap of CsPbBr3−yXy (X = Cl, I) for Optimal Interfacial Charge Transfer and Enhanced Photocatalytic Hydrogen Generation. *J. Mater. Chem. A* **2023**, *11* (12), 6226–6236. https://doi.org/10.1039/D2TA09920A.

(30) Knezevic, M.; Hoang, T.-H.; Wang, C.; Johar, M.; Manjón, A. G.; Rauret, D. L.; Scheu, C.; Erard, M.; Berardan, D.; Arbiol, J.; Colbeau-Justin, C.; Ghazzal, M. N. Amplified

View Article Online
DOI: 10.1039/D6EL00019C

Photoluminescence of CsPbX3 Perovskites Confined in Silica Film with a Chiral Nematic Structure. *Adv. Mater. Interfaces* **2024**, *11* (3), 2300636. https://doi.org/10.1002/admi.202300636.

(31) Wu, L.-Y.; Zhang, M.-R.; Feng, Y.-X.; Zhang, W.; Zhang, M.; Lu, T.-B. Two-Dimensional Metal Halide Perovskite Nanosheets for Efficient Photocatalytic CO2 Reduction. *Sol. RRL* **2021**, *5* (8), 2100263. https://doi.org/10.1002/solr.202100263.

(32) Smith, I. C.; Hoke, E. T.; Solis-Ibarra, D.; McGehee, M. D.; Karunadasa, H. I. A Layered Hybrid Perovskite Solar-Cell Absorber with Enhanced Moisture Stability. *Angew. Chem. Int. Ed.* **2014**, *53* (42), 11232–11235. https://doi.org/10.1002/anie.201406466.

(33) Byun, J.; Cho, H.; Wolf, C.; Jang, M.; Sadhanala, A.; Friend, R. H.; Yang, H.; Lee, T.-W. Efficient Visible Quasi-2D Perovskite Light-Emitting Diodes. *Adv. Mater.* **2016**, *28* (34), 7515–7520. https://doi.org/10.1002/adma.201601369.

(34) Knezevic, M.; Hoang, T.-H.; Quach, V. D.; Garzón Manjón, A.; Llorens Rauret, D.; Erard, M.; Gayral, A.; Benoit, M.; Berardan, D.; Arbiol, J.; Colbeau-Justin, C.; Ghazzal, M. N. Impact of Bi^{3+} and Cu^{2+} Doping on the Optical and Electronic Properties of $CsPbBr_3$ for Photocatalytic Toluene Oxidation. *Nanoscale* **2025**, *17* (35), 20280–20291. https://doi.org/10.1039/D5NR02442K.

(35) Jiang, X.; Zhou, Q.; Lu, Y.; Liang, H.; Li, W.; Wei, Q.; Pan, M.; Wen, X.; Wang, X.; Zhou, W.; Yu, D.; Wang, H.; Yin, N.; Chen, H.; Li, H.; Pan, T.; Ma, M.; Liu, G.; Zhou, W.; Su, Z.; Chen, Q.; Fan, F.; Zheng, F.; Gao, X.; Ji, Q.; Ning, Z. Surface Heterojunction Based on N-Type Low-Dimensional Perovskite Film for Highly Efficient Perovskite Tandem Solar Cells. *Natl. Sci. Rev.* **2024**, *11* (5), nwae055. https://doi.org/10.1093/nsr/nwae055.

(36) Euvrard, J.; Yan, Y.; Mitzi, D. B. Electrical Doping in Halide Perovskites. *Nat. Rev. Mater.* **2021**, *6* (6), 531–549. https://doi.org/10.1038/s41578-021-00286-z.

(37) Thiesbrummel, J.; Milić, J. V.; Deibel, C.; Garnett, E. C.; Tao, S.; Kirchartz, T.; Guerrero, A.; Cameron, P.; Tress, W.; Saiful Islam, M.; Ehrler, B. Ion Migration in Perovskite Solar Cells. *Nat. Rev. Chem.* **2026**, *10* (3), 179–195. https://doi.org/10.1038/s41570-025-00790-8.

(38) Li, X.; Ibrahim Dar, M.; Yi, C.; Luo, J.; Tschumi, M.; Zakeeruddin, S. M.; Nazeeruddin, M. K.; Han, H.; Grätzel, M. Improved Performance and Stability of Perovskite Solar Cells by Crystal Crosslinking with Alkylphosphonic Acid ω-Ammonium Chlorides. *Nat. Chem.* **2015**, *7* (9), 703–711. https://doi.org/10.1038/nchem.2324.

(39) Song, W.; Wang, Y.; Wang, C.; Wang, B.; Feng, J.; Luo, W.; Wu, C.; Yao, Y.; Zou, Z. Photocatalytic Hydrogen Production by Stable CsPbBr3@PANI Nanoparticles in Aqueous Solution. *ChemCatChem* **2021**, *13* (7), 1711–1716. https://doi.org/10.1002/cctc.202001955.

(40) Li, X.; Wang, Y.; Sun, H.; Zeng, H. Amino-Mediated Anchoring Perovskite Quantum Dots for Stable and Low-Threshold Random Lasing. *Adv. Mater.* **2017**, *29* (36), 1701185. https://doi.org/10.1002/adma.201701185.

View Article Online
DOI: 10.1039/D6EL00019C

(41) Ball, J. M.; Petrozza, A. Defects in Perovskite-Halides and Their Effects in Solar Cells. *Nat. Energy* **2016**, *1* (11), 16149. https://doi.org/10.1038/nenergy.2016.149.

(42) Jin, H.; Debroye, E.; Keshavarz, M.; Scheblykin, I. G.; Roeffaers, M. B. J.; Hofkens, J.; Steele, J. A. It's a Trap! On the Nature of Localised States and Charge Trapping in Lead Halide Perovskites. *Mater. Horiz.* **2020**, *7* (2), 397–410. https://doi.org/10.1039/C9MH00500E.

(43) Li, Y.; Wu, H.; Qi, W.; Zhou, X.; Li, J.; Cheng, J.; Zhao, Y.; Li, Y.; Zhang, X. Passivation of Defects in Perovskite Solar Cell: From a Chemistry Point of View. *Nano Energy* **2020**, *77*, 105237. https://doi.org/10.1016/j.nanoen.2020.105237.

(44) Guo, Z.; Yuan, M.; Chen, G.; Liu, F.; Lu, R.; Yin, W. Understanding Defects in Perovskite Solar Cells through Computation: Current Knowledge and Future Challenge. *Adv. Sci.* **2024**, *11* (20), 2305799. https://doi.org/10.1002/advs.202305799.

(45) Xiang, D.; Ma, Z.; Li, Y.; Lv, Z.; Chen, B.; Liu, K.; Du, H.; Zhang, Q.; Gou, F.; Du, Z.; You, W.; Xu, R.; Chen, L.; Xiang, Y.; Huang, C.; Yu, J.; Zhu, L.; Ding, Y.; Tang, C.; Luo, B.; Guo, H.; Hu, Y.; Sun, K. Perovskite-Based Photoanode with Surface Defect Passivation for Efficient Photoelectrochemical Water Splitting. *J. Alloys Compd.* **2025**, *1049*, 185441. https://doi.org/10.1016/j.jallcom.2025.185441.

(46) Sun, J.; Liu, N.; Wang, D.; Li, Q.; Qiu, F. Maximizing Defect Formation Energies via Collaborative Passivation Achieves High-Performance Perovskite Solar Cells. *ACS Appl. Mater. Interfaces* **2025**, *17* (50), 67926–67933. https://doi.org/10.1021/acsami.5c18376.

(47) Zhu, Z.; Ke, B.; Sun, K.; Jin, C.; Song, Z.; Jiang, R.; Li, J.; Kong, S.; Liu, C.; Bai, S.; He, S.; Ge, Z.; Huang, F.; Cheng, Y.-B.; Bu, T. High-Performance Inverted Perovskite Solar Cells and Modules *via* Aminothiazole Passivation. *Energy Environ. Sci.* **2025**, *18* (9), 4120–4129. https://doi.org/10.1039/D5EE01083G.

(48) Xu, X.; Zhang, Z.; Liu, T.; Zhu, P.; Zhang, Z.; Xing, G. Suppressing the Penetration of 2D Perovskites for Enhanced Stability of Perovskite Solar Cells. *J. Mater. Chem. A* **2025**, *13* (17), 12097–12103. https://doi.org/10.1039/D4TA08811E.

(49) Li, J.-A.; Ma, H.; Ding, X.; Li, S.; Han, B.; Chen, W.; Huang, S.; Chen, S.; Kuang, Y.; Liu, Z.; Yan, C. Synergistic Passivation and Stable Carrier Transport Enable Efficient Blade-Coated Perovskite Solar Cells Fabricated in Ambient Air. *J. Mater. Chem. A* **2025**, *13* (36), 30140–30150. https://doi.org/10.1039/D5TA04703J.

(50) Kumar, A.; Gupta, S. K.; Dhamaniya, B. P.; Pathak, S. K.; Karak, S. Understanding the Origin of Defect States, Their Nature, and Effects on Metal Halide Perovskite Solar Cells. *Mater. Today Energy* **2023**, *37*, 101400. https://doi.org/10.1016/j.mtener.2023.101400.

(51) Ye, J.; Byranvand, M. M.; Martínez, C. O.; Hoye, R. L. Z.; Saliba, M.; Polavarapu, L. Defect Passivation in Lead-Halide Perovskite Nanocrystals and Thin Films: Toward Efficient LEDs and Solar Cells. *Angew. Chem. Int. Ed.* **2021**, *60* (40), 21636–21660. https://doi.org/10.1002/anie.202102360.

View Article Online
DOI: 10.1039/D6EL00019C

(52) Niazi, Z.; Goharshadi, E. K. Biopolymers for Perovskite Solar Cells. In *Bio-Based Polymers: Farm to Industry. Volume 3: Emerging Trends and Applications*; ACS Symposium Series; American Chemical Society, 2024; Vol. 1487, pp 35–56. https://doi.org/10.1021/bk-2024-1487.ch003.

(53) Wang, S.; Gong, X.-Y.; Li, M.-X.; Li, M.-H.; Hu, J.-S. Polymers for Perovskite Solar Cells. *JACS Au* **2024**, *4* (9), 3400–3412. https://doi.org/10.1021/jacsau.4c00615.

(54) Zou, H.; Bi, H.; Chen, Y.; Guo, M.; Hou, W.; Su, P.; Zhou, K.; Yang, C.; Gong, X.; Xiao, L.; Liu, L. Functionalized Polymer Modified Buried Interface for Enhanced Efficiency and Stability of Perovskite Solar Cells. *Nanoscale* **2023**, *15* (5), 2054–2060. https://doi.org/10.1039/D2NR06290A.

(55) Sangale, S. S.; Mann, D. S.; Lee, H.-J.; Kwon, S.-N.; Na, S.-I. Influence of Interfacial Roughness on Slot-Die Coatings for Scaling-up High-Performance Perovskite Solar Cells. *Commun. Mater.* **2024**, *5* (1), 201. https://doi.org/10.1038/s43246-024-00645-7.

(56) Ji, T.; Niu, T.; Wang, J.; Lu, R.; Wen, Z.; Luo, D.; Huang, J. C.; Min, Y.; Wang, S.; Luponosov, Y. N.; Pan, S.; Chen, Y.; Xue, Q. Crystallization Regulation of Solution-Processed Two-Dimensional Perovskite Solar Cells. *J. Mater. Chem. A* **2022**, *10* (26), 13625–13650. https://doi.org/10.1039/D2TA02574D.

(57) Hu, Y.; Schlipf, J.; Wussler, M.; Petrus, M. L.; Jaegermann, W.; Bein, T.; Müller-Buschbaum, P.; Docampo, P. Hybrid Perovskite/Perovskite Heterojunction Solar Cells. *ACS Nano* **2016**, *10* (6), 5999–6007. https://doi.org/10.1021/acsnano.6b01535.

(58) Liu, T.; Yang, Z. Self-Healing Perovskite Solar Cells: Introduction, Recent Progresses and Perspective. *SmartMat* **2025**, *6* (4), e70033. https://doi.org/10.1002/smm2.70033.

(59) Zhang, Y.; Siegler, T. D.; Thomas, C. J.; Abney, M. K.; Shah, T.; De Gorostiza, A.; Greene, R. M.; Korgel, B. A. A "Tips and Tricks" Practical Guide to the Synthesis of Metal Halide Perovskite Nanocrystals. *Chem. Mater.* **2020**, *32* (13), 5410–5423. https://doi.org/10.1021/acs.chemmater.0c01735.

(60) Zheng, Q.; Wang, J.; Li, X.; Bai, Y.; Li, Y.; Wang, J.; Shi, Y.; Jiang, X.; Li, Z. Surface Halogen Compensation on CsPbBr3 Nanocrystals with SOBr2 for Photocatalytic CO2 Reduction. *ACS Mater. Lett.* **2022**, *4* (9), 1638–1645. https://doi.org/10.1021/acsmaterialslett.2c00482.

(61) Wang, J.-C.; Li, N.; Idris, A. M.; Wang, J.; Du, X.; Pan, Z.; Li, Z. Surface Defect Engineering of CsPbBr3 Nanocrystals for High Efficient Photocatalytic CO2 Reduction. *Sol. RRL* **2021**, *5* (7), 2100154. https://doi.org/10.1002/solr.202100154.

(62) Pan, J.; Shang, Y.; Yin, J.; De Bastiani, M.; Peng, W.; Dursun, I.; Sinatra, L.; El-Zohry, A. M.; Hedhili, M. N.; Emwas, A.-H.; Mohammed, O. F.; Ning, Z.; Bakr, O. M. Bidentate Ligand-Passivated CsPbI3 Perovskite Nanocrystals for Stable Near-Unity Photoluminescence Quantum Yield and Efficient Red Light-Emitting Diodes. *J. Am. Chem. Soc.* **2018**, *140* (2), 562–565. https://doi.org/10.1021/jacs.7b10647.

View Article Online
DOI: 10.1039/D6EL00019C

(63) Alharbi, E. A.; Alyamani, A. Y.; Kubicki, D. J.; Uhl, A. R.; Walder, B. J.; Alanazi, A. Q.; Luo, J.; Burgos-Caminal, A.; Albadri, A.; Albrithen, H.; Alotaibi, M. H.; Moser, J.-E.; Zakeeruddin, S. M.; Giordano, F.; Emsley, L.; Grätzel, M. Atomic-Level Passivation Mechanism of Ammonium Salts Enabling Highly Efficient Perovskite Solar Cells. *Nat. Commun.* **2019**, *10* (1), 3008. https://doi.org/10.1038/s41467-019-10985-5.

(64) Kim, Y.-H.; Kim, S.; Kakekhani, A.; Park, J.; Park, J.; Lee, Y.-H.; Xu, H.; Nagane, S.; Wexler, R. B.; Kim, D.-H.; Jo, S. H.; Martínez-Sarti, L.; Tan, P.; Sadhanala, A.; Park, G.-S.; Kim, Y.-W.; Hu, B.; Bolink, H. J.; Yoo, S.; Friend, R. H.; Rappe, A. M.; Lee, T.-W. Comprehensive Defect Suppression in Perovskite Nanocrystals for High-Efficiency Light-Emitting Diodes. *Nat. Photonics* **2021**, *15* (2), 148–155. https://doi.org/10.1038/s41566-020-00732-4.

(65) Kim, Y.-H.; Kim, S.; Kakekhani, A.; Park, J.; Park, J.; Lee, Y.-H.; Xu, H.; Nagane, S.; Wexler, R. B.; Kim, D.-H.; Jo, S. H.; Martínez-Sarti, L.; Tan, P.; Sadhanala, A.; Park, G.-S.; Kim, Y.-W.; Hu, B.; Bolink, H. J.; Yoo, S.; Friend, R. H.; Rappe, A. M.; Lee, T.-W. Comprehensive Defect Suppression in Perovskite Nanocrystals for High-Efficiency Light-Emitting Diodes. *Nat. Photonics* **2021**, *15* (2), 148–155. https://doi.org/10.1038/s41566-020-00732-4.

(66) Liang, A.; Wang, K.; Gao, Y.; Finkenauer, B. P.; Zhu, C.; Jin, L.; Huang, L.; Dou, L. Highly Efficient Halide Perovskite Light-Emitting Diodes via Molecular Passivation. *Angew. Chem. Int. Ed.* **2021**, *60* (15), 8337–8343. https://doi.org/10.1002/anie.202100243.

(67) Bai, Z.-J.; Yang, A.-J.; Tian, S.; Chen, L.; Wang, B.-H.; Hu, B.; Wang, X.; Zeng, T.-Q.; Peng, C.; Mao, Y.; Tulu, M.; Au, C.-T.; Yin, S.-F. Multi-Dimensional Lead-Free Hybrid Double Perovskite toward Efficient and Stable Photocatalytic Selective Oxidation of Toluene. *Chem. Eng. Sci.* **2023**, *282*, 119334. https://doi.org/10.1016/j.ces.2023.119334.

(68) Fang, Z.; Chen, W.; Shi, Y.; Zhao, J.; Chu, S.; Zhang, J.; Xiao, Z. Dual Passivation of Perovskite Defects for Light-Emitting Diodes with External Quantum Efficiency Exceeding 20%. *Adv. Funct. Mater.* **2020**, *30* (12), 1909754. https://doi.org/10.1002/adfm.201909754.

(69) Zheng, X.; Deng, Y.; Chen, B.; Wei, H.; Xiao, X.; Fang, Y.; Lin, Y.; Yu, Z.; Liu, Y.; Wang, Q.; Huang, J. Dual Functions of Crystallization Control and Defect Passivation Enabled by Sulfonic Zwitterions for Stable and Efficient Perovskite Solar Cells. *Adv. Mater.* **2018**, *30* (52), 1803428. https://doi.org/10.1002/adma.201803428.

(70) Choi, K.; Lee, J.; Kim, H. I.; Park, C. W.; Kim, G.-W.; Choi, H.; Park, S.; Park, S. A.; Park, T. Thermally Stable, Planar Hybrid Perovskite Solar Cells with High Efficiency. *Energy Environ. Sci.* **2018**, *11* (11), 3238–3247. https://doi.org/10.1039/C8EE02242A.

(71) Yang, Y.; Peng, H.; Liu, C.; Arain, Z.; Ding, Y.; Ma, S.; Liu, X.; Hayat, T.; Alsaedi, A.; Dai, S. Bi-Functional Additive Engineering for High-Performance Perovskite Solar Cells with Reduced Trap Density. *J. Mater. Chem. A* **2019**, *7* (11), 6450–6458. https://doi.org/10.1039/C8TA11925B.

(72) Ciro, J.; Mesa, S.; Uribe, J. I.; Mejía-Escobar, M. A.; Ramirez, D.; Montoya, J. F.; Betancur, R.; Yoo, H.-S.; Park, N.-G.; Jaramillo, F. Optimization of the Ag/PCBM Interface by a

View Article Online
DOI: 10.1039/D6EL00019C

Rhodamine Interlayer to Enhance the Efficiency and Stability of Perovskite Solar Cells. *Nanoscale* **2017**, *9* (27), 9440–9446. https://doi.org/10.1039/C7NR01678F.

(73) Kim, J.-H.; Kim, Y. R.; Park, B.; Hong, S.; Hwang, I.-W.; Kim, J.; Kwon, S.; Kim, G.; Kim, H.; Lee, K. Simultaneously Passivating Cation and Anion Defects in Metal Halide Perovskite Solar Cells Using a Zwitterionic Amino Acid Additive. *Small* **2021**, *17* (3), 2005608. https://doi.org/10.1002/smll.202005608.

(74) Zhang, L.; Cao, K.; Qian, J.; Huang, Y.; Wang, X.; Ge, M.; Shen, W.; Huang, F.; Wang, M.; Zhang, W.; Chen, S.; Qin, T. Crystallization Control and Multisite Passivation of Perovskites with Amino Acid to Boost the Efficiency and Stability of Perovskite Solar Cells. *J. Mater. Chem. C* **2020**, *8* (48), 17482–17490. https://doi.org/10.1039/D0TC04186F.

(75) Cho, Y.; Soufiani, A. M.; Yun, J. S.; Kim, J.; Lee, D. S.; Seidel, J.; Deng, X.; Green, M. A.; Huang, S.; Ho-Baillie, A. W. Y. Mixed 3D–2D Passivation Treatment for Mixed-Cation Lead Mixed-Halide Perovskite Solar Cells for Higher Efficiency and Better Stability. *Adv. Energy Mater.* **2018**, *8* (20), 1703392. https://doi.org/10.1002/aenm.201703392.

(76) Tavakoli, M. M.; Yadav, P.; Prochowicz, D.; Sponseller, M.; Osherov, A.; Bulović, V.; Kong, J. Controllable Perovskite Crystallization via Antisolvent Technique Using Chloride Additives for Highly Efficient Planar Perovskite Solar Cells. *Adv. Energy Mater.* **2019**, *9* (17). https://doi.org/10.1002/aenm.201803587.

(77) Lee, S.; Park, J. H.; Lee, B. R.; Jung, E. D.; Yu, J. C.; Di Nuzzo, D.; Friend, R. H.; Song, M. H. Amine-Based Passivating Materials for Enhanced Optical Properties and Performance of Organic–Inorganic Perovskites in Light-Emitting Diodes. *J. Phys. Chem. Lett.* **2017**, *8* (8), 1784–1792. https://doi.org/10.1021/acs.jpclett.7b00372.

(78) Wang, F.; Geng, W.; Zhou, Y.; Fang, H.-H.; Tong, C.-J.; Loi, M. A.; Liu, L.-M.; Zhao, N. Phenylalkylamine Passivation of Organolead Halide Perovskites Enabling High-Efficiency and Air-Stable Photovoltaic Cells. *Adv. Mater.* **2016**, *28* (45), 9986–9992. https://doi.org/10.1002/adma.201603062.

(79) Zhou, Y.; Wang, F.; Cao, Y.; Wang, J.-P.; Fang, H.-H.; Loi, M. A.; Zhao, N.; Wong, C.-P. Benzylamine-Treated Wide-Bandgap Perovskite with High Thermal-Photostability and Photovoltaic Performance. *Adv. Energy Mater.* **2017**, *7* (22), 1701048. https://doi.org/10.1002/aenm.201701048.

(80) Zheng, Y.-Z.; Li, X.-T.; Zhao, E.-F.; Lv, X.-D.; Meng, F.-L.; Peng, C.; Lai, X.-S.; Huang, M.; Cao, G.; Tao, X.; Chen, J.-F. Hexamethylenetetramine-Mediated Growth of Grain-Boundary-Passivation CH3NH3PbI3 for Highly Reproducible and Stable Perovskite Solar Cells. *J. Power Sources* **2018**, *377*, 103–109. https://doi.org/10.1016/j.jpowsour.2017.12.011.

(81) Kim, S.-G.; Chen, J.; Seo, J.-Y.; Kang, D.-H.; Park, N.-G. Rear-Surface Passivation by Melaminium Iodide Additive for Stable and Hysteresis-Less Perovskite Solar Cells. *ACS Appl. Mater. Interfaces* **2018**, *10* (30), 25372–25383. https://doi.org/10.1021/acsami.8b06616.

View Article Online
DOI: 10.1039/D6EL00019C

(82) Xu, L.; Li, J.; Cai, B.; Song, J.; Zhang, F.; Fang, T.; Zeng, H. A Bilateral Interfacial Passivation Strategy Promoting Efficiency and Stability of Perovskite Quantum Dot Light-Emitting Diodes. *Nat. Commun.* **2020**, *11* (1), 3902. https://doi.org/10.1038/s41467-020-17633-3.

(83) Wang, R.; Xue, J.; Wang, K.-L.; Wang, Z.-K.; Luo, Y.; Fenning, D.; Xu, G.; Nuryyeva, S.; Huang, T.; Zhao, Y.; Yang, J. L.; Zhu, J.; Wang, M.; Tan, S.; Yavuz, I.; Houk, K. N.; Yang, Y. Constructive Molecular Configurations for Surface-Defect Passivation of Perovskite Photovoltaics. *Science* **2019**, *366* (6472), 1509–1513. https://doi.org/10.1126/science.aay9698.

(84) Li, X.; Chen, C.-C.; Cai, M.; Hua, X.; Xie, F.; Liu, X.; Hua, J.; Long, Y.-T.; Tian, H.; Han, L. Efficient Passivation of Hybrid Perovskite Solar Cells Using Organic Dyes with □COOH Functional Group. *Adv. Energy Mater.* **2018**, *8* (20), 1800715. https://doi.org/10.1002/aenm.201800715.

(85) Zhang, J.; Yu, H. Reduced Energy Loss Enabled by Thiophene-Based Interlayers for High Performance and Stable Perovskite Solar Cells. *J. Mater. Chem. A* **2021**, *9* (7), 4138–4149. https://doi.org/10.1039/D0TA10270A.

(86) Qu, G.; Khan, D.; Yan, F.; Atsay, A.; Xiao, H.; Chen, Q.; Xu, H.; Nar, I.; Xu, Z.-X. Reformation of Thiophene-Functionalized Phthalocyanine Isomers for Defect Passivation to Achieve Stable and Efficient Perovskite Solar Cells. *J. Energy Chem.* **2022**, *67*, 263–275. https://doi.org/10.1016/j.jechem.2021.09.041.

(87) Cao, J.; Yin, J.; Yuan, S.; Zhao, Y.; Li, J.; Zheng, N. Thiols as Interfacial Modifiers to Enhance the Performance and Stability of Perovskite Solar Cells. *Nanoscale* **2015**, *7* (21), 9443–9447. https://doi.org/10.1039/C5NR01820J.

(88) Xu, T.; Xie, Y.; Qi, S.; Zhang, H.; Ma, W.; Wang, J.; Gao, Y.; Wang, L.; Zong, X. Simultaneous Defect Passivation and Co-Catalyst Engineering Leads to Superior Photocatalytic Hydrogen Evolution on Metal Halide Perovskites. *Angew. Chem. Int. Ed.* **2024**, *63* (41), e202409945. https://doi.org/10.1002/anie.202409945.

(89) Meng, G.; Zhen, L.; Sun, S.; Hai, J.; Zhang, Z.; Sun, D.; Liu, Q.; Wang, B. Confining Perovskite Quantum Dots in the Pores of a Covalent-Organic Framework: Quantum Confinement- and Passivation-Enhanced Light-Harvesting and Photocatalysis. *J. Mater. Chem. A* **2021**, *9* (43), 24365–24373. https://doi.org/10.1039/D1TA07733C.

(90) Li, M.; Yan, X.; Kang, Z.; Huan, Y.; Li, Y.; Zhang, R.; Zhang, Y. Hydrophobic Polystyrene Passivation Layer for Simultaneously Improved Efficiency and Stability in Perovskite Solar Cells. *ACS Appl. Mater. Interfaces* **2018**, *10* (22), 18787–18795. https://doi.org/10.1021/acsami.8b04776.

(91) Kim, M.; Motti, S. G.; Sorrentino, R.; Petrozza, A. Enhanced Solar Cell Stability by Hygroscopic Polymer Passivation of Metal Halide Perovskite Thin Film. *Energy Environ. Sci.* **2018**, *11* (9), 2609–2619. https://doi.org/10.1039/C8EE01101J.

(92) Feng, W.; Zhao, Y.; Lin, K.; Lu, J.; Liang, Y.; Liu, K.; Xie, L.; Tian, C.; Lyu, T.; Wei, Z. Polymer-Assisted Crystal Growth Regulation and Defect Passivation for Efficient Perovskite

View Article Online
DOI: 10.1039/D6EL00019C

Light-Emitting Diodes. *Adv. Funct. Mater.* **2022**, *32* (34), 2203371. https://doi.org/10.1002/adfm.202203371.

(93) Peng, J.; Khan, J. I.; Liu, W.; Ugur, E.; Duong, T.; Wu, Y.; Shen, H.; Wang, K.; Dang, H.; Aydin, E.; Yang, X.; Wan, Y.; Weber, K. J.; Catchpole, K. R.; Laquai, F.; De Wolf, S.; White, T. P. A Universal Double-Side Passivation for High Open-Circuit Voltage in Perovskite Solar Cells: Role of Carbonyl Groups in Poly(Methyl Methacrylate). *Adv. Energy Mater.* **2018**, *8* (30), 1801208. https://doi.org/10.1002/aenm.201801208.

(94) Li, J.; Shan, X.; Bade, S. G. R.; Geske, T.; Jiang, Q.; Yang, X.; Yu, Z. Single-Layer Halide Perovskite Light-Emitting Diodes with Sub-Band Gap Turn-On Voltage and High Brightness. *J. Phys. Chem. Lett.* **2016**, *7* (20), 4059–4066. https://doi.org/10.1021/acs.jpclett.6b01942.

(95) Song, L.; Guo, X.; Hu, Y.; Lv, Y.; Lin, J.; Liu, Z.; Fan, Y.; Liu, X. Efficient Inorganic Perovskite Light-Emitting Diodes with Polyethylene Glycol Passivated Ultrathin CsPbBr3 Films. *J. Phys. Chem. Lett.* **2017**, *8* (17), 4148–4154. https://doi.org/10.1021/acs.jpclett.7b01733.

(96) Lao, Y.; Yang, S.; Yu, W.; Guo, H.; Zou, Y.; Chen, Z.; Xiao, L. Multifunctional π-Conjugated Additives for Halide Perovskite. *Adv. Sci.* **2022**, *9* (17), 2105307. https://doi.org/10.1002/advs.202105307.

(97) Lin, Y.; Shen, L.; Dai, J.; Deng, Y.; Wu, Y.; Bai, Y.; Zheng, X.; Wang, J.; Fang, Y.; Wei, H.; Ma, W.; Zeng, X. C.; Zhan, X.; Huang, J. π-Conjugated Lewis Base: Efficient Trap-Passivation and Charge-Extraction for Hybrid Perovskite Solar Cells. *Adv. Mater.* **2017**, *29* (7), 1604545. https://doi.org/10.1002/adma.201604545.

(98) Wang, K.; Liu, J.; Yin, J.; Aydin, E.; Harrison, G. T.; Liu, W.; Chen, S.; Mohammed, O. F.; De Wolf, S. Defect Passivation in Perovskite Solar Cells by Cyano-Based π-Conjugated Molecules for Improved Performance and Stability. *Adv. Funct. Mater.* **2020**, *30* (35), 2002861. https://doi.org/10.1002/adfm.202002861.

(99) Park, Y.; Jana, A.; Myung, C. W.; Yoon, T.; Lee, G.; Kocher, C. C.; Ying, G.; Osokin, V.; Taylor, R. A.; Kim, K. S. Enhanced Photoluminescence Quantum Yield of MAPbBr3 Nanocrystals by Passivation Using Graphene. *Nano Res.* **2020**, *13* (4), 932–938. https://doi.org/10.1007/s12274-020-2718-8.

(100) Xu, Y.-F.; Yang, M.-Z.; Chen, B.-X.; Wang, X.-D.; Chen, H.-Y.; Kuang, D.-B.; Su, C.-Y. A CsPbBr3 Perovskite Quantum Dot/Graphene Oxide Composite for Photocatalytic CO2 Reduction. *J. Am. Chem. Soc.* **2017**, *139* (16), 5660–5663. https://doi.org/10.1021/jacs.7b00489.

(101) Bai, Y.; Lin, Y.; Ren, L.; Shi, X.; Strounina, E.; Deng, Y.; Wang, Q.; Fang, Y.; Zheng, X.; Lin, Y.; Chen, Z.-G.; Du, Y.; Wang, L.; Huang, J. Oligomeric Silica-Wrapped Perovskites Enable Synchronous Defect Passivation and Grain Stabilization for Efficient and Stable Perovskite Photovoltaics. *ACS Energy Lett.* **2019**, *4* (6), 1231–1240. https://doi.org/10.1021/acsenergylett.9b00608.

View Article Online
DOI: 10.1039/D6EL00019C

(102) Purohit, S.; Singh, S.; Yadav, K. L.; Pant, K. K.; Satapathi, S. Enhanced CO2 Reduction with Cs2AgBiBr6-gC3N4 Heterojunction Photocatalysts Prepared by Green Synthesis. *ACS Appl. Energy Mater.* **2023**, *6* (10), 5580–5587. https://doi.org/10.1021/acsaem.3c00717.

(103) Jia, L.; Chen, M.; Yang, S. Functionalization of Fullerene Materials toward Applications in Perovskite Solar Cells. *Mater. Chem. Front.* **2020**, *4* (8), 2256–2282. https://doi.org/10.1039/D0QM00295J.

(104) Shao, Y.; Xiao, Z.; Bi, C.; Yuan, Y.; Huang, J. Origin and Elimination of Photocurrent Hysteresis by Fullerene Passivation in CH3NH3PbI3 Planar Heterojunction Solar Cells. *Nat. Commun.* **2014**, *5* (1), 5784. https://doi.org/10.1038/ncomms6784.

(105) Niu, T.; Lu, J.; Munir, R.; Li, J.; Barrit, D.; Zhang, X.; Hu, H.; Yang, Z.; Amassian, A.; Zhao, K.; Liu, S. (Frank). Stable High-Performance Perovskite Solar Cells via Grain Boundary Passivation. *Adv. Mater.* **2018**, *30* (16), 1706576. https://doi.org/10.1002/adma.201706576.

(106) Zhang, F.; Shi, W.; Luo, J.; Pellet, N.; Yi, C.; Li, X.; Zhao, X.; Dennis, T. J. S.; Li, X.; Wang, S.; Xiao, Y.; Zakeeruddin, S. M.; Bi, D.; Grätzel, M. Isomer-Pure Bis-PCBM-Assisted Crystal Engineering of Perovskite Solar Cells Showing Excellent Efficiency and Stability. *Adv. Mater.* **2017**, *29* (17), 1606806. https://doi.org/10.1002/adma.201606806.

(107) Zhang, F.; Bi, D.; Pellet, N.; Xiao, C.; Li, Z.; Berry, J. J.; Zakeeruddin, S. M.; Zhu, K.; Grätzel, M. Suppressing Defects through the Synergistic Effect of a Lewis Base and a Lewis Acid for Highly Efficient and Stable Perovskite Solar Cells. *Energy Environ. Sci.* **2018**, *11* (12), 3480–3490. https://doi.org/10.1039/C8EE02252F.

(108) Cheng, P.-P.; Zhang, Y.-W.; Liang, J.-M.; Tan, W.-Y.; Chen, X.; Liu, Y.; Min, Y. A Facile Route to Surface Passivation of Both the Positive and Negative Defects in Perovskite Solar Cells via a Self-Organized Passivation Layer from Fullerene. *Sol. Energy* **2019**, *190*, 264–271. https://doi.org/10.1016/j.solener.2019.08.026.

(109) Zhang, M.; Chen, Q.; Xue, R.; Zhan, Y.; Wang, C.; Lai, J.; Yang, J.; Lin, H.; Yao, J.; Li, Y.; Chen, L.; Li, Y. Reconfiguration of Interfacial Energy Band Structure for High-Performance Inverted Structure Perovskite Solar Cells. *Nat. Commun.* **2019**, *10* (1), 4593. https://doi.org/10.1038/s41467-019-12613-8.

(110) Yang, Z.; Dou, J.; Kou, S.; Dang, J.; Ji, Y.; Yang, G.; Wu, W.-Q.; Kuang, D.-B.; Wang, M. Multifunctional Phosphorus-Containing Lewis Acid and Base Passivation Enabling Efficient and Moisture-Stable Perovskite Solar Cells. *Adv. Funct. Mater.* **2020**, *30* (15), 1910710. https://doi.org/10.1002/adfm.201910710.

(111) Abate, A.; Saliba, M.; Hollman, D. J.; Stranks, S. D.; Wojciechowski, K.; Avolio, R.; Grancini, G.; Petrozza, A.; Snaith, H. J. Supramolecular Halogen Bond Passivation of Organic–Inorganic Halide Perovskite Solar Cells. *Nano Lett.* **2014**, *14* (6), 3247–3254. https://doi.org/10.1021/nl500627x.

(112) Song, D.; Wei, D.; Cui, P.; Li, M.; Duan, Z.; Wang, T.; Ji, J.; Li, Y.; Mbengue, J. M.; Li, Y.; He, Y.; Trevor, M.; Park, N.-G. Dual Function Interfacial Layer for Highly Efficient and Stable

View Article Online
DOI: 10.1039/D6EL00019C

Lead Halide Perovskite Solar Cells. *J. Mater. Chem. A* **2016**, *4* (16), 6091–6097. https://doi.org/10.1039/C6TA00577B.

(113) Abdi-Jalebi, M.; Pazoki, M.; Philippe, B.; Dar, M. I.; Alsari, M.; Sadhanala, A.; Divitini, G.; Imani, R.; Lilliu, S.; Kullgren, J.; Rensmo, H.; Grätzel, M.; Friend, R. H. Dedoping of Lead Halide Perovskites Incorporating Monovalent Cations. *ACS Nano* **2018**, *12* (7), 7301–7311. https://doi.org/10.1021/acsnano.8b03586.

(114) Hu, T.; Wang, Y.; Liu, K.; Liu, J.; Zhang, H.; Khan, Q. U.; Dai, S.; Qian, W.; Liu, R.; Wang, Y.; Li, C.; Zhang, Z.; Luo, M.; Yue, X.; Cong, C.; Yongbo, Y.; Yu, A.; Zhang, J.; Zhan, Y. Understanding the Decoupled Effects of Cations and Anions Doping for High-Performance Perovskite Solar Cells. *Nano-Micro Lett.* **2025**, *17* (1), 145. https://doi.org/10.1007/s40820-025-01655-x.

(115) Lu, Y.; Alam, F.; Shamsi, J.; Abdi-Jalebi, M. Doping Up the Light: A Review of A/B-Site Doping in Metal Halide Perovskite Nanocrystals for Next-Generation LEDs. *J. Phys. Chem. C* **2024**, *128* (24), 10084–10107. https://doi.org/10.1021/acs.jpcc.4c00749.

(116) Bera, S.; Saha, A.; Mondal, S.; Biswas, A.; Mallick, S.; Chatterjee, R.; Roy, S. Review of Defect Engineering in Perovskites for Photovoltaic Application. *Mater. Adv.* **2022**, *3* (13), 5234–5247. https://doi.org/10.1039/D2MA00194B.

(117) Wu, L.; Zhang, M.; Yang, S.; Wu, R.; Gong, S.; Han, Q.; Wu, W. Spectral and Dynamic Analysis of CsPbBr3 Perovskite Nanocrystals with Enhanced Water Stability Using Sodium Passivation. *J. Alloys Compd.* **2021**, *889*, 161721. https://doi.org/10.1016/j.jallcom.2021.161721.

(118) Bi, C.; Zheng, X.; Chen, B.; Wei, H.; Huang, J. Spontaneous Passivation of Hybrid Perovskite by Sodium Ions from Glass Substrates: Mysterious Enhancement of Device Efficiency Revealed. *ACS Energy Lett.* **2017**, *2* (6), 1400–1406. https://doi.org/10.1021/acsenergylett.7b00356.

(119) Zhang, M.; Hu, W.; Shang, Y.; Zhou, W.; Zhang, W.; Yang, S. Surface Passivation of Perovskite Film by Sodium Toluenesulfonate for Highly Efficient Solar Cells. *Sol. RRL* **2020**, *4* (6), 2000113. https://doi.org/10.1002/solr.202000113.

(120) Zhang, J.; Yin, C.; Yang, F.; Yao, Y.; Yuan, F.; Chen, H.; Wang, R.; Bai, S.; Tu, G.; Hou, L. Highly Luminescent and Stable CsPbI3 Perovskite Nanocrystals with Sodium Dodecyl Sulfate Ligand Passivation for Red-Light-Emitting Diodes. *J. Phys. Chem. Lett.* **2021**, *12* (9), 2437–2443. https://doi.org/10.1021/acs.jpclett.1c00008.

(121) Son, D.-Y.; Kim, S.-G.; Seo, J.-Y.; Lee, S.-H.; Shin, H.; Lee, D.; Park, N.-G. Universal Approach toward Hysteresis-Free Perovskite Solar Cell via Defect Engineering. *J. Am. Chem. Soc.* **2018**, *140* (4), 1358–1364. https://doi.org/10.1021/jacs.7b10430.

(122) Abdi-Jalebi, M.; Andaji-Garmaroudi, Z.; Cacovich, S.; Stavrakas, C.; Philippe, B.; Richter, J. M.; Alsari, M.; Booker, E. P.; Hutter, E. M.; Pearson, A. J.; Lilliu, S.; Savenije, T. J.; Rensmo, H.; Divitini, G.; Ducati, C.; Friend, R. H.; Stranks, S. D. Maximizing and Stabilizing

View Article Online
DOI: 10.1039/D6EL00019C

Luminescence from Halide Perovskites with Potassium Passivation. *Nature* **2018**, *555* (7697), 497–501. https://doi.org/10.1038/nature25989.

(123) Bu, T.; Liu, X.; Zhou, Y.; Yi, J.; Huang, X.; Luo, L.; Xiao, J.; Ku, Z.; Peng, Y.; Huang, F.; Cheng, Y.-B.; Zhong, J. A Novel Quadruple-Cation Absorber for Universal Hysteresis Elimination for High Efficiency and Stable Perovskite Solar Cells. *Energy Environ. Sci.* **2017**, *10* (12), 2509–2515. https://doi.org/10.1039/C7EE02634J.

(124) Yue, D.; Zhang, T.; Wang, T.; Yan, X.; Guo, C.; Qian, X.; Zhao, Y. Potassium Stabilization of Methylammonium Lead Bromide Perovskite for Robust Photocatalytic H2 Generation. *EcoMat* **2020**, *2* (1), e12015. https://doi.org/10.1002/eom2.12015.

(125) Abdi-Jalebi, M.; Andaji-Garmaroudi, Z.; Pearson, A. J.; Divitini, G.; Cacovich, S.; Philippe, B.; Rensmo, H.; Ducati, C.; Friend, R. H.; Stranks, S. D. Potassium- and Rubidium-Passivated Alloyed Perovskite Films: Optoelectronic Properties and Moisture Stability. *ACS Energy Lett.* **2018**, *3* (11), 2671–2678. https://doi.org/10.1021/acsenergylett.8b01504.

(126) Guo, Y.; Zhao, F.; Tao, J.; Jiang, J.; Zhang, J.; Yang, J.; Hu, Z.; Chu, J. Efficient and Hole-Transporting-Layer-Free CsPbI2Br Planar Heterojunction Perovskite Solar Cells through Rubidium Passivation. *ChemSusChem* **2019**, *12* (5), 983–989. https://doi.org/10.1002/cssc.201802690.

(127) Xu, C.; Chen, X.; Ma, S.; Shi, M.; Zhang, S.; Xiong, Z.; Fan, W.; Si, H.; Wu, H.; Zhang, Z.; Liao, Q.; Yin, W.; Kang, Z.; Zhang, Y. Interpretation of Rubidium-Based Perovskite Recipes toward Electronic Passivation and Ion-Diffusion Mitigation. *Adv. Mater.* **2022**, *34* (14), 2109998. https://doi.org/10.1002/adma.202109998.

(128) Kubicki, D. J.; Prochowicz, D.; Hofstetter, A.; Zakeeruddin, S. M.; Grätzel, M.; Emsley, L. Phase Segregation in Cs-, Rb- and K-Doped Mixed-Cation (MA)x(FA)1–xPbI3 Hybrid Perovskites from Solid-State NMR. *J. Am. Chem. Soc.* **2017**, *139* (40), 14173–14180. https://doi.org/10.1021/jacs.7b07223.

(129) Ling, X.; Zhou, S.; Yuan, J.; Shi, J.; Qian, Y.; Larson, B. W.; Zhao, Q.; Qin, C.; Li, F.; Shi, G.; Stewart, C.; Hu, J.; Zhang, X.; Luther, J. M.; Duhm, S.; Ma, W. 14.1% CsPbI3 Perovskite Quantum Dot Solar Cells via Cesium Cation Passivation. *Adv. Energy Mater.* **2019**, *9* (28), 1900721. https://doi.org/10.1002/aenm.201900721.

(130) Yuan, S.; Cai, Y.; Yang, S.; Zhao, H.; Qian, F.; Han, Y.; Sun, J.; Liu, Z.; Liu, S. (Frank). Simultaneous Cesium and Acetate Coalloying Improves Efficiency and Stability of FA0.85MA0.15PbI3 Perovskite Solar Cell with an Efficiency of 21.95%. *Sol. RRL* **2019**, *3* (9), 1900220. https://doi.org/10.1002/solr.201900220.

(131) Zhang, Y.; Wu, C.; Wang, D.; Zhang, Z.; Qi, X.; Zhu, N.; Liu, G.; Li, X.; Hu, H.; Chen, Z.; Xiao, L.; Qu, B. High Efficiency (16.37%) of Cesium Bromide—Passivated All-Inorganic CsPbI2Br Perovskite Solar Cells. *Sol. RRL* **2019**, *3* (11), 1900254. https://doi.org/10.1002/solr.201900254.

View Article Online
DOI: 10.1039/D6EL00019C

(132) Guo, X.; Koh, T. M.; Febriansyah, B.; Han, G.; Bhaumik, S.; Li, J.; Jamaludin, N. F.; Ghosh, B.; Chen, X.; Mhaisalkar, S.; Mathews, N. Cesium Oleate Passivation for Stable Perovskite Photovoltaics. *ACS Appl. Mater. Interfaces* **2019**, *11* (31), 27882–27889. https://doi.org/10.1021/acsami.9b08026.

(133) Abdi-Jalebi, M.; Pazoki, M.; Philippe, B.; Dar, M. I.; Alsari, M.; Sadhanala, A.; Divitini, G.; Imani, R.; Lilliu, S.; Kullgren, J.; Rensmo, H.; Grätzel, M.; Friend, R. H. Dedoping of Lead Halide Perovskites Incorporating Monovalent Cations. *ACS Nano* **2018**, *12* (7), 7301–7311. https://doi.org/10.1021/acsnano.8b03586.

(134) Lu, M.; Zhang, X.; Bai, X.; Wu, H.; Shen, X.; Zhang, Y.; Zhang, W.; Zheng, W.; Song, H.; Yu, W. W.; Rogach, A. L. Spontaneous Silver Doping and Surface Passivation of CsPbI3 Perovskite Active Layer Enable Light-Emitting Devices with an External Quantum Efficiency of 11.2%. *ACS Energy Lett.* **2018**, *3* (7), 1571–1577. https://doi.org/10.1021/acsenergylett.8b00835.

(135) Chen, Q.; Chen, L.; Ye, F.; Zhao, T.; Tang, F.; Rajagopal, A.; Jiang, Z.; Jiang, S.; Jen, A. K.-Y.; Xie, Y.; Cai, J.; Chen, L. Ag-Incorporated Organic–Inorganic Perovskite Films and Planar Heterojunction Solar Cells. *Nano Lett.* **2017**, *17* (5), 3231–3237. https://doi.org/10.1021/acs.nanolett.7b00847.

(136) Gong, X.; Guan, L.; Pan, H.; Sun, Q.; Zhao, X.; Li, H.; Pan, H.; Shen, Y.; Shao, Y.; Sun, L.; Cui, Z.; Ding, L.; Wang, M. Highly Efficient Perovskite Solar Cells via Nickel Passivation. *Adv. Funct. Mater.* **2018**, *28* (50), 1804286. https://doi.org/10.1002/adfm.201804286.

(137) Chakraborty, R.; Maiti, A.; Ghorai, U. K.; Pal, A. J. Defect Passivation of Mn2+-Doped CsPbCl3 Perovskite Nanocrystals as Probed by Scanning Tunneling Spectroscopy: Toward Boosting Emission Efficiencies. *ACS Appl. Nano Mater.* **2021**, *4* (10), 10155–10163. https://doi.org/10.1021/acsanm.1c01623.

(138) Zhao, W.; Shi, J.; Tian, C.; Wu, J.; Li, H.; Li, Y.; Yu, B.; Luo, Y.; Wu, H.; Xie, Z.; Wang, C.; Duan, D.; Li, D.; Meng, Q. CdS Induced Passivation toward High Efficiency and Stable Planar Perovskite Solar Cells. *ACS Appl. Mater. Interfaces* **2021**, *13* (8), 9771–9780. https://doi.org/10.1021/acsami.0c18311.

(139) Wu, W.-Q.; Rudd, P. N.; Ni, Z.; Van Brackle, C. H.; Wei, H.; Wang, Q.; Ecker, B. R.; Gao, Y.; Huang, J. Reducing Surface Halide Deficiency for Efficient and Stable Iodide-Based Perovskite Solar Cells. *J. Am. Chem. Soc.* **2020**, *142* (8), 3989–3996. https://doi.org/10.1021/jacs.9b13418.

(140) Ji, M.; Jin, M.; Du, Q.; Zheng, J.; Feng, Y.; Shen, Z.; Li, F.; Li, H.; Chen, C. Defect Passivation with Metal Cations toward Efficient and Stable Perovskite Solar Cells Exceeding 22.7% Efficiency. *ACS Appl. Energy Mater.* **2021**, *4* (10), 11144–11150. https://doi.org/10.1021/acsaem.1c02048.

(141) Yan, L.; Li, Z.; Niu, T.; Xu, X.; Xie, S.; Dong, G.; Xue, Q.; Yip, H.-L. Effects of ZnI2 Doping on the Performance of Methylammonium-Free Perovskite Solar Cells. *J. Appl. Phys.* **2020**, *128* (4), 043102. https://doi.org/10.1063/5.0012370.

View Article Online
DOI: 10.1039/D6EL00019C

(142) Xiong, L.; Xu, M.; Wang, J.; Chen, Z.; Li, L.; Yang, F.; Zhang, Q.; Jiang, G.; Li, Z. Passivating Defects and Constructing Catalytic Sites on CsPbBr3 with ZnBr2 for Photocatalytic CO2 Reduction. *Inorg. Chem.* **2024**, *63* (28), 12703–12707. https://doi.org/10.1021/acs.inorgchem.4c02313.

(143) Chen, Q.; Cao, S.; Xing, K.; Ning, M.; Zeng, R.; Wang, Y.; Zhao, J. Mg2+-Assisted Passivation of Defects in CsPbI3 Perovskite Nanocrystals for High-Efficiency Photoluminescence. *J. Phys. Chem. Lett.* **2021**, *12* (45), 11090–11097. https://doi.org/10.1021/acs.jpclett.1c03258.

(144) Shen, W.; Zhang, J.; Dong, R.; Chen, Y.; Yang, L.; Chen, S.; Su, Z.; Dai, Y.; Cao, K.; Liu, L.; Chen, S.; Huang, W. Stable and Efficient Red Perovskite Light-Emitting Diodes Based on Ca2+-Doped CsPbI3 Nanocrystals. *Research 2021*. https://doi.org/10.34133/2021/9829374.

(145) Chen, J.-K.; Ma, J.-P.; Guo, S.-Q.; Chen, Y.-M.; Zhao, Q.; Zhang, B.-B.; Li, Z.-Y.; Zhou, Y.; Hou, J.; Kuroiwa, Y.; Moriyoshi, C.; Bakr, O. M.; Zhang, J.; Sun, H.-T. High-Efficiency Violet-Emitting All-Inorganic Perovskite Nanocrystals Enabled by Alkaline-Earth Metal Passivation. *Chem. Mater.* **2019**, *31* (11), 3974–3983. https://doi.org/10.1021/acs.chemmater.9b00442.

(146) Yao, J.-S.; Ge, J.; Wang, K.-H.; Zhang, G.; Zhu, B.-S.; Chen, C.; Zhang, Q.; Luo, Y.; Yu, S.-H.; Yao, H.-B. Few-Nanometer-Sized α-CsPbI3 Quantum Dots Enabled by Strontium Substitution and Iodide Passivation for Efficient Red-Light Emitting Diodes. *J. Am. Chem. Soc.* **2019**, *141* (5), 2069–2079. https://doi.org/10.1021/jacs.8b11447.

(147) Chen, C.; Xuan, T.; Bai, W.; Zhou, T.; Huang, F.; Xie, A.; Wang, L.; Xie, R.-J. Highly Stable CsPbI3:Sr2+ Nanocrystals with near-Unity Quantum Yield Enabling Perovskite Light-Emitting Diodes with an External Quantum Efficiency of 17.1%. *Nano Energy* **2021**, *85*, 106033. https://doi.org/10.1016/j.nanoen.2021.106033.

(148) Lu, M.; Zhang, X.; Zhang, Y.; Guo, J.; Shen, X.; Yu, W. W.; Rogach, A. L. Simultaneous Strontium Doping and Chlorine Surface Passivation Improve Luminescence Intensity and Stability of CsPbI3 Nanocrystals Enabling Efficient Light-Emitting Devices. *Adv. Mater.* **2018**, *30* (50), 1804691. https://doi.org/10.1002/adma.201804691.

(149) Yang, L.; Shan, Q.; Zhang, S.; Zhou, Y.; Li, Y.; Zou, Y.; Zeng, H. Improving Anion-Exchange Efficiency and Spectrum Stability of Perovskite Quantum Dots via an Al3+ Bonding-Doping Synergistic Effect. *Nanoscale* **2023**, *15* (12), 5696–5704. https://doi.org/10.1039/D2NR07091J.

(150) Zhu, M.; Qin, L.; Xia, Y.; Mao, L.; Zhao, P.; Zhao, C.; Hu, Y.; Hong, D.; Tian, Y.; Tie, Z.; Jin, Z. Indium-Doped CsPbI2.5Br0.5 with a Tunable Band Structure and Improved Crystallinity for Thermo-Stable All-Inorganic Perovskite Solar Cells. *ACS Appl. Energy Mater.* **2023**, *6* (15), 8237–8244. https://doi.org/10.1021/acsaem.3c01345.

(151) Begum, R.; Parida, M. R.; Abdelhady, A. L.; Murali, B.; Alyami, N. M.; Ahmed, G. H.; Hedhili, M. N.; Bakr, O. M.; Mohammed, O. F. Engineering Interfacial Charge Transfer in

View Article Online
DOI: 10.1039/D6EL00019C

CsPbBr3 Perovskite Nanocrystals by Heterovalent Doping. *J. Am. Chem. Soc.* **2017**, *139* (2), 731–737. https://doi.org/10.1021/jacs.6b09575.

(152) Oku, T.; Ohishi, Y.; Suzuki, A. Effects of Antimony Addition to Perovskite-Type CH3NH3PbI3 Photovoltaic Devices. *Chem. Lett.* **2016**, *45* (2), 134–136. https://doi.org/10.1246/cl.150984.

(153) Duan, J.; Zhao, Y.; Yang, X.; Wang, Y.; He, B.; Tang, Q. Lanthanide Ions Doped CsPbBr3 Halides for HTM-Free 10.14%-Efficiency Inorganic Perovskite Solar Cell with an Ultrahigh Open-Circuit Voltage of 1.594 V. *Adv. Energy Mater.* **2018**, *8* (31), 1802346. https://doi.org/10.1002/aenm.201802346.

(154) Mir, W. J.; Sheikh, T.; Arfin, H.; Xia, Z.; Nag, A. Lanthanide Doping in Metal Halide Perovskite Nanocrystals: Spectral Shifting, Quantum Cutting and Optoelectronic Applications. *NPG Asia Mater.* **2020**, *12* (1), 9. https://doi.org/10.1038/s41427-019-0192-0.

(155) Zhou, Y.; Chen, J.; Bakr, O. M.; Sun, H.-T. Metal-Doped Lead Halide Perovskites: Synthesis, Properties, and Optoelectronic Applications. *Chem. Mater.* **2018**, *30* (19), 6589–6613. https://doi.org/10.1021/acs.chemmater.8b02989.

(156) Wang, J. T.-W.; Wang, Z.; Pathak, S.; Zhang, W.; deQuilettes, D. W.; Wisnivesky-Rocca-Rivarola, F.; Huang, J.; Nayak, P. K.; Patel, J. B.; Mohd Yusof, H. A.; Vaynzof, Y.; Zhu, R.; Ramirez, I.; Zhang, J.; Ducati, C.; Grovenor, C.; Johnston, M. B.; Ginger, D. S.; Nicholas, R. J.; Snaith, H. J. Efficient Perovskite Solar Cells by Metal Ion Doping. *Energy Environ. Sci.* **2016**, *9* (9), 2892–2901. https://doi.org/10.1039/C6EE01969B.

(157) Lee, W.; Hong, S.; Kim, S. Colloidal Synthesis of Lead-Free Silver–Indium Double-Perovskite Cs2AgInCl6 Nanocrystals and Their Doping with Lanthanide Ions. *J. Phys. Chem. C* **2019**, *123* (4), 2665–2672. https://doi.org/10.1021/acs.jpcc.8b12146.

(158) Han, P.; Zhou, W.; Zheng, D.; Zhang, X.; Li, C.; Kong, Q.; Yang, S.; Lu, R.; Han, K. Lead-Free All-Inorganic Indium Chloride Perovskite Variant Nanocrystals for Efficient Luminescence. *Adv. Opt. Mater.* **2022**, *10* (1), 2101344. https://doi.org/10.1002/adom.202101344.

(159) Zhou, X.; Zhang, J.; Tong, X.; Sun, Y.; Zhang, H.; Min, Y.; Qian, Y. Near-Unity Quantum Yield and Superior Stable Indium-Doped CsPbBrxI3−x Perovskite Quantum Dots for Pure Red Light-Emitting Diodes. *Adv. Opt. Mater.* **2022**, *10* (2), 2101517. https://doi.org/10.1002/adom.202101517.

(160) Sarkar, P.; Mazumder, J.; Tripathy, S. K.; Baishnab, K. L.; Palai, G. Structural, Optoelectronic, and Morphological Study of Indium-Doped Methylammonium Lead Chloride Perovskites. *Appl. Phys. A* **2019**, *125* (8), 580. https://doi.org/10.1007/s00339-019-2877-1.

(161) Sun, H.-T.; Zhou, J.; Qiu, J. Recent Advances in Bismuth Activated Photonic Materials. *Prog. Mater. Sci.* **2014**, *64*, 1–72. https://doi.org/10.1016/j.pmatsci.2014.02.002.

(162) Abdelhady, A. L.; Saidaminov, M. I.; Murali, B.; Adinolfi, V.; Voznyy, O.; Katsiev, K.; Alarousu, E.; Comin, R.; Dursun, I.; Sinatra, L.; Sargent, E. H.; Mohammed, O. F.; Bakr, O. M.

View Article Online
DOI: 10.1039/D6EL00019C

Heterovalent Dopant Incorporation for Bandgap and Type Engineering of Perovskite Crystals. *J. Phys. Chem. Lett.* **2016**, *7* (2), 295–301. https://doi.org/10.1021/acs.jpclett.5b02681.

(163) Zhou, Y.; Yong, Z.-J.; Zhang, W.; Ma, J.-P.; Sadhanala, A.; Chen, Y.-M.; Liu, B.-M.; Zhou, Y.; Song, B.; Sun, H.-T. Ultra-Broadband Optical Amplification at Telecommunication Wavelengths Achieved by Bismuth-Activated Lead Iodide Perovskites. *J. Mater. Chem. C* **2017**, *5* (10), 2591–2596. https://doi.org/10.1039/C6TC05539G.

(164) Zhang, J.; Shang, M.; Wang, P.; Huang, X.; Xu, J.; Hu, Z.; Zhu, Y.; Han, L. N-Type Doping and Energy States Tuning in CH3NH3Pb1–xSb2x/3I3 Perovskite Solar Cells. *ACS Energy Lett.* **2016**, *1* (3), 535–541. https://doi.org/10.1021/acsenergylett.6b00241.

(165) Wang, L.; Zhou, H.; Hu, J.; Huang, B.; Sun, M.; Dong, B.; Zheng, G.; Huang, Y.; Chen, Y.; Li, L.; Xu, Z.; Li, N.; Liu, Z.; Chen, Q.; Sun, L.-D.; Yan, C.-H. A Eu3+-Eu2+ Ion Redox Shuttle Imparts Operational Durability to Pb-I Perovskite Solar Cells. *Science* **2019**, *363* (6424), 265–270. https://doi.org/10.1126/science.aau5701.

(166) Chen, Z.-Y.; Huang, N.-Y.; Xu, Q. Metal Halide Perovskite Materials in Photocatalysis: Design Strategies and Applications. *Coord. Chem. Rev.* **2023**, *481*, 215031. https://doi.org/10.1016/j.ccr.2023.215031.

(167) Fathalizadeh, N.; Ghahrizjani, R. T.; Shojaei, S.; Mohajerani, E.; Ahmadi-Kandjani, S. Enhancing Metal Halide Perovskite LED Performance by Minimizing Ion Migration through the Design of a Mixed 2D(RP+DJ)/3D Active Layer Structure. *J. Alloys Compd.* **2025**, *1010*, 177813. https://doi.org/10.1016/j.jallcom.2024.177813.

No data availability statement is required for the review

View Article Online
DOI: 10.1039/D6EL00019C